The influence of water on the méchanical behaviour of argillaceous rocks

Harald Freissmuth

HAL Id: **pastel-00579409**
https://pastel.hal.science/pastel-00579409

Submitted on 23 Mar 2011

Écote des Mines de Paris

N° attribué par la bibliothèque

/__/__/__/__/__/__/__/__/__/__/

Thèse

pour obtenir le grade de

Docteur de l'École des Mines de Paris

Spécialité : Technique et Economie de l'Exploitation du
Sous-Sol

présentée et soutenue publiquement

par

Harald FREISSMUTH

le 17 décembre 2002

**Influence de l'eau sur le comportement
mécanique des roches argileuses**

Directeurs de thèse : Joël BILLIOTTE et Michel TIJANI

Jury

Madame	Brigitte WEINHARDT	Rapporteur
Monsieur	Peter MOSER	Rapporteur
Monsieur	Jack-Pierre PIGUET	Examinateur
Madame	Kun SU	Examinateur
Monsieur	Joël BILLIOTTE	Directeur
Monsieur	Michel TIJANI	Directeur

I Executive Summary

This thesis was done in collaboration with the French national radioactive waste agency ANDRA. The aim is to contribute to a better understanding of the mechanical behaviour of argillaceous rocks under the influence of aqueous solutions, as they are considered to be a possible host rock for a nuclear waste disposal site.

Shale, can depending on the composition, change its mechanical and petrophysical properties in a wide range due to fluid-clay mineral interactions. One and the same shale can be soft or hard, ductile or rigid, permeable or sealing – depending on the environmental conditions the sample is exposed to. Shale can be very sensitive to a change of conditions such as humidity, stress state, temperature, and chemical potential gradients.

One of the most obvious shale reactions is the swelling and shrinking as a function of it's saturation and the chemical potential gradient in the fluid system. Theses volume changes also sometimes alter other properties. Depending on the nature and the concentration of a liquid, a shale can either shrink or swell when in contact with a liquid. The material may sometimes also disperse in the liquid and deteriorate completely.

An understandable description of the clay-minerals from the site of Est is given. The physico-chemical micro mechanism of the fluid solid interaction such as adsorption, absorption, capillarity and osmosis are also presented. The possible consequences of these mechanisms on the macro mechanical behaviour, such as swelling and shrinking, crack induction and others was analysed.

X-ray microfocus technology was introduced and used to analyse shale under different environmental conditions. The advantage of this technology is it's non-destructive character. The preparation of classical thin cross section is a rather inappropriate method, concerning micro cracks and deterioration in shale, because of the grinding of the material.

A solution test was conducted to qualitatively observe the real-time reaction of the shale, from the site of Est, when in contact with different aqueous solutions and under uniaxial load. The cracking as well as the strain and the general behaviour of the material was investigated by using the X-ray µRG technology while the material was immersed in a solution. It could be shown, that the deterioration, the development of micro cracks and the strain are partially governed by the ion concentration and the ion species of the solution.

In the kinetic test arrangement the shale was exposed to different relative humidity and uniaxial load conditions. A computer controlled air conditioning system, with online data transfer of the axial strain and the environmental parameters, was used. The relation between environmental humidity, axial strain, axial load condition and micro cracks was analyzed. X-ray microfocus technology was used to take images of the specimen before and after the test. The material was tested in a range of relative humidity from 5% to 99%, in order to evaluate the influence of the humidity on the crack and strain behaviour. A cyclical test was conducted to asses the crack sensitivity in a range from 35% RH to 75% RH.

Finally a combined test was realized, to determine whether the material reacts to pure water in a different way after being saturated in a humid environment, compared to its reaction to water in its initial saturation state. The material was initially exposed to 5% and 99% relative humidity and subsequently immersed into pure water. A hydration phenomenon was discovered through this test, which is believed to be of importance with reference to commonly applied testing procedures.

II   Résumé général

Cette thèse a été réalisée en coopération avec ANDRA, l'agence nationale française des déchets radioactives. Son objectif est de donner une meilleure compréhension des propriétés mécaniques des roches argileuses sous l'influence de solutions aqueuses, en admettant qu'elles sont considérées comme des roches susceptibles d'héberger des déchets nucléaires.

L'ardoise peut, selon sa composition, modifier dans un large domaine ses propriétés mécaniques et pétro-physiques à cause des interactions minérales de la glaise liquide. L'ardoise peut être molle ou dure, extensible ou rigide, perméable ou imperméable et ce selon les conditions environnementales auxquelles elle est exposée. Elle peut être très sensible aux changements des conditions environnantes, comme par exemple l'humidité, la contrainte, la température et les gradients du potentiel chimique.

Une des réactions les plus apparentes de l'ardoise est le gonflement et le dégonflement comme résultat de sa saturation et des gradients du potentiel chimique dans le système liquide. Ces variations de volume modifient parfois d'autres propriétés. Selon la consistance et la concentration d'un liquide, l'ardoise peut soit gonfler soit se dégonfler en entrant en contact avec un liquide. Le matériau peut aussi se dissoudre dans le liquide et se désintégrer complètement.

Une description compréhensible des minéraux argileux du site de l'Est a été élaborée. Les micro-mécanismes physico-chimiques de l'interaction liquide-solide, comme l'adsorption, l'absorption, la capillarité et l'osmose y sont également présentés. Les conséquences possibles de ces mécanismes sur le comportement macro-mécanique, comme le gonflement et le dégonflement, fissuration et autres ont également été analysées.

La technologie des rayons X en microfocus a été introduite et utilisée pour analyser l'ardoise dans des conditions environnementales différentes. L'avantage de cette méthode est son caractère non-déstructif. Dû à la friabilité du matériau, la préparation des lames minces classiques est une méthode inappropriée pour analyser les micro-fissures et la désintégration de l'ardoise.

Les solutions ont été examinées pour observer la réaction en temps réel de l'ardoise dans le site de l'Est quand elle entre en contact avec différentes solutions aqueuses et sous charge uniaxial. La désintégration et la déformation ainsi que les propriétés générales de ce matériau ont été analysées en utilisant la technologie des rayons X µRG en immergeant le matériau dans une solution. On a pu constater que la désintégration, le développement des cracks et la déformation dépendent en partie de la concentration des ions ainsi que des types des ions de la solution.

Lors d'un test cinétique l'ardoise a été exposée à des degrés différents d'humidité relative et à des conditions de pressions uniaxiales. Une enceinte climatique électronique, contrôlée par une ordinateur a été utilisée pour créer des degrés d'humidité différents et on a transféré directement les résultats de la déformation axiale et des paramètres environnementaux. La relation entre l'humidité environnementale, la déformation axiale, la charge axiale et les micro fissures a été analysée. La technologie des rayons X en microfocus a été utilisée pour radiographier des spécimens avant et après les essais. Le matériau a été testé sous une humidité relative de 5% à 99%, pour évaluer l'influence de l'humidité sur le comportement des micro fissures et de la déformation.

Un test cyclique a été développé afin de définir le degré de friabilité dans un secteur entre 35% et 75% d'humidité relative.

Finalement, un test combiné a été réalisé afin de comparer la réaction dans l'eau pure d'un matériau saturé dans un environnement humide avec sa réaction dans l'eau en étant dans son état initial de saturation. Le matériau a été d'abord exposé à une humidité relative de 5% et 99% et ensuite immergé dans l'eau pure. Grâce à ce test on a découvert un phénomène d'hydratation qui pourrait être important pour les procédures des essais normalement appliquées.

1.   Introduction

This chapter examines a brief description about the importance of clay minerals and why they are of high interest for the nuclear waste management industry and others. The aim is to give general insights about the problems we face with argillaceous (clay rich) rocks as well as the positive aspects that make them attractive.
The goal of this thesis and the ideas and reflections leading to those aims will also be presented in this chapter.

1.a   Resumé de l'introduction

On prévoit le stockage de déchets caractérisés par une haute activité radioactive et par une vie longue en formations géologiques profondes. La formation de stockage devrait constituer une barrière pour séparer les déchets du reste de la biosphère afin d'empêcher sa contamination. Le risque le plus élevé de contamination provient de la migration des nucléides qui utilisent le système d'eau souterraine. Une des principales exigences auxquelles doit donc satisfaire le matériau est de retarder les effets des agents contaminateurs - et cela pour quelques milliers d'années.

Si l'on considère que les sédiments argileux peuvent avoir une très basse perméabilité (de 10^{-17} à 10^{-22} m²) et présentent ainsi une très forte capacité d'absorption des polluants, ils possèdent un certain potentiel de roche de stockage idéal. De plus, ces sédiments montrent parfois des structures géologiques très homogènes sans grandes perturbations, ce qui est également exigé.

Pour déterminer la capacité d'une formation argileuse à accueillir le stockage des déchets l'ANDRA a installé un laboratoire de recherche souterrain à une profondeur de 500 m. Ce laboratoire permettra l'application directe des expériences destinées à juger le comportement et l'évolution de la formation argileuse dans laquelle des cellules de dépôt devront être creusées.

Les matériaux argileux peuvent changer leurs propriétés mécaniques et pétro-physiques si les conditions environnementales comme la température, l'humidité, la contrainte, la composition ou la pression interstitielle varient. Le résultat obtenu est tel que les paramètres classiques pour décrire le comportement d'un matériau sont, dans la plupart des cas, insuffisants pour les matériaux argileux. A cause de la modification des paramètres tels que le module de Young, le coefficient de poison, la perméabilité ou la porosité ils ne sont pas considérés comme stables et doivent donc être traités comme des variables d'état. La constatation de la variabilité de ces paramètres est importante.

Les analyses du matériau commencent par le carottage, suivi par l'échantillonnage et enfin le stockage des spécimens pour une période déterminée sous des conditions déterminées. Parfois, ces dernières ne sont ni connus ni contrôlées. Mais les matériaux argileux peuvent réagir à ces conditions d'une manière très sensible. Pour cela les résultats obtenus pour l'ardoise doivent être pris en considération par rapport aux conditions appliquées lors des analyses, le stockage, le carottage et l'échantillonnage. Vu que ces conditions influencent considérablement les résultats.

Il existe de nombreux modèles pour décrire les matériaux argileux qui sont tous confrontés aux mêmes problèmes : comment intégrer les mécanismes de l'interaction solide-liquide qui changent fortement les propriétés du matériau ? et comment décrire la plasticité et la relation micro-macro ?

Jusqu'à présent, il n'existe aucun modèle basé sur une approche analytique qui considère l'interaction entre le solide et le liquide. Il y a, bien sûr, des approches pour simuler et prévoir le comportement mais les résultats demeurent empirique et ne concernent que des matériaux spécifiques. L'application d'un modèle approprié pour prévoir et décrire les propriétés argileuses demande aussi l'utilisation de résultats fiables. C'est pour cela que les matériaux argileux posent des problèmes d'un point de vue pratique. La variation des résultats obtenus pour le même matériau peut être trop grande pour permettre une interprétation appropriée du résultat.

1.1 The world of clay minerals

Numerous varying clay minerals exist in different combinations. We encounter them in many distinct situations in our daily lifes as they are an important component of the earths shallow crustal materials. Between 60% to 75% of the geological column comprises argillaceous rocks. Their importance is not only due to the quantity in which they appear, but also because of the enormous variety of their physical, mechanical and chemical properties. Their characteristics allow for the application of clayish materials in many different disciplines as for example the food industry, pharmaceutical industry, biology and many others. Of course we also deal with them in geology, mining, civil and petroleum engineering.

Clay minerals, so called fine grained Phylosilicates, have therefore been the issue of a wide variety of studies and scientific research programs, and they still are. Despite the enormous efforts of investigations and the vast amount of literature that appeared in the last decades, some important aspects concerning the comportment of this material under certain circumstances are not yet completely understood – for example when in contact with aqueous solutions.

This is why argillaceous materials occasionally still cause serious problems in civil and petroleum engineering such as landslides, subsidence of the surface or the loss of oil wells and tunnels. As much as they can be considered as tricky, they sometimes are the only material that meets the required properties, for example in the waste repository industry. In the case of waste disposal facilities we use the highly advantageous properties of clay minerals to retard and absorb certain contaminants and thus avoid the migration of pollutants beyond the barrier into the biosphere.

By the same token the annual extra costs in the petroleum industry due to problems with argillaceous formations are estimated to be in the magnitude of 500 million US$. Unfortunately about 75% of the world's drilled wells pass formations which contain clay minerals and thus may cause problems.

The main reason for the problems we face in the previously mentioned disciplines with some clayish materials is their aptitude to change their mechanical and petrophysical properties in a wide range due to fluid-clay mineral interactions. One and the same shale can be soft or hard, ductile or rigid, permeable or sealing – depending on the environmental conditions the sample is exposed to. This means argillaceous materials can be very sensitive to a change of conditions such as humidity, stress state, temperature, and chemical potential gradients.

One of the most obvious shale reactions is the swelling and shrinking as a function of it's saturation and the chemical potential gradient in the fluid system. Theses volume changes also sometimes alter other properties. Depending on the nature and the concentration of a liquid, a shale can either shrink or swell when in contact with a liquid. The material can also sometimes disperse in the liquid and thus becomes completely deteriorated.

However, the nuclear industry is interested in evaluating the potential of argillaceous formations as the host rock of an underground waste disposal facility as some argillaceous formations exhibit the previously mentioned retarding and absorbing properties for some contaminants.

1.2 ANDRA and nuclear waste

ANDRA (National Radioactive Waste Management Agency of France) is a public industrial organisation under control of the French government, who is responsible for the national nuclear waste management. The activities of ANDRA include all operative activities as well as research activities concerning the question of radioactive contaminated waste.

Nuclear waste is the end product of several different technical processes of the nuclear energy industry, the medical industry and others. The garbage is classified into different groups with

reference to the period of its radiation and the radiation intensity. Varying solutions are applied to store or transmute the contaminated materials according to the distinct risks of the groups.

The long lived high level waste is foreseen to be disposed in deep geological repository facilities. The material of the host rock should act as a barrier to separate the waste from the rest of the biosphere to avoid it's contamination. The highest risk of contamination is through the migration of nuclides within the groundwater system and one of the most important requirements for the material is therefore the retardation of the contaminants – for some thousand years.

Argillaceous sediments posses a certain potential of being an ideal host rock as they may have very low permeability (from 10^{-17} to 10^{-22} m²) and show a high sorption capacity for the pollutants. Furthermore they sometimes exhibit very homogeneous geological structures with very few disturbances which is also a demand.
Other materials like granite or dolomite are also being considered and research has also been undertaken to evaluate their potential of serving as a host rock.

In order to determine the ability of a an argillaceous formation to contain a waste disposal facility ANDRA, in 1999, installed the Meuse/Haute Marne underground research laboratory in a shale formation at a depth of about 500 m. (The site is located in the east between Chaumont and Toul) This laboratory allows the conduction of on site experiments to asses the behaviour and evolution of the shale formation in which disposal cells and galleries shall be excavated.
The research activities can be divided into four groups that are firmly interlinked to each other: geomechanics, hydrogeology, geology and geochemistry.

The geomechanical tests are undertaken to determine the mechanical behaviour of the host rock under the influence of the excavation activities and the waste material in order to assure the mechanical stability of the underground galleries.

Hydrogeological tests are supposed to resolve the question as to whether or not water-dissolved nuclear contaminants can migrate through the shale formation. The interest is thus focused on the mass transport mechanism like diffusion, advection and dispersion.

As the disposal of nuclear waste is a matter for some thousands of years it is imperative to understand the genesis of the formation to predict the possible future evolution of the site from a geological point of view. This concern is treated by the geology group in the laboratory.

The modification of the physico-chemical properties of the clayish material due to excavation works and the storage of the garbage is evaluated by geochemical studies in the underground site. Temperature changes (the waste has a temperature of about 130 °C) as well as alteration of the initial water content of the material are main issues of these tests.

Hence we deal with an enormous time scale in terms of a nuclear waste disposal repository, the biggest difficulty is obvious. Is it possible to accurately predict the behaviour of the whole system for a period of thousands of years? Can we possibly foresee all scenarios that could influence the performance of the disposal site for such a period of time?

What we can rather attempt do to is to draw different probable case scenarios, in order to highlight a range between the best and the worst possibilities.

But before reaching this goal, we have to find solutions to more recent problems such as the understanding of the mechanical behaviour of clayish materials, which will be discussed in the next chapter.

1.3   The problems we face with argillaceous materials

The aim of this chapter is not to present an exhaustive listing of all the problems we have with this material, but rather to give an overall idea about them for a better understanding.

It was previously mentioned that argillaceous materials can significantly alter their mechanical and petrophysical properties when the environmental conditions like temperature, humidity, stress state or the chemistry of the pore-liquid or the pore-liquid pressure are altered.

The consequence is that the classical parameters we use in rock mechanics, in order to describe the behaviour of a material, are in most cases not sufficient for argillaceous materials. As the parameters, such as elasticity modulus, poison ratio or permeability and porosity alter, they must not be considered as stable, but have to be treated like state variables.

The consideration of these parameters as state variables is of great importance from the authors point of view, because, as practice has shown several times in the past, any other approach to describe this sort of material is doomed to fail.

The question is how these parameters change if the environmental conditions alter. An example is given by the change of the strength of shale as a function of it's water saturation and the trial to establish a realistic hydro mechanical model. No model exists as yet, to predict this comportment, based on a sound analytical basis which takes the interaction between the solid and the fluid phase into consideration. Of course empirical approaches exist to simulate and predict the changes in strength, but the basis is of an empirical nature for one specific material and thus not applicable for other argillaceous materials.

Tests in a lab normally begin by sampling and storing the specimen for a certain period under certain conditions (they are sometimes not controlled or may even be unknown). In the case of argillaceous materials many problems are created by using incorrect sampling, preservation or conditioning technologies such as incorrect drilling mud or rehydration with reconditioned pore liquid and many others. These very commonly made mistakes may later create false test results because the sample no longer represents the initial state of the material and may have irreversible changed due to the reactivity of clay minerals. This means the chain of problems we face with argillaceous materials already starts with sampling and preservation.

The mechanisms responsible for the liquid solid interaction are not of a simple nature. They are of chemical, physico-chemical or physical nature, governed by the mineralogical and petrophysical properties of the solid part of the rock as well as the chemical and physical characteristics of the pore liquid. It can be rather difficult to understand all the different models, of all these disciplines, and to combine them in one model in order to predict the mechanical behaviour of such a material under the influence of changing environmental conditions.

The problem is also one of knowledge management. As the transfer of know how between the different disciplines has been poorly organized in the past, leading to errors and false assumptions that could have been avoided (sampling, storage, resaturation…).

In some cases it was found for example, that tap water was used for mechanical tests in order to analyse the mechanical behaviour of shale in different saturation states. In the case of shale, tap water must not be considered as water, as it contains many other different minerals and chemical species than just water. The point is the high sensitivity of this material, which is in complete contrast to classical rocks like granite or sandstone. The consequence is, that due to this hyper sensitivity the same tests with the same material conducted by different labs often lead to different results. This aspect will be presented in chapter 1.4.2 concerning the reliability of obtained mechanical data.

Another problem due to the physico chemical interaction of shale - and thus stress, strain and porosity alteration - is the transport (mainly advection and Fick diffusion) and pressure propagation of liquid through shale as the permeability is very stress state sensitive. Darcy's law is only valid for a laminar and steady state one-phase flow through a porous medium (moreover the fluid has to be largely incompressible [45]). It is not sufficient to describe the magnitude or direction of liquid movement in argillaceous rocks. Several attempts have been made to extend the validity of Darcy's law for shale by adding some terms contributing to the physico-chemical interaction between the fluid and the rock [94,60].

The creeping behaviour of argillaceous materials – it can be stable for a certain period of time under constant conditions and start, all of a sudden, a creeping stabilizing cycle, which means the material creeps and stabilizes afterwards - is not yet understood and we are far away from having a recognized theory about that phenomenon.

Other problems exist such as the problem of measuring the pore pressure and the permeability, how to evaluate the Biot factor, the drained-undrained controversy, the specimen scale problem and many others.

By now the reader should have a better idea regarding the problems faced, and thus we will not go into any further detail.

The next point of interest is how these problems are handled in mechanical models. In the following chapter we therefore present a short introduction of the classical Terzaghi and Biot model to give an idea about the attempts made to model clayish materials including the solid-liquid interaction.

1.3.1 A short introduction into the stress strain model

This simplified short examination of a possible stress strain model is presented in the chapter of introduction as it strongly influenced the set up and definition of the goals of this thesis. It allows a general insight of the main problem in finding a realistic approach to model argillaceous materials.

Terzaghi developed the fundamental effective stress theory for granular soils:

$$s = s' + p_{pore} \qquad\qquad 1$$

s   total normal stress [Pa]
s'   effective normal stress [Pa]
p_{pore} pore pressure [Pa]

The statement of this theory is that an increase of the external isotropic pressure produces the same volume change of the material as a reduction of the pore pressure (by the same amount). The effective stress rather than the total stress determines the deformation and thus whether or not the rock fails due to external load, as the shear strength depends on the difference between the normal stress and the pore pressure.

Biot applied Terzaghi's relation for saturated soil by introducing the Biot coefficient which is a material constant. It takes into account grain contact areas over which the pore pressures do not act. Initially it was developed for large grains in combination with a small porosity.

$$s = s' + a \; p_{pore} \qquad\qquad 2$$

a   Biot coefficient [ ]

If a=0 there is no interconnected porosity and thus no communicating pore liquid. The material doesn't exhibit hydro-mechanical coupling and is normally less deformable. On the other hand a=1 corresponds to the Terzaghi relation and the coupling is maximal. For shale a is seldom found to be less than 0.95 [21,29]

Although the effective stress principal remains valid for argillaceous rocks, the relation of Terzaghi and the Biot factor are not really applicable for these materials, as they don't take into account the physico-chemical pore-liquid rock interaction and thus phenomena like shrinkage or swelling.

_____

Seedsman developed a possible model, including the forces of repulsion (osmosis, double layer theory) and attraction (electrical and Van der Waals) [37] due to shale liquid interaction:

$$s = s\prime + p_{pore} + R - A \qquad\qquad 3$$

R   stress due to repulsion between particle [Pa]
A   stress due to attraction between particle [Pa]

Unfortunately it is not yet possible to determine exactly the attractive and repulsive parameter by calculation nor measurements for different shale and fluid conditions. But high accuracy would be necessary concerning the enormous number of clay particles in argillaceous structures, as the cumulative error would otherwise lead to useless results.

Wong [98] used the series-configuration model of Hueckel (cf figure 1) to decompose the total strain into two separate strain components, based on the theory that the total strain could be the result of:

I.: A volume change in connected (intramatrix) pores due to change in pore pressure or skeleton contact stress.

II.: Volume increase between the clay platelets (interlamellar) due to changes in the electrochemical properties of the clay particle surface - or decrease due to increase in contact stress transmitted to clay platelets.

III.: Volume change in interlamellar pores due to osmosis. Thus, the strains can be induced by changes in mechanical load in intramatrix pores, repulsive-attractive forces in interlamellar pores, and osmotic pressure
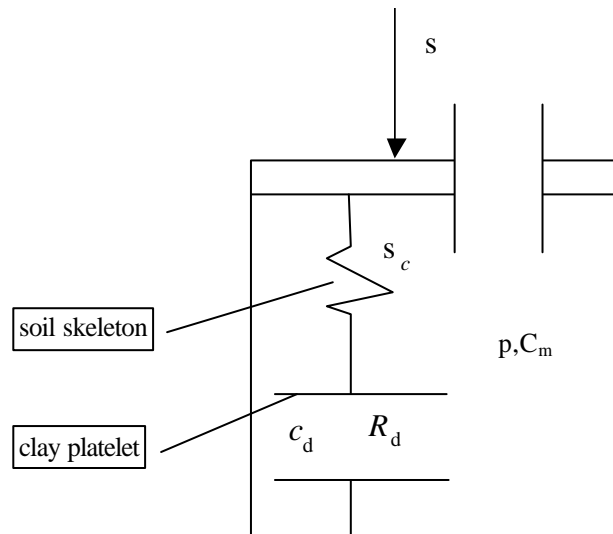

Figure 1: series model of Hueckel, decomposing
the total strain into separate strain components

s   total stress
s_c average mineral contact stress
c_d concentration within the clay platelet (interlamellar)
c_m concentration of bulk water (intramatrix)
R_d repulsive attractive force within the platelet
p   bulk water pressure

_____

$$e_v = e_{sk} + e_d \qquad\qquad 4$$

e_v total strain
e_{sk} skeleton strain
e_d intramatrix strain

$$e_{sk} = m_v \, \Delta s \text{,} \qquad\qquad 5$$

m_v compressibility coefficient of intramatrix pores

$$\Delta s = \Delta s \text{,} + \Delta p \quad \wedge \quad \Delta s \text{,} = \Delta s_c = \Delta R \qquad\qquad 6$$

R   average repulsive attractive force

$$\Delta R = b \; \Delta R_d \qquad\qquad 7$$

ß   volume coefficient (ratio of interlamellar to total bulk volume)

$$e_d = m_d \, (\Delta R + \Delta \Pi) \qquad\qquad 8$$

?   osmotic pressure

One of the main assumptions in this model is that the mineral contact stress is equal to the effective stress and to the average repulsive-attractive stress.

For undrained conditions in this model there would not be any volume change due to an increase of total stress, only the intramatrix pore pressure would increase. (The effective stress is equal to the difference between total stress and pore pressure, or contact stress)

For the drained model the pore pressure would remain constant and the change in total stress causes an equal change in contact stress and in the repulsive/attractive stress. The deformation is the sum of skeleton and platelets which is equal to the net change in bulk bore fluid volume. A change in the environmental load also causes an inward or outward flow of ions according to the chemical gradient. This could result in the development of an osmotic pressure difference.

This linearized model has been incorporated into mass balance equations for fluid and solute, to form a frame work to analyse problems involving the swelling process in shale. It considers the whole system as reversible as it doesn't distinguish between elastic and irreversible inelastic strains. Furthermore it doesn't contribute to the often observed irreversible stress strain relationship and the well known plastical behaviour of clayish materials.

There exist, of course, many other models to describe clayish materials, but they have all one common problem: how to integrate the clay-liquid interaction mechanism that obviously causes serious stress strain changes and how to account for the irreversible transition from elasticity to plasticity.

The use of an appropriate model also requires the use of reliable data, and this is where argillaceous materials cause problems from a practical point of view (as will be shown in the next chapter).

_____

1.3.2   The reliability of obtained mechanical data

Between 1995 and 2000 many tests were conducted in order to evaluate the mechanical properties of the clayish material of the Meuse-Haute Marne underground research laboratory of ANDRA [4]. Among theses investigations, more than 300 uniaxial and triaxial tests were done by four different institutions. These were the G3S, ANTEA, ENSG and LML.

Miehe B. [57] analysed all the results obtained from the tests with reference to their variation. The Elasticity module, the Poisson ratio and the failure stresses were determined in correspondence to an elastic-plastic model taking post rupture softening into account. The data variation was characterized as a function of the depth, the radial confining stress and the different laboratories.

Figure 2 and 3 illustrate the variation of the different Elasticity modules for several depths obtained from the different labs by running uniaxial and triaxial tests. The spread for both charts is in the range of about 400% between the minimum and the maximum value obtained for most depths! The plots don't allow a reliable interpretation about a relation between the depth and the Elasticity module, as the variation is too strong.
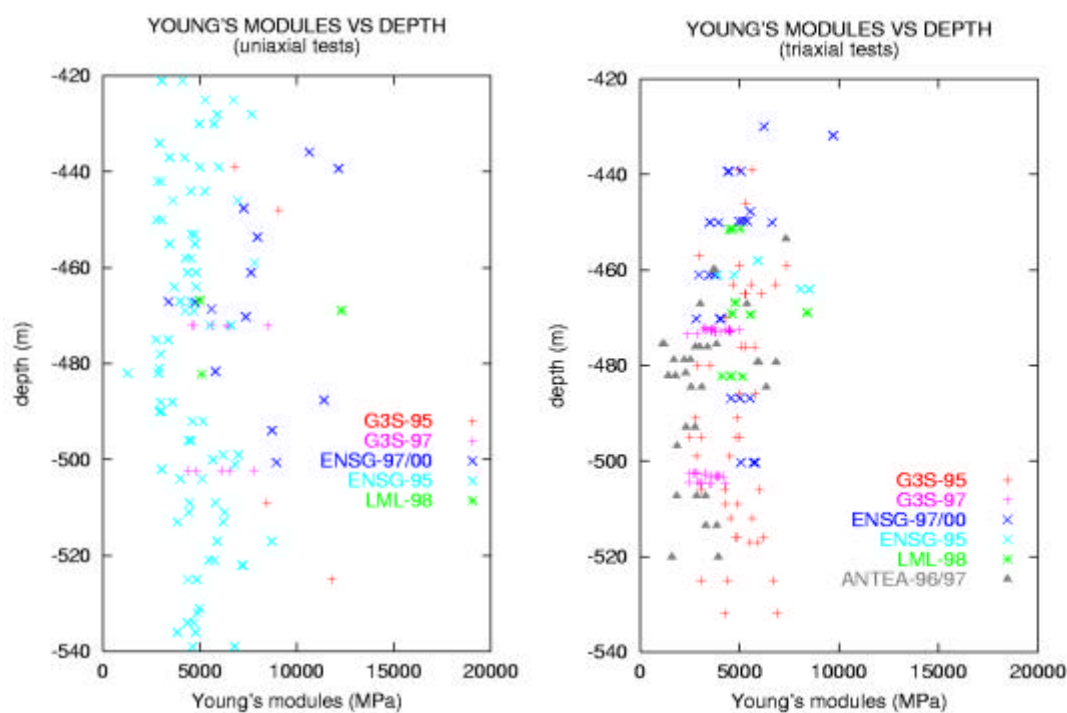

Figure 2 and figure 3: The Elasticity modules over the depth of the shale from the site of Est obtained by different laboratories running uniaxial and triaxial tests. Remarkable is the strong variation between values for the same specific depth. [Miehe 2002]

Besides this rather natural variation of the depth values, Miehe found a strong variation of the breaking stress results between the different labs. He concluded that this dispersion might be due to differing preservation and testing procedures in the labs that fostered physico-chemical solid liqid reactions (cf figure 4).

The breaking stresses obtained by ANTEA for example were much lower than the results of the other laboratories. ANTEA resaturated the samples by using water, which influences the material enormously as will be shown later on in this thesis. As did G3S before running some creeping tests.

_____

_____

The other labs used untreated initial samples without resaturation.

Contrary to this, the results of LML show, in general, higher values than those of the other institutions. A possible explanation is the usage of slower load rates, relaxation-load cycles and the drained conditions of the test, which may have led to a higher mechanical resistance. All values allow more or less the interpretation of an average Mohr Coulomb criteria as shown in the graph.
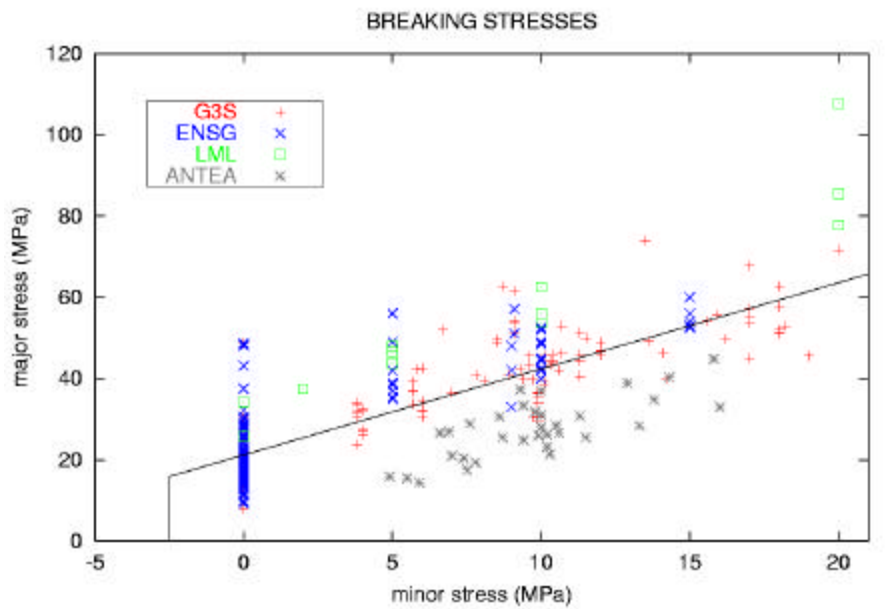

Figure 4: breaking stress over the minimum stress of shale from the site of Est obtained by triaxial tests. The spread pf the values is due to different testing procedures and sample preparation methods. [Miehe 2002]

The interpretation of the ANTEA values led Miehe to the conclusion that other phenomena besides the classical hydro-mechanical coupling effect influence the behaviour of the material. The rehydration of the material obviously strongly effected the initial material properties and degraded its mechanical strength.

Finally we can conclude that the test results obtained for shale always have to be considered with reference to the applied testing conditions, the storage, preservation and sampling technology, as they influence the results quite remarkably. But what are the most representative conditions to simulate the on site conditions?

_____

1.4   The goal of the thesis

Throughout the first months of the literature review one thing was striking: The physico-chemical interaction is not taken into consideration in so many cases, even though it seems to play a momentous role. The reasons may be simply ignorance or an underestimation of it's importance.
It appeared to be imperative to understand the mechanisms of this interaction in order to understand clayish materials and the first goal was thus defined.

> An understandable description of the clay-minerals from the site of Est and their physico-chemical interactions with aqueous solutions, including the possible consequences of these mechanisms.

One of the most noticeable consequences of these reactions is the swelling and shrinking of the material. The result can be either high swelling stresses - in the case of a constant sample volume - or remarkable volume changes - if the sample volume is variable. It is easy to imagine that these volume-stress alterations could influence the properties of the material. But could it be possible that they lead to a micro cracking of the shale?
In general there is no doubt about the importance of cracks with regard to the strength and permeability of the material. They could also have a noticeable effect on the irreversible phenomena such as creep or plasticity. It's also a fact that micro cracks are very often the origin of macro cracks, as they propagate. But nevertheless nothing essential was found in literature to answer the question of micro cracking in argillaceous materials. As there is a limited amount of reference material, the issue became a goal.

> To find the technology that enables the non destructive detection of micro-cracks in the argillaceous material from the site of Est of ANDRA.

In the case that we could find some micro cracks, the logical consequence was to find out more about the conditions and parameters that govern the micro-crack induction and propagation in the material, from a qualitative point of view.
We therefore have to have a look at the conditions the material is exposed to in an underground laboratory. The underground excavation works create an excavation damage zone (EDZ) around the construction facility. In the EDZ the material is somehow disturbed due to different stress states, desaturation and contact with new chemical species in aqueous solutions. The points of interest were clear and determined the further goals.

> To qualitatively analyse the influence of saturation changes of the shale on the micro fissures and strain, and if the kinetic of dehydration/hydration is of relevance

The term kinetic is used with reference to the saturation gradient over time – the hydration or dehydration speed. To put a saturated sample in a very dry environment creates a strong suction effect and causes a fast dehydration and thus a high saturation/time gradient.
It was found that the chemical composition of the water within the same gallery varies significantly in the ANDRA laboratory. Water based solutions could change their migration path within the EDZ and encounter shale which was initially in contact with another solution. The reactions it could provoke are of interest and therefore the next point.

> To qualitatively analyse the influence of different water based salt solutions on the micro cracking and strain of the material

Once the nuclear waste is stored, the galleries are refilled with a special Bentonite mixture, and the partially desaturated EDZ will be resaturated after a certain time. It is very alike that the shale may pass the limit of the air entry point during dehydration. After the refilling the air would remain in the porous material. The entrapped air bubbles could theoretically be responsible for micro cracking due to capillary pressurisation when resaturation occurs. The goal is therefore:

> To determine whether entrapped air in the material influences the cracking comportment

As all these experiments would be in combination with the swelling and the shrinking of the material, we wanted the strain changes to be documented during the tests.

Classical swelling tests normally evaluate the swelling stress. In these tests the sample is either restricted to a constant volume, or has a variable volume. But in both cases the method is not very representative for on site conditions in a gallery. To conduct a swelling test in which the sample is under a certain constant load seems to be more appropriate. The sample holder should also allow real time crack detection under load and the influence of different water solutions. The requirement was thus:

> To design a sample holder that allows for the application of different constant loads and the documentation of the strain development during the test. In addition to this, the real time crack detection has to be possible when the sample is in contact with aqueous solutions

As the humidity and temperature conditions in the underground repository may change, the previously mentioned test to evaluate the influence of the saturation change on the micro cracks is of very high interest. The facility must thus enable swelling tests under load in controlled environmental conditions to create a certain suction. The only problem is that a sample holder that loads the sample and a strain gauge would be too big for classical desiccator tests. Furthermore it's not very practical to change the salt solution in the desiccator each time there is a humidity change required. The sample would be exposed to uncontrolled conditions during each change. The aim was therefore:

> To install a precise air conditioning system, allowing for the greatest possible range of controlled temperature and humidity, as well as the application of the sample holder under load with real time data monitoring.

All theses goals are more qualitative than quantitative. The overall goal is to deliver a sound basis in order to understand clay minerals and their physico-chemical interactions with water based solutions. The insights gained from this work shall contribute to a better modelling of clayish materials as well as to provide a sound lasting basis for further research regarding argillaceous materials at the CGES. Lasting also with reference to new laboratory equipment that enables the future conduction of new tests.

2.   Theoretical background of shale liquid systems

An understandable description of the clay-minerals from the site of Est and their physico-chemical interactions with aqueous solutions shall be given in this chapter. The discussion also includes the possible consequences of these mechanisms on the mechanical behaviour such as swelling and shrinking, crack induction and others.

2.a   Résumé sur l'interaction solide-liquide des roches argileuses

Les minéraux argileux possèdent une structure interfoliaire d'atomes cristallines. Ils sont caractérisés par le type de couches, la composition de feuillets qui constituent la structure des couches, la charge électrique des couches, leur force de liaison et par la composition des inter-feuillets. Quelques minéraux montrent une très haute affinité pour les liquides polaires et réagissent à ces liquides.

Les deux structures élémentaires les plus importantes, qui composent la forme des couches des minéraux argileux, sont les unités tétraédriques de silicium et les unités octaédriques d'aluminium ou de magnésium. Les minéraux argileux consistent de piles de feuillets basés sur la combinaison de couches tétraédriques et octaédriques en forme 1 :1, 2 :1 et 2 :1 :1.

Le manque d'équilibre de la charge de la surface minérale est en partie neutralisé par des soi-disant cations compensateurs. On différencie entre les cations compensateurs absorbés et les ions compensateurs adsorbés qui peuvent être échangés par d'autres ions (ions compensateurs échangeables). Cette capacité d'échange cationique (CEC) représente la réactivité globale.

Les molécules d'eau peuvent être liées de manière distinctes aux différentes couches des minéraux argileux et aux différents types d'eau : l'eau libre, l'eau adsorbée, l'eau absorbée et l'eau cristalline. La teneur en minéraux argileux dans l'ardoise du site de l'Est varie entre 30% et 60% et se constitue surtout des types inter-stratifiés (Illite-Smectite) et d'une petite part de Kaolinite. La teneur en Smectite domine la fraction de l'ardoise et le matériau possède des propriétés typiques de la Smectite. Le matériau montre aussi des propriétés de gonflement et dégonflement.

La Kaolinit faite partie du groupe des serpentines (structure 1:1) et ne montre pas de gonflement interfoliaire . L'Illite (structure 2 :1) montre un gonflement interfoliaire très faible. Dans le groupe des Smectites (structure 2 :1) le gonflement interfoliaire peut atteindre des valeurs très élevées. Les minéraux inter-stratifiés du type Illite-Smectite montrent des propriétés similaires au groupe des Smectites et sont caractérisés par un gonflement interfoliaire moyen voire élevé.

A cause du caractère dipolaire de l'eau et des solutions aqueuses les particules argileuses sèches adsorbent les différents feuillets d'eau mono-moléculaire à la surface des cristaux (le principe des 2 couches). L'eau adsorbée provoque le gonflement interfoliaire pour tous les types de minéraux, avec des degrés de gonflement inférieurs à ceux de l'absorption. L'absorption est l'intégration des masses d'eau dans la couche interfoliaire et/ou l'hydratation des cations interfoliaires et/ou leur échange par d'autres espèces (non-)hydratés (groupe des Smectites). L'absorption peut mener à un gonflement très élevé et à une perte totale des forces de liaison entre les couches minérales ce qui conduit à une détérioration totale du matériau.

La capillarité s'exprime en fonction des forces adhésives, cohésives et superficielles du système à 3 phases : le solide, le gaz et le liquide. La capillaire dans l'ardoise peut être couverte d'un film d'eau adsorbée. Dans ce cas, il y a présence de forces cohésives entre l'eau adsorbée et le liquide libre des pores au lieu des forces adhésives. Ces forces contrôlent le mécanisme et ainsi la pression capillaire. Le gaz piégé à l'intérieur de l'ardoise peut être soumis à une augmentation de la pression générée par la capillarité. Cette pression pourrait dépasser la résistance au cisaillement du matériau œ qui peut provoquer la détérioration du matériau.

L'osmose peut causer de hautes pressions anormales du liquide interstitiel qui sont plus hautes que la pression extérieure (advective) . L'ardoise peut réagir comme une membrane semi-perméable et peut montrer un gradient de potentiel chimique ce qui conduire à l'insertion de l'eau dans le matériau physiquement saturé.

2.1 Introduction of clay minerals and the structure of shale

From the geological perspective, argillaceous rocks encompass a wide range of litho-types ranging from unlithified muds and clays, through moderately indurated mudstones and claystones to fissile and often highly indurated shale. Metamorphosed rocks such as argillite and slates also belong to the family of argillaceous rocks. Across this large spectrum, the properties and characteristics of the material can vary enormously [103, 59, 49].

The term clay and shale are often used in a fairly non-specific way in the geomechanical and radioactive waste disposal literature. Table 1 represents a useful classification scheme of the correct terms according to Potter et al. [71] The correct term for the material from the site of Est is rather mudshale with reference to this classification. Nevertheless we retain using the terms shale and clay in this thesis, as it facilitates the understanding.

		amount of clay particles in vol [%]		
		0-32	33-65	66-100
non-indurated	beds	bedded silt	bedded mud	bedded clay
	laminae	laminated silt	laminated mud	laminated clay
indurated	beds	siltstone	mudstone	claystone
	laminae	siltshale	mudshale	clayshale
metamorphosed	low	quartz argilite	argilite	argilite
	medium	quartz shale	slate	slate
	high	phyllite and / or mica schist		

Table 1: classification scheme according to Potter et al. for argillaceous rocks

Clays are commonly defined as consisting of grains less than 2µm in diameter and their crystallographic habit is sheet-like (Phylosilicat). Clay materials have a very high specific surface area relative to the mass of material in the clay mineral crystal grains and a residual imbalanced electrical surface charge. The combination of these factors is the reason why clay particles absorb and/or adsorb polar molecules like water and therefore have a high affinity for polar liquids.

The key properties for a better understanding of clay materials are thus the electronegative charge of the clay minerals (crystal surface), their size and their structural arrangement. A discussion of the structure of shale and clay minerals at atomic level is therefore very useful in order to understand their reactivity. This is why a brief examination about this issue is presented throughout the following paragraphs.

2.1.1   The micro structure of shale

According to Collins and Stepkowska [90] we can describe the microstructure of shale using three basic micro fabric features (cf figure 5). These are the clay particles, the elementary particle clusters and the pore spaces.

The clay particles consist of a various number of layers of clay minerals, whereas the elementary particle clusters are formed by several of these clay particles in a parallel configuration. The assembly of elementary particle clusters are formed by arrays, which represent the solid matrix of the rock. The pores between the elementary particle clusters are the so-called intramatrix pores and the space between the particles is defined as interlamellar porosity.
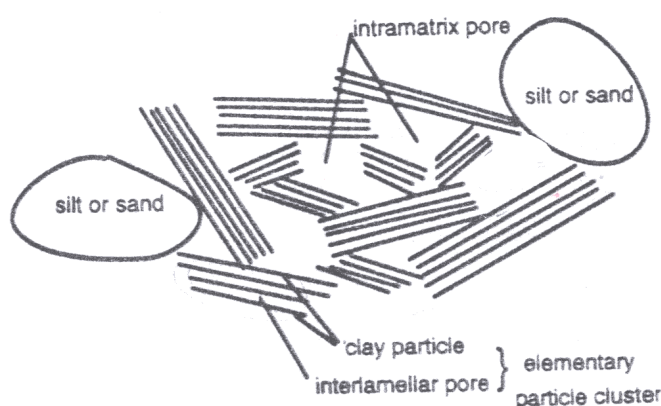

Figure 5: Scheme of the microstructure of shale using three basic micro fabric features: the clay particles, the elementary particle clusters and the pore spaces (Collins and Stepkowska 1990).

Griffiths and Joshi [28] use the same model for the micro-structure of the particles (referred to as crystallite) and the elementary particle clusters (referred to as particles) but distinguish between the types of pores (cf figure 6):

The interlamellar pores between the particles (intra-particle), the intramatrix pores between the elementary particle clusters (inter particle), the pores within the assemblage of several particle clusters (intra-assemblage) and the pores between these assemblages consisting of particle clusters (inter-assemblage).

Furthermore we have to distinguish between the geometrical and the effective porosity of argillaceous rocks. The geometrical porosity is not equal to the effective porosity as clay minerals may have a strong affinity for water. This interaction of the clay minerals with polar liquids exists due to their electronegative nature and is a function of the types of clay minerals. It may lead to the attraction of several monomolecular layers of water around the particles, which may in turn reduce the geometrical porosity (see chapter 2.3).

This interaction may also influence the rheological behaviour of a migrating fluid in the rock as will be described in the following chapters. This can for example lead to a non-Newtonian comportment of water and is one of the reasons why the law of Darcy becomes inappropriate for shale. In addition the shale may exhibit inter-crystalline and/or inter particular swelling that also changes the structural geometry.
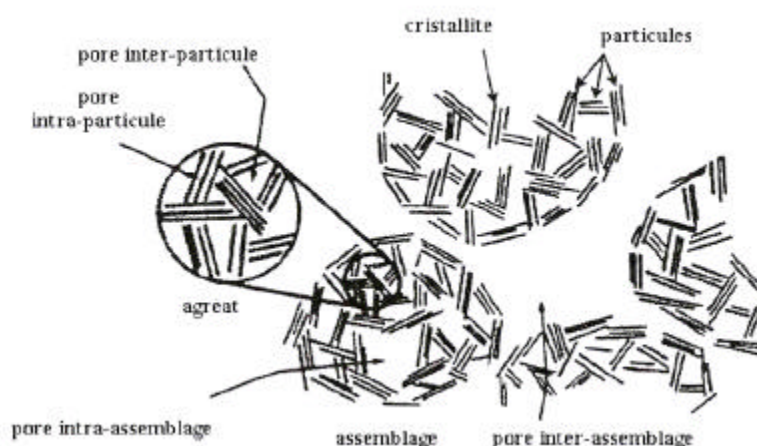
_____

Figure 6: Scheme of the micro-structure of clay: the particles (crystallite), the elementary particle clusters (particules) and pores as following: interlamellar (intra-particule), intramatrix (inter particule), intra-assemblage and inter-assemblage. (ENSMP 2000)

This is what was meant by the statement in the introductory chapter, that petrophysical parameters of clays like porosity or permeability are not constant as for classical sedimentary rocks but state variables depending on the solid liquid interaction of the clay minerals. These special variable properties of clay minerals are some of the reasons contributing to the problems we face in finding reliable models and testing procedures to describe and predict their behaviour when in contact with a fluid.

A better understanding of the physico-chemical interaction between the clay particles and the pore fluids therefore requires a detailed discussion of the structure and the arrangement of the clay particles at atomic level.

2.1.2   The classification of clay minerals

This chapter is confined to an introduction of the structure and the properties of the most important clay minerals found in the shale of 'Est d'Andra'. These are the minerals of the Smectite group (2:1 type), Kaolinit (1:1 type) and Illit (2:1 type).

Clay minerals are Phylosilicates (sheet silicates) with a crystalline atomic sheet-stacking structure and belong to the large group of silica minerals. They are also referred to as aluminum silicates as their basic composition is hydrous aluminum silicate.

A large number of different clay minerals exists and their classification in literature is not uniform. A general scheme of the nomenclature is given in figure 7. As the swelling property is one of the most evident problems of clay minerals in material-mechanics we use a simplified but sufficient classification into swelling and non-swelling types (cf figure 8).

They are characterized by the type of layer structure, the composition of the sheets that make up their layer structure, the layer charge, their bonding forces and the composition of the interlayer material. The two most important elementary structures that form the sheets of the clay minerals are the silicon tetrahedron and the aluminium or magnesium octahedron and are presented in the next chapter [27, 95].

_____

Layer type	Interlayer	Group	Subgroup
1:1	None or H_2O only	Serpentine + kaolinite $(x \pm 0)$	Serpentines, kaolins
2:1	None	Talc + pyrophyllite $(x \pm 0)$	Talcs, pyrophyllites
	Hydrated exchangeable cations	Smectite $(x \pm 0.2-0.6)$	Saponites, montmorillonites
	Hydrated exchangeable cations	Vermiculite $(x \pm 0.6-0.9)$	Trioctahedral vermiculites, dioctahedral vermiculites
	Nonhydrated cations	True mica $(x \pm 0.5-1)$	Trioctahedral true micas, dioctahedral true micas
	Nonhydrated cations	Brittle mica $(x \pm 2.0)$	Trioctahedral brittle micas dioctahedral brittle micas
	Hydroxide sheet	Chlorite $(x$ variable$)$	Trioctahedral chlorites dioctahedral chlorites

x = Charge per formula unit.

Figure 7: general scheme of the clay nomenclature [Clauer 1995]

	Dominant elements	Basal spacing (Å) Glycol	Dry
SWELLING TYPES			
Smectites			
Beidellite	Al	17	10
Montmorillonite	Al (Mg, Fe^{2+} minor)	17	10
Nontronite	Fe^{3+}	17	10
Saponite	Mg, Al	17	10
Vermiculite	Mg, Fe^{2+}, Al (Fe^{3+} minor)	15.5	10-12
Mixed layer minerals*		10-17	<10
NON-SWELLING TYPES			
Illite	K, Al (Fe, Mg minor)	10	
Glauconite	K, Fe^{2+}, Fe^{3+}	10	
Celadonite	K, Fe^{2+}, Mg, Fe^{3+}, Al^{3+}	10	
Chlorite	Mg, Fe, Al	14	
Berthiérine	Fe^{2+}, Al^{3+} (minor Mg)	7	
Kaolinite	Al	7	
Halloysite	Al	10.2	
Sepiolite	Mg, Al	12.4	
Palygorskite	Mg, Al	10.5	
Talc	Mg, Fe^{2+}	9.6	

* Two or more types of basic layer interstratified in the same crystal

Figure 8: simplified but sufficient classification into swelling and non-swelling types [Velde 1992].

_____

2.1.3 Silicon tetrahedron sheet

The silicon tetrahedron, illustrated in figure 9 comprises of four O-2 anions surrounding a central Si 4+ cation, which fits snugly into the center.
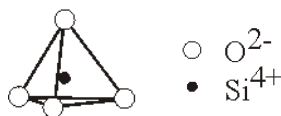

Figure 9: the silicon tetrahedron, an elementary structure of the layer clay minerals

These tetrahedrons are linked together by highly covalent bonding through the sharing of the basal O-2 (cf figure 10). The linked tetrahedrons form a two dimensional array of atoms, which is the basis of the sheet structure.
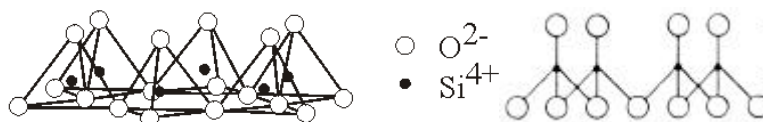

Figure 10: linked silicon tetrahedrons forming a two dimensional array and thus a layer

The arrangement of the interlinked basal oxygen occurs in such a way as to leave a hexagonal shaped "hole" in the network of oxygen atoms (cf figure 11) in the plan view.
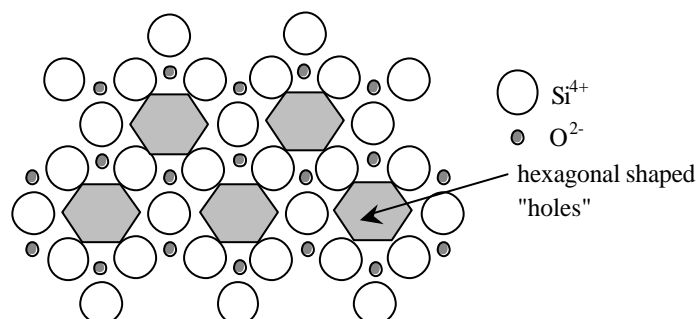

Figure 11: shows an orthogonal plan view of a theoretically ideal Si layer. The stripe pattern symbolizes the hexagonal shaped "holes" due to the arrangement of the interlinked basal oxygen atoms.

On the opposite end of the linked tetrahedron we find the apical oxygens (on the top), which are pointing away from the interlinked tetrahedral basis. Basel oxygens are only linked to shared tetrahedrons while apical oxygens are shared with other cations to form another polyhedron and thus can be firmly linked with another layer of cations.

Cations found in the tetrahedrally coordinated sheet are principally Si. Some substitution of Al^{3+}, Fe^{2+} or Cr^{+} is common, and occasionally Fe^{3+} is present. All of the anions in the two fundamental planes are oxygen atoms. [28, 27, 95, 59, 49]

_____

2.1.4   Aluminium octahedron sheet

The octahedron illustrated in figure 12 consists of six hydroxyls (OH-) surrounding one Al^{3+} or Mg^{2+} both of which are frequently present in clay minerals. Instead of the six hydroxyls the cations can also be coordinated with six oxygens.
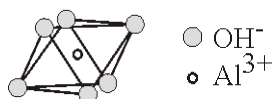

Figure 12: the aluminum octahedron tetrahedron, an elementary structure of clay minerals

As in the case of tetrahedrons the octahedrally coordinated cations are interlinked by shared anions (cf figure 13) in a two dimensional sheet sheet structure that forms hexagonal "holes".
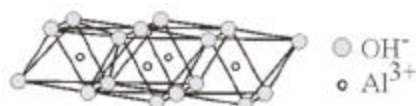

Figure 13: linked aluminum octahedrons forming a sheet structure

Ideally, with OH anions coordinating the octahedral cation, the sheet forms either a tri-octahedral structure, in which all cation positions are filled, or when only two thirds of the cation positions are filled, a so-called di-octahedral structure (cf figure 14). That means some of the cation positions remain unoccupied in a di-octahedral structure.

Figure 14: tri-octahedral (all cation positions filled) and di-octahedral structure (2/3 of the positions filled)

Due to substitutions cations other than the principle species Al and Mg can be found. These cations found in the octahedrally coordinated layer are more varied in species than in the tetrahedral ones. Fe^{2+}, Fe^{3+}, Ti^+, Ni^+, Zn^+, and Mn^+ can be present. [28, 27, 95, 59, 49]

2.1.5   Layer types and sheet combinations

As already mentioned clay minerals are sheet silicates and their chemical and mechanical properties are also determined by the type of layer structure and the composition of the sheets that make up their layer structure.
The clay mineral structures consist of stacks of octahedral and tetrahedral sheets and are based on the combination of tetrahedral and octahedral sheets in the form of 1:1, 2:1 and 2:1:1 types.

In the 1:1 types (cf figure 15) consisting of one tetrahedral and one octahedral sheet. The plane of apical oxygens of the tetrahedral sheet is superimposed on the OH plane of the octahedral sheet. The stacking is provided by hydrogen bonds between two 1:1 layers. Kaolinit and Illite exhibit a 1:1 structure.
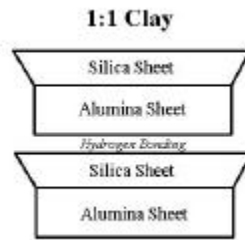
_____

Figure 15: the 1:1 type of clay (stacking of octahedral and tetrahedral sheets)

The 2:1 type is the stacking of a octahedral sheet sandwiched between two tetrahedral sheets (cf figure 16). The planes of apical oxygens of the tetrahedral sheets face toward each other. The common planes between the two tetrahedral sheets and the octahedral sheet consist of shared oxygens and unshared OH's. Each unshared OH is at the centre of tetrahedral hexagonal 2D rings. The smectite group represents this 2:1 structure.
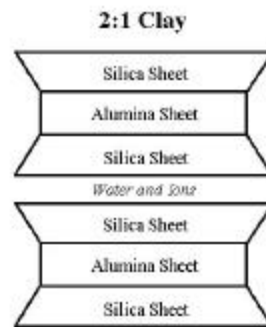

Figure 16: the 2:1 type clay (stacking of a octahedral sheet sandwiched between two tetrahedral sheets)

The 2:1:1 structure consists of a 2:1 layer arranged with an additional octahedral sheet between the 2:1 layers.

All these structures allow a good cleavability in the sheet plane and explain why the clay particles morphology often exhibit a needle or lamina shape. Furthermore this structure explains the high anisotropy of argillaceous materials as well as the crack induction between the sheets.[104, 27, 95]

2.1.6 Compensator cations and the net negative charge

The preliminary described cation substitutions in both sheet structures by cations that carry a lower negative charge create a charge imbalance in the layer and give the clay mineral its electronegative character (cf figure 17).

On top of this, structural errors in the planes such as dislocation densities, the geometrical limitation of the sheets, and the possibility of vacant central cation positions increase this electronegative charge. Due to the limited geometrical size and therefore open bonds of the crystal sheets the particle carries a positive charge at the edge.

The charge imbalance is partially neutralized by inserting cations into the holes in the basel hexagonal 2D oxygen array. These so called interlayer compensator ions also enable the bond of two tetrahedrical sheets which are held firmly together by sharing these cations.

As an ideal hexagonal array of oxygens rarely exists and the holes are not always occupied, a net negative charge always remains, which has a very dominant influence on the reactivity of the material. This negative charge can reach values up to 2 coulomb per unit cell.

We distinguish between absorbed interlayer compensator cations as described and adsorbed surface compensator ions linked to the surface (cf figure 18). Both types may be exchanged by other ions and are therefore referred to as exchangeable compensator ions.
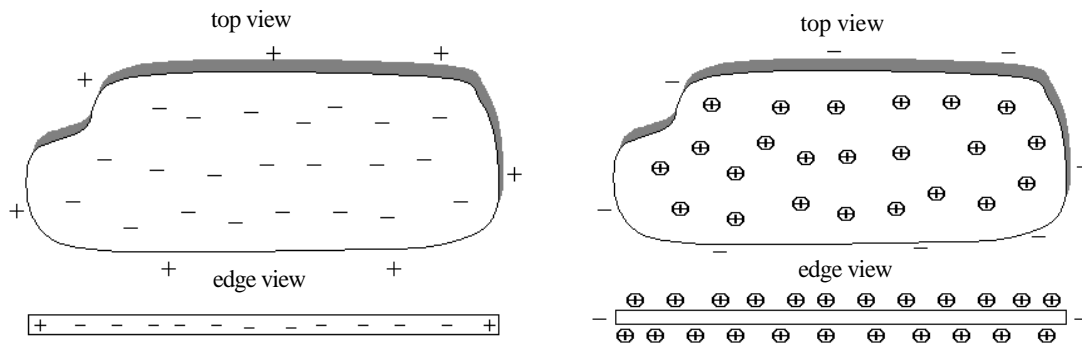
Figure 17: charge imbalance of a classical 2:1 type clay particle without and with compensator cations

Potassium compensator ions are usually not exchangeable because of their high bonding forces with the clay crystals and play a major rule in the understanding of clay behaviour. Most of the exchangeable ions are Ca^{2+}, Na^+ or Mg^{2+}. The capacity to exchange these cations (CEC) is a fundamental property of clays in characterizing their reactivity (cf chapter 2.1.7).

The hydration and/or exchange of these cations is the main mechanism responsible for the swelling or shrinking of some clay minerals when they are hydrated (cf chapter 2.3.2 and 2.3.3).
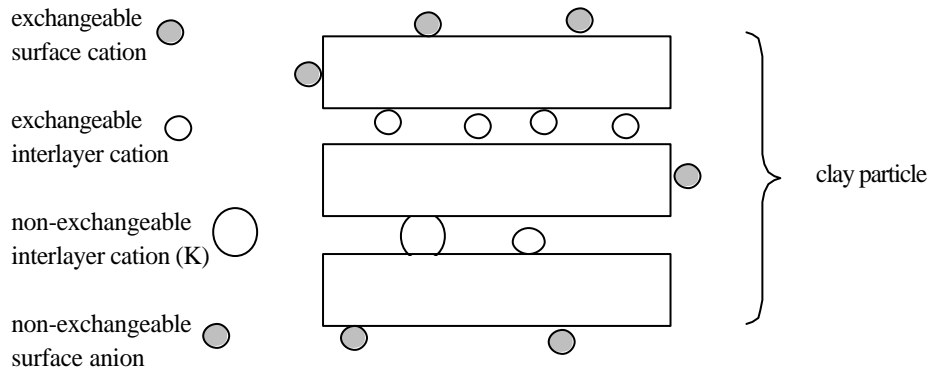
Figure 18: adsorbed surface compensator cations and absorbed interlayer compensator cations

According to their charge, the structures can be classified into three groups:

1. The neutral structures, where the 2:1 or 1:1 interlinked tetrahedral and octahedral have a net charge of zero and are thus electrostatically non-reactive.

2. High-charge 2:1 structures carry a charge of 0,9-1,0 C. The charge is compensated by nonexchangeable strongly bound interlayer Potassium compensator ions, which are an integral part of the structure.

3. Low charge 2:1 structures with a net negative charge of (0,2-0,9 C). Loosley held and easily exchangeable interlayer compensator ions balance the charge. These ions can be easily exchanged by aqueous solutions and replaced by other polar ions leading to a swelling of the material.

Kaolinit and Illit posses only surface sited exchangeable ions, whereas clay minerals of the smectite group have exchangeable interlayer and surface ions.

2.1.7   The cation exchange capacity (CEC)

The CEC is one of the most important properties of clays representing their overall reactivity.

The external surface, the internal surface and the charge of the surfaces of clays are measured by the CEC. The external surface CEC measures the average crystalline size and thus the adsorption capacity, whereas the internal one reflects the overall charge imbalance on the layer structure and the absorption capacity. The CEC is thus an estimate of the number of ions absorbed between the layers of a clay structure and of those adsorbed on the outer surfaces.

Immersing the clay in certain salt solutions and extracting i afterwards by drying estimates the CEC, which is given in milliequivalents per 100g of dried material (meq/100g or meq).
In general clays are divided into those with low CEC (10 - 40 meq) and those with high CEC (40-120 meq) (cf figure 19).[75]
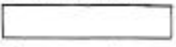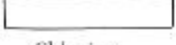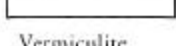
Figure 19: CEC and surface area of the most common clay minerals [Rowe 1997]

2.1.8   The different types of water

As already introduced, water molecules may be linked in different ways and to several sites of the clay minerals. Therefore we have to distinguish between different types of water in a clay mineral system (cf figure 20). Present are at least two different types of water but, may sometimes be as many as four types, depending on the clay species and thus their properties.

Figure 20: scheme of the different types of water of a clay particle

1. Free water is located in the intramatrix pores where the influence of the clay particle surface on the water is negligible. The physical characteristics of this water is close to normal liquid water (hydrostatical tensor, Newtonian fluid). Free water is the water of macroscopic liquid transfer within the argillaceous rock due to advection (hydraulic gradient) or other drives.

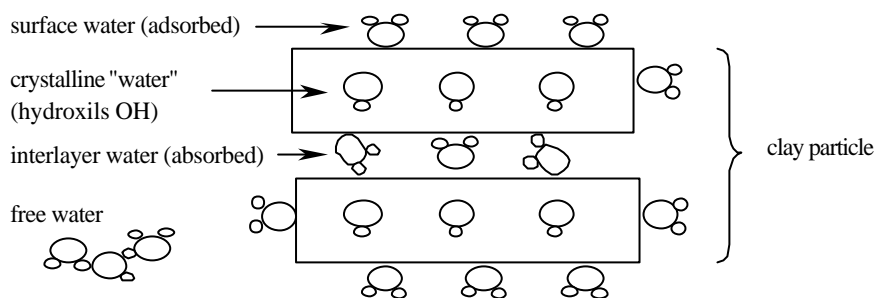2. Adsorbed water is located at the surface of the clay particles (1 to 4 monomolecular water layers). The electrical nature of the particles attracts the water molecule which are dipoles - as already explained in chapter 2.3.1. This type of water is anisotropic and exhibits a bi-dimensional orientated structure that is comparable to the structure of frozen water (no longer a hydrostatic tensor). The water molecules are only mobile in the plane parallel to the clay particle surface and they are never part of macroscopic water transfers. The quantity of this water is proportional to the outer surface of the clay mineral and the amount of the adsorbed water from one species to another is in the same range. This type of water is normally eliminated at temperatures between 80 and 100°C. By using the quasi elastic neutron scattering technique it was found that the adsorbed water has a mobile and an immobile component. The mobile component exhibits a rapid but spatially restricted jump diffusion whereas the immobile phase corresponds to water molecules in the hydration shells of surface cations.[75, 29, 95, 49]

3. Absorbed (also referred to as bound or interlayer) water is located between the clay platelets of a clay particle and exists only in minerals of the Smectite group (2:1 structure) as the attractive forces between the platelets are weak and thus the incorporation of water molecules in interlayer sites of the sheet structure is possible. It is usually associated with cations (hydrated ion) found between the layers. This type of water has an essential influence on the mechanical behaviour of the material as it fosters swelling and drastically reduces the strength of the material. The quantity of this type of water may be very high compared to the adsorbed water, depending on the interlayer ion species in the 2:1 structure. This type of water is normally eliminated at temperatures between 100 and 200°C.

4. Crystalline water is a fixed part of the crystalline structure in the minerals, present in the form of OH units, which oxidize upon heating and thus form water molecules. As crystalline water is strongly linked to the structure it requires temperatures of more than 500°C to be eliminated.

To identify and quantify the different types of water in a clay species the Thermo-gravimetric-analysis (TGA) and the Differential Thermal Analysis (DTA) are commonly used. As the water system of a clay mineral is a characteristic of each clay species, the method of identifying the clays by estimating their water quantities may also be used.

The principle of the TGA (cf figure 21) is a loss in weight of the sample after heating due to evaporation of the water, dependant upon the retention of the water by the clay. The retention energy among several types of water is different and allows the qualitative estimation of the water. The DTA (cf figure 22) method is based on the type of reaction that occurs when a clay is heated, whether the reaction is endothermic or exothermic. This analysis considers not only water loss but also observed recrystallization and recombinations.[95]
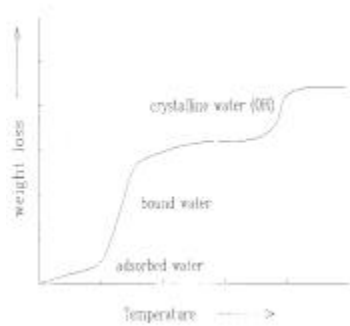
_____

Figure 21: Illustration of a typical weight loss over temperature (TGA) for a 2:1 Smectite type with rel. high amounts of absorbed water.[Velde 1992]
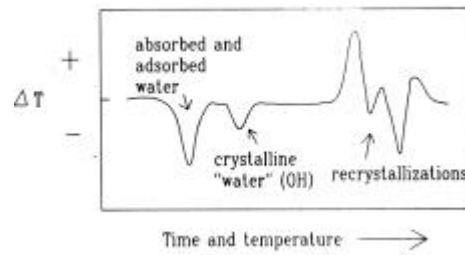
Figure 22: The DTA curve shows the exothermic (+) and endothermic (-) reactions of water loss and re-crystallization (?T over t with incr. T). [Velde 1992]

However both of the methods (TGA and DTA) are limited in exactly estimating the type of water. The transition between adsorbed and absorbed is rather diffuse and one can't say exactly whether the loss of weight is due to the loss of adsorbed water or because of a loss of absorbed water. For practical purposes the TGA is more commonly used and nevertheless provides sufficient information concerning the water clay system.

Shale may also contain anhydrite ($CaSO_4$), which can be transferred into gypsum ($CaSO_4 + H_2O$) by water contact. The normal TGA and DTA method will produce erratic results when gypsum is present, as a big portion of the removed water is crystal water of the gypsum, and not of the shale. The drying in a desiccator by using P_2O_5 and following heating to 200°C have to be applied for gypsum containing shale [54, 32]. The material from the site of Est does not contain anhydrite and the TGA (cf figure 23) as well as the DTA are applicable.
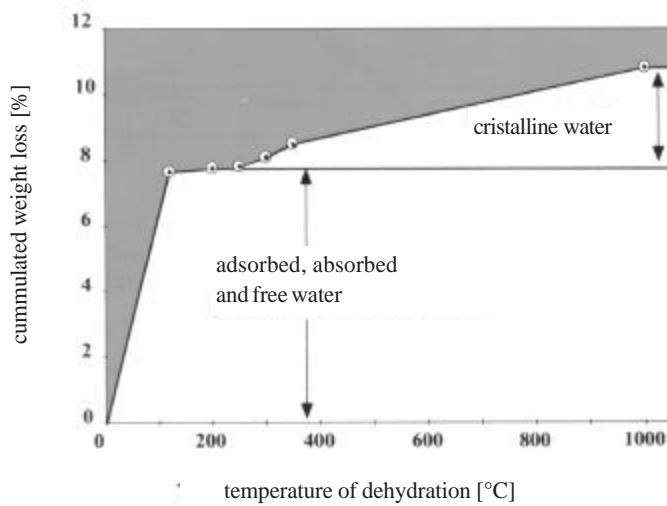
Figure 23: TGA curve for a Callovo Oxfordian shale sample from the site of Est [Andra 1999]

The absorbed, adsorbed and free water of the material from the site of Est form about 7,8 % of the overall weight. The quantity of the crystalline water is approximately 3% of the material weight. The adsorbed and free water of the material in the original state have a portion of 6 – 6,8% of the weight. The average total water content of the material from the site of Est can therefore be estimated to be as much as 11,2% of the shale weight (including crystalline water).[3]

_____

2.2 The average mineralogical composition of the material from the site of Est

The material of interest for a theoretically possible stocking site is at a depth of between 400 m and 600 m and is characterized as a silteuse carbonatic shale of the Callovo-Oxfordian.

Hence the composition of the material and the portions of each fraction vary with depth. We only present the general range of the specific components. Figure 24 illustrates the average mineralogical composition of the material.

range of some physical properties of the shale from the site of Est

natural density	[kg/m^3]	2,32 - 2,61
water content	[%]	2,8 - 8,7
porosity	[%]	9 - 18
uniaxial compr.		
strength	[Mpa]	12 - 49
triaxial compr.		
strength	[Mpa]	50 - 150
tension strength	[Mpa]	0,9 - 5,4
Young modulus	[Mpa]	2300 - 11000
poisson ratio	[ ]	0,17 - 0,4

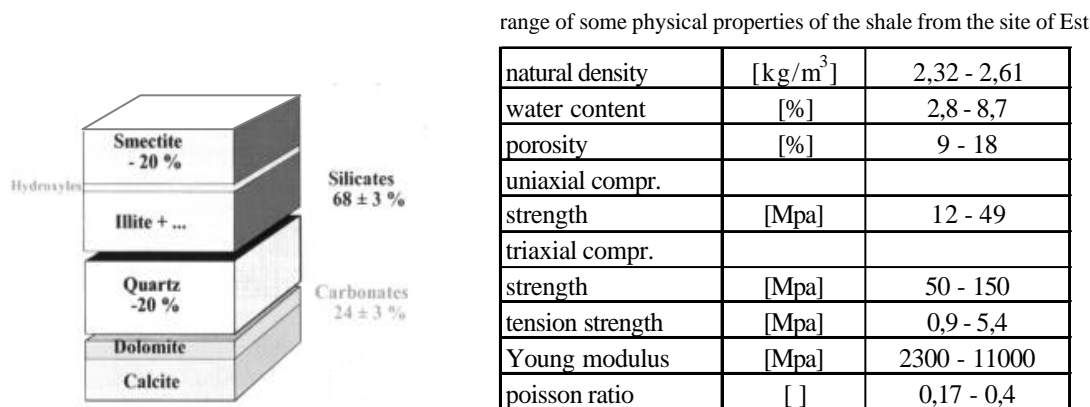Figure 24: Average mineralogical composition of the Callovo Oxfordian shale from the site of Est. The percentage is with reference to the overall weight of the material. The table presents the range of some important physical properties of the shale [Andra 1999]

The content of clay minerals varies between 30% and 60% and consists mainly of interstratified Illite-Smectite types and a small portion of Kaolinit. The Illit particles show a high Potassium content in their interlayer site which gives them strong cohesive bonding resulting in mechanically rigid and chemical unreactive behaviour. As the Smectite portion is dominant in the clay fraction the material has typical Smectite properties. The material therefore exhibits a relatively high CEC (15 to 25 meq/100g) and swelling and shrinking comportment. [4]

20% to 40% of the material consists of carbonates, mainly $CaCO_3$. Between the clay mineral layers Calcite was found which fosters the volume changing behaviour due to it's high solvability and the incorporation of other ion water complexes. This interlayer incorporation of water complexes is explained in chapter 2.3.3 (Absorption). The content of $CaCO_3$ strongly influences the material strength. An increased content may increase the strength (up to 150 MPa) and vice versa. [10]

Quartz is found to be imbedded into the clay matrix with a fraction of 5% up to 20%. Pyrite and other minerals are estimated with a portion between 1% and a maximum of 5%. [5, 4, 3]

The following paragraphs give a brief summary of the structure and the main properties of the most common clay minerals found in the Callovo Oxfordian material. Knowing the composition and the properties of each fraction makes it easier to understand the overall behaviour of the material from the site of Est.

Kaolinit is a member of the Serpentine group exhibiting a 1:1 di-octahedral sheet structure with a very low degree of cation substitution (morphological pure). The material is therefore mostly electro-statically neutral, in some cases carrying a weak electronegative charge. The 1:1 sheets are linked via relatively strong hydrogen bonds between the hydroxyl groups. This strong link between the stacked layers avoids water molecules in the interlayer sites and Kaolinit therefore doesn't exhibit inter-crystalline swelling. The CEC is in a range of 3 to 15 meq/100g which indicates the low reactivity of the material.

1:1 clay: Kaolinite
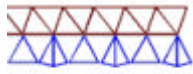
very low degree of cation substitution and therefore
neutral to very weak electronegatively charged sheets.

Strongly linked by hydrogene bonding
between hydroxyl groups

Illit is part of the Mica group possessing a di-octahedral 2:1 structure with a low degree of substitution. The highly electronegative charged sheets (due to the di-octahedral structure) are strongly linked by K^+ ions or NH_4^+ molecules in the interlayer site which neutralize the negative charge of the minerals.
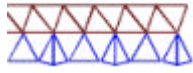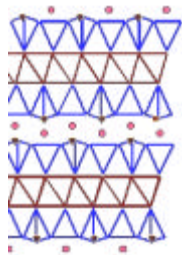
The inter-crystalline swelling is normally zero but may be very weak depending on the type of interlayer complex. With a CEC of 10 to 40 meq/100g the material belongs to the low to moderately reactive group.

2:1 clay: Illite

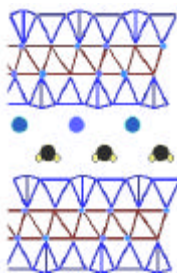highly electronegative charged sheets due to
Al^{3+} substitutes for Si^{4+} in tetrahedral sheets

Strongly linked by interlayer K+ ions
which also ballance the negative charge

Montmorillonit is one of the most important materials representing the Smectite group. The materials of this group exhibit a di or tri-octahedral 2:1 structure with a relatively high degree of cation substitution in the mineral. The sheets carry a strong negative charge due to Mg^{2+} or Fe^{2+} substitutes for Al^{3+} in the octahedral sheets, which is compensated by exchangeable Ca^{2+}, Mg^{2+}, Na^+ or H^+ ions.

The member of the Smectite group show very high values of inter-crystalline swelling, sometimes leading to a complete loss of the bonding forces between the mineral sheets and a complete dispersion of the material. The high reactivity of this clay type is indicated by its high CEC of 80 to 150meq/100g.

2:1 clay:Smectite

highly electronegative charged due to
Mg2+ or Fe 2+ substitutes foe Al3+ in
the octahedral sheets.

Weakly long bonding by exchangeable interlayer
cations which allow the incorporation of water
complexes leading to intercristalline swelling

The mixed layer minerals, also called interstratified minerals, result from a combination of two or more kinds of clay mineral species. The most common interstratification is the Illit/Smectite type which is present in the site of Est. The Illit/Smectite minerals are composed of fundamental particles that have an internal interlayer of illitic composition and are bound by hydrous interfaces. We could also see it as a Smectite like compound of Illit via hydrated exchangeable cations. The properties of this material are rather more like Smectite than Illit. They show small to high values of inter–crystalline swelling and a relatively high CEC. [27, 104, 95, 49]

2.3   The mechanisms of clay liquid interaction

The aim of this chapter is to describe the mechanism of clay-liquid interaction and the mechanical consequences. One of the main intentions is to do it in an understandable manner, as these mechanisms are of high importance in understanding the mechanical behaviour of shale.

The reactions are mainly an interaction between the clay particle surface and the pore liquid. Swelling, shrinking, cracking, mechanical weakening and mineralogical mutation are some of the consequences.

Water based solutions are of high interest regarding the clay reaction as they are a good solvent for contaminants and ionic bonds and because the initial pore liquid of a shale is mostly a sort of brine. It's therefore useful to briefly describe the general characteristics of aqueous solutions. After which we will look at the mechanisms of adsorption, absorption, capillarity and osmosis as they explain the high affinity of shale to polar liquids.

2.3.1   Aqueous Solutions

Water exhibits a dipolar character because of the asymmetrical coordination of the hydrogen atoms around the oxygen atom (cf figure 25). The internal charge distribution is such that the hydrogen side has a slight excess of positive charge and the oxygen end is correspondingly negative.
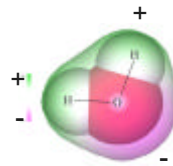
Figure 25: water molecule with its dipolar character

Being dipole and because of hydrogen bonds, water molecules are a very good solvent of ionic bonds by attracting the anion with the positive pole and the cation with the negative pole. The attraction forces of this compound may be very strong and the ion is normally hydrated by several water molecules forming a hydration shell around the ion (cf figure26).
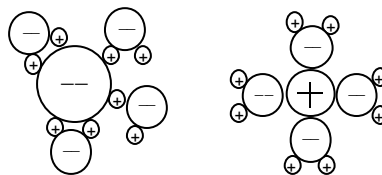
Figure 26: hydrated cation/anion forming a hydration shell

The orientation of the water molecules in the hydration shell results in a net charge on the outside of this shell, a charge of the same sign as that of the ion in the centre.
Water molecules in the vicinity can be linked to the first primary hydration shell via hydrogen bonds leading to a second hydration shell. [62]

Hence the hydrated ion may be covered by several hydration shells, the effective radius of the water-ion complex is much bigger than the radius of the unhydrated ion (cf table 2).
The level of hydration of an ion depends on the ionic potential which is defined as the ratio of the charge to the ionic radius. The higher the electrical charge of the ion the higher the bonding forces

_____

and the number of hydrating water molecules will be. This means that elements with a small ionic radius and a high valence may form larger hydrated ions than elements with a large ionic radius and a small charge.

This implies that Mg^{2+} and Ca^{2+} ions can be strongly hydrated because of their relatively small ionic radius and their valence. Hence Na^+, K^+ and Cs^+ have relatively great ionic radii and carry a simple negative charge they therefore form smaller hydration shells.

Element	Stoke radius [pm]	Ionic radius [pm]	Covalent radius [pm]
Mg	345	78	136
Ca	307	100	175
Na	183	102	155
K	124	130	203
Rb	120	150	230
Cs	119	165	247

Table 2: The different radii of different ions. The Stokes radius is the effective hydrated radius including the hydration shell and was evaluated by using the law of Stokes. The Anti Stokes ion don't obey this law because they are to small in diameter. The reason is their inability to get hydrated. [Millot 1963]

The K, Rb, and Cs represent a very special species among the ions in terms of hydration. They belong to the group of so called anti-Stokes ions. This means they are very poorly hydrated in an aqueous solution and therefore stay too small to obey the law of Stokes (cf table 2) when descending in a tube filled with a solvent (Descending test for spherical particles according to Stokes). The explanation is given by their small ionic potential - they have large ionic radii and carry a small ionic charge (cf figure 27). The specific surface charge thus seem to be too weak to orientate the water molecules and thus to attract them. [59]

As Potassium and Caesium are two major elements in the nuclear clay barrier system these properties are of great importance concerning the mechanical behaviour (swelling/shrinking) of clayish materials and will be discussed in detail in the chapter 'swelling and shrinking of shale'.
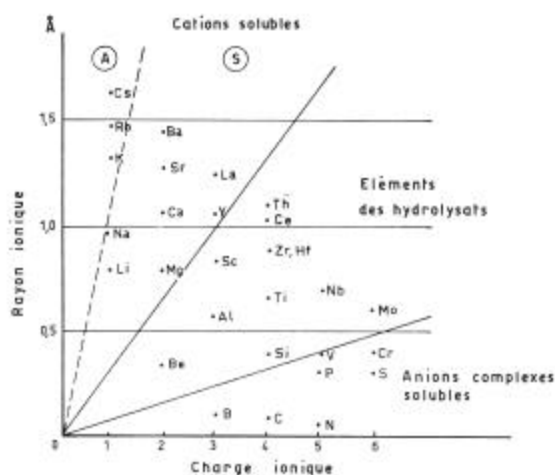

Figure 27: The ionic potential is defined as the ratio of the ion radius to the ion charge and governs the ability to hydrate an ion species. [Millot 1964]

_____

2.3.2   Adsorption and inter-particle swelling

The term adsorption implies the enrichment or depletion of a chemical species in the region of an interface. When positive adsorption (enrichment) occurs, the concentration of the adsorbed species is greater at the interface than in the bulk fluid phase. The same applies vice versa for negative adsorption (depletion). That means in the case of positive adsorption a chemical species accumulates at the surface of the clay particle. [62]

Due to the dipole character and the presence of hydrated cations in the aqueous solution, a dry clay particle being in contact with it develops a layer of monomolecular water at the surface of the clay crystal (Stern layer). Above this first layer several other monomolecular layers of water molecules can be superposed, forming the so called double (multi) layer water (cf figure 28).

The water molecules and hydrated cations are usually linked to the defect sites, broken bonds and compensator ions on the surface trying to equilibrate the structure. The number of layers depends on the electrostatic interaction range of the clay particle in the solution and the character of the hydrated ions.
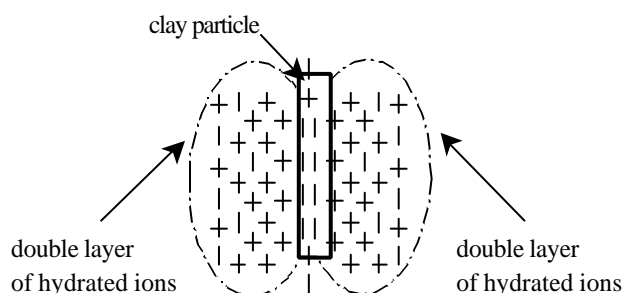
Figure 28: clay particle with adsorbed water double layer

Depending on the radius of the hydrated ion, and their net charge, they approach more or less close to the surface of the mineral. The closer they get, the better they equilibrate the net negative charge of the clay platelet, as the electrostatic interaction radius is limited. Therefore it needs more strongly hydrated large cations to equilibrate the clay platelet than it would need smaller ones (other type of cation or level of hydration). Furthermore osmotic forces (see chapter 2.3.5) can repel the cations from the surface so that they can't approach close enough to the surface of the clay mineral.
This results in the development of several monomolecular layers of water. If the water is chemically pure, the number of layers depends only on the electronegative charge and range of interaction of the clay mineral .

Once the system is electro-statically equilibrated, the cations are organized in a so called double layer distribution (cf figure 29). This configuration exhibits a negative concentration coefficient in the direction from the particle. This means, the concentration of hydrated cations is highest next to the charged particle, decreasing with distance to the same value as in the free pore water. Hence the anions in the solution are affected by the same mechanism, they show an inversely configured distribution to the cations.

The double layer thickness is in the order of nanometers to micrometers and we distinguish between the first Stern layer and the further Diffuse or Gouy layer. The Stern layer can be divided into the inner Helmholz plane and the outer Helmholz plane. The molecules in the first one are completely fixed to the surface, whereas the outer Helmholz plane allows some movement. With increasing distance from the particle surface the electrical interacting potential of the clay platelet decreases. [72, 75, 27, 95]

_____
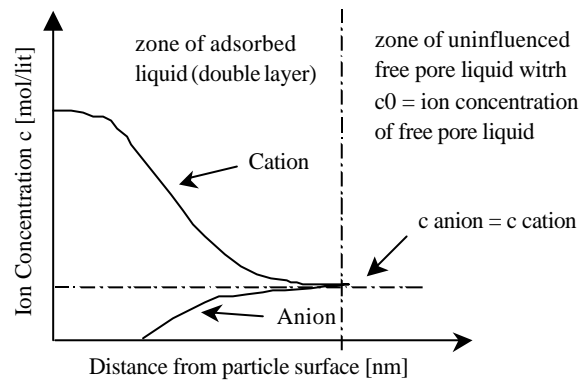
Figure 29: ion distribution close to the particle surface according to the double layer theory

The close proximity of the first layer of firmly attached cations results in an abrupt drop in electrical potential through the Stern-layer. That's why the second Diffuse or Gouy layer is less firmly linked to the particle than the Stern-layer (cf figure 30).
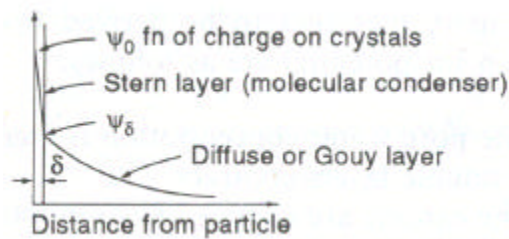
Figure 30: Illustration of the Stern layer and the Diffuse
layer with the electrical potential over the particle distance

The double layer system is a dynamic one with reference to the water layer thickness. It may contract or expand depending on several factors. According to the Gouy Chapman theory an increasing pore water concentration as well as a cation change from monovalent to divalent or trivalent contracts the double layer (cf figure 31). Contraction also occurs by decreasing the dielectric constant of the pore liquid which could be achieved by increasing the temperature of the pore liquid (cf figure 31). [72, 27]
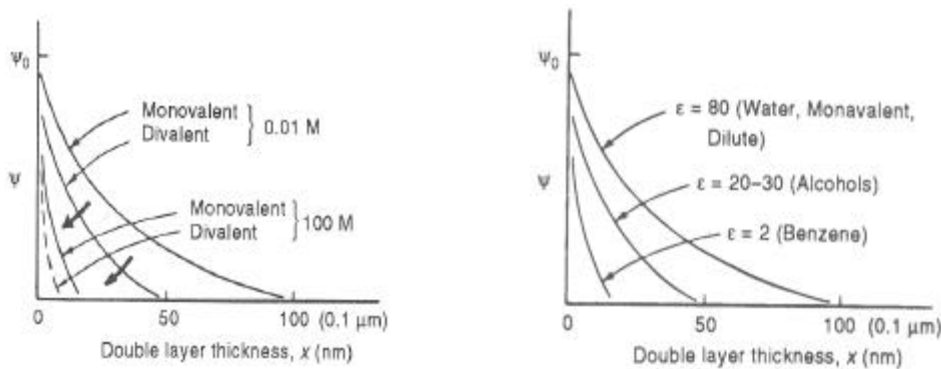
Figure 31: The influence of the valency and concentr. of the cations on the double layer thickness and the electrostatic potential (?) distribution as well as the effect of the dielectric constant (e) of the adsorbed water.

_____

These double layer thickness variations, at constant void ratio of the material, can have an enormous affect concerning the petrophysical properties such as permeability and effective porosity. This influence can be illustrated by the ratio of possible pore radii in shale to the thickness variation of the adsorbed water. The water layer varies from several nanometers up to 0,1 micrometer causing a change in free void space (effective porosity) and thus, influencing the previously mentioned parameters.

Furthermore Osmosis relies on the way the adsorbed water layers are developed, as the free pore space might be small enough to act as a semi-permeable membrane (cf chapter 2.3.5). Mechanical parameters like the friction angle, the resistance and creep as well as the heat conductivity of the material could be influenced by the water. Unfortunately no investigations could be found in literature that try to correlate the influence of adsorbed water on these parameters.

The quantity of this water is proportional to the outer surface area (cf chapter 2.1.7) and the net negative charge of the particles and can be found in all types of clays, with relatively small differences in quantities. If we take into account the large specific surface of clay materials (up to 850 m²/g) - and also the small size of the clay particles (micro-nano) - one can imagine that the adsorbed water increases the volume and represents a great portion of the whole absorbed water in the material.

This kind of swelling produces, in general, smaller swelling rates than the swelling due to absorption of water molecules. In the case of a very fine grain size distribution like for some Kaolinit the swelling pressures and volume changes can nevertheless be very high.

2.3.3   Absorption and inter-layer swelling

This swelling mechanism is also referred to as inter-lamellar or inter-crystalline swelling in literature. Contrary to the process of adsorption, absorption does not accumulate a chemical species at the interface, but diffuses into the solid. In the case of clay minerals, ions or molecules can be incorporated between the crystal layer of the clay particle.

When a low charge 2:1 structure clay particle (Smectite group, cf chapter 2.1.5) is in contact with a hydrous solution, the less firmly linked interlayer cation (usually Ca^{2+}, Na^+) can be hydrated or replaced by another ion (ion exchange) and other polar or ionic molecules can be incorporated into the interlayer site.

Depending upon the ionic potential (valence and ionic radius) of the interlayer cation, it will be hydrated by more or less water molecules. The different cations in their hydrated state have different dimensions (hydration shell) creating different interlayer spacing in the structures and thus swelling or shrinking of the material. Monovalent hydrated ions cause, in general, a smaller spacing than divalent hydrated ions.

Another interlayer distance defining factor is the level of hydration of the cations. (cf figure 32).
The solvation of loosely held exchangeable interlayer cations of such a 2:1 structure and their exchange (cf chapter 2.1.7) by other ionic species of the aqueous solution, with different diameters and electrical charges also leads to a change of the distance between the layers. This means that the swelling depends not only on the type of interlayer cations, but also on the ion concentration, the ionic species and their hydration in the solution in contact with the clay.

The incorporation of water molecules can lead to a complete deterioration and dispersion of the material, if the linkage between the layers in the clay particle is weak enough to be disrupted. This comportment was observed under certain circumstances, using the shale from the site of Est and will be discussed in the chapter 'practical clay testing program'.

The saturation of a dry Smectite particle, may alternatively reduce the interlayer spacing and thus shrink the material (cf figure 32) as in the case of Potassium ions in the solution. The unhydrated

ions can replace the bigger hydrated interlayer ions and fit perfectly into the 2D hexagonal holes of the layer (chapter 2.1.3).

As the poorly hydrated K ions are small and their net charge is relatively high, compared to the exchanged hydrated ions, they are tightly fixed to the layers on both sides, which leads to the described reduction of the spacing. Once the K ions are fixed into the interlayer site, the clay particle can't add any other polar molecules into the interlayer site as the bonding forces of the K and the layers are too strong. The particle no longer shows intercristalline swelling when in contact with water. From the mineralogical point of view the Smectite was transferred into a Mica type which does not exhibit swelling. [47]

This shrinking is usually accompanied by a strong micro and macro fissuration (cf figure 33) and a complete change in the mechanical and petrophysical properties of the material, such as permeability, porosity and mechanical strength.

Dehydration also causes Smectite types to shrink, as the spacing is reduced due to water molecule evacuation. Very often, the shrinking is accompanied by crack induction which can be easily observed at the surface of the sample (cf chapter 4.6.2).

These cracks, of course, modify the solid structure of the material, as well as influence the mechanical and petrophysical properties of it. This means that a variation in the saturation of the shale may cause structural changes that are irreversible. This irreversible influence of saturation and desaturation, on the material properties, was often observed. Tests with originally saturated shale and rehydrated shale led to different results, even though the material was identical. [4, 72, 75, 27, 95, 59, 49]

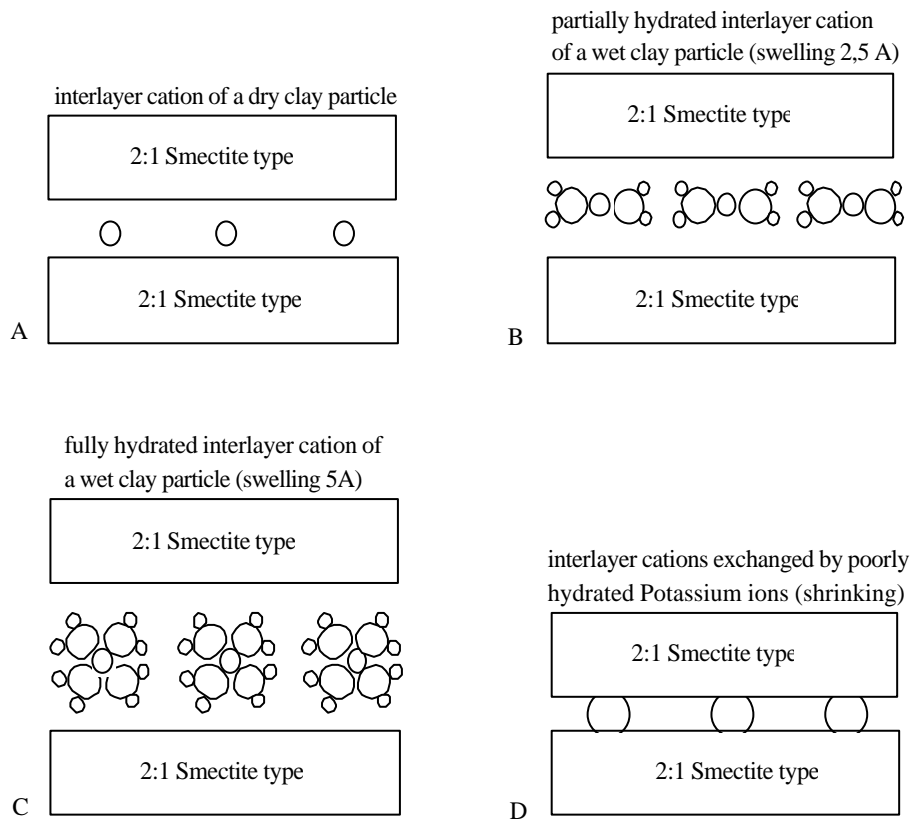Figure 32: the different cases that cause either swelling or shrinking of a 2:1 type Smectite clay particle. Picture A shows a dry particle with loosely linked interlayer compensator cations. Pictures B and C exhibit these cations in different hydration states causing different interlayer spacing. In the last picture D the initial interlayer cations have been exchanged by Potassium ions which results in shrinkage of the material.

_____

The concept of ion exchange and cation hydration is very important as it may change the mechanical, petrophysical and chemical properties of clayish materials. It should therefore be taken into consideration for models that dry to describe and predict the behaviour of those materials.

Figure 33: exhibits strong fissuring in the bedding plane of
a shale sample from the site of Est, after immersing into a 2 molar KCl solution.
The specimen is a cylinder with 16mm in diameter and a height of 30 mm.

2.3.4   Capillarity

Capillary phenomena play, in general, an important role concerning the saturation of unsaturated materials. This physical affinity for wetting liquids is not related to the physico chemical affinity of the clay minerals due to their surface activity but is of a physical nature.

Having a fine porous network, due to their small particles size, clays foster capillarity and may create high capillary suction in the magnitude of 100 MPa. Capillarity is a function of the adhesive, cohesive and superficial forces of the three phase system solid, gas and liquid. The term wettability defines in general whether a liquid will raise or descend in a capillary tube.

Wettability and Superficial Tension

If two different and immiscible liquids (for example gas and water) are in contact, forces at the contact interface will be developed (interfacial tension).
If we consider, for example, a water gas system, a water molecule inside the liquid is surrounded by other water molecules and their attracting Van der Waals forces are balanced (cf figure 34). A surface sited water molecule is not completely surrounded and attracted by other water molecules. The residual attraction force therefore points into the liquid as the attraction to the gas molecules is not strong enough to balance the liquid forces. To keep this water molecule at the surface, energy is required to overcome this force. Surface water molecules therefore have a higher level of potential energy than molecules inside the liquid. [62]
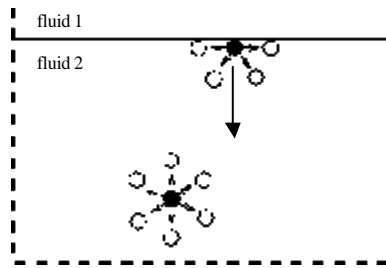
Figure 34: the origin of the superficial tension is a result of the residual attraction force pointing into the liquid, as molecules at the surface have unbalanced attraction forces

If the surface of a liquid should be enlarged, molecules have to be brought to the surface. This means we have to overcome the forces that try to keep the molecule inside. The energy required to enlarge the surface per unit, is called superficial or interfacial tension. The required work for the enlargement of a rectangular liquid surface is thus:

$$\Delta W = F \Delta s = F \frac{\Delta A}{l}$$
9

ΔW mechanical enlargement work [Nm]
F   force [N]
Δs enlargement along s [m]
ΔA enlarged surface [m²]
l   width of the surface [m]

and the superficial tension can be written as:

$$g = \frac{\Delta W}{\Delta A} = \frac{F}{l}$$
10

γ superficial (interfacial) tension [N/m]

If the system is in an energetic equilibrated state - the surface is part of the system – its energy will be a minimum. Thus the surface energy will be a minimum if there are few molecules at the surface - resulting in a small surface. This means the higher the attracting forces of the liquid molecules, the smaller the surface of the liquid will be. The superficial tension (interfacial tension with air at standard conditions) for water is 72 N/m and for mercury 243 N/m.

A fluid drop brought into contact with a solid phase, is shaped depending upon the relation of the interfacial tensions and the gravity acting upon it (cf figure 35).
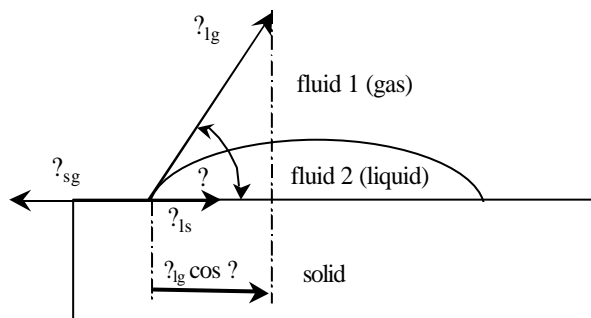
Figure 35: definition of the contact angle in a three phase system using the interfacial tension

Young (1805) defined the contact angle ? of the system as a consequence of the static equilibrium between the interfacial forces by projecting them in the horizontal plane:

$$\cos q = \frac{g_{sg} - g_{ls}}{g_{lg}} \qquad\qquad 11$$

?ls   interfacial tension between solid and liquid [N/m]
?lg   interfacial tension between liquid and gas [N/m]
?sg   interfacial tension between solid an gas [N/m]

This contact angle defines whether a liquid is wetting (?<90°)or non wetting (?>90°) for a given solid material and whether the liquid will rise or descend in a capillary tube. According to picture 36, either fluid 2 or fluid 1 exhibit wetting properties. In most cases the wettability will be of partial character rather than of a total one (?=180° or ?=0°).

The wettability is furthermore used to define whether the displacement of a fluid by another is called imbibition or drainage. Imbibition is the displacement of the non wetting fluid by a wetting fluid in a porous medium. Drainage is referred to as displacement of the wetting fluid by a non wetting fluid. Drainage implies that a force has to be applied to counterbalance the capillary forces of the system. [79, 45]
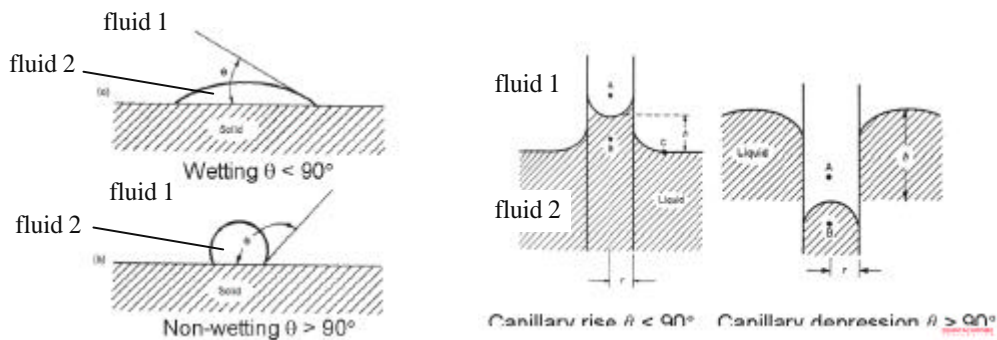
Figure 36: wetting (capillary rise) and non-wetting properties (capillary depression) of a liquid determined by the contact angle

The Capillary Pressure

The previously described interfacial tensions between two immiscible fluids are counterbalanced by a pressure difference called capillary pressure if the system is in an equilibrated state. This means the pressure at both sides of the fluid interface is different.
The diphasic interface in figure 37 is formed by the two curvature radii r_1 and r_2. As these radii are proportional to the interfacial tension between the two fluids they represent the activity of the system.
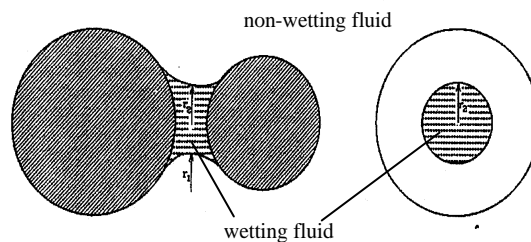
Figure 37: illustration of the principal curvature radii of two fluids in a pore (Heinemann 1995)

_____

We can therefore calculate the pressure difference by using the Laplace equation 12:

$$p_c = g_{lg}\left(\frac{1}{r_1} + \frac{1}{r_2}\right) \qquad\qquad 12$$

In a capillary tube the meniscus can be considered as a portion of a sphere limited by the internal diameter of the capillary at the angle ? (cf figure 38). Under these assumptions the curvature radii may be expressed by equation 13:

$$r_1 = r_2 = r_m = \frac{R}{\cos q} \qquad\qquad 13$$

r_m radius of the meniscus of the liquid [m]
R   radius of the capillary [m]

The combination of equation 12 with equation 13 leads to the relation 14 which is known as the law of Turin:

$$\Delta p = p_c = p_g - p_l = \frac{2g_{lg}}{r_m} = 2g_{lg}\frac{\cos q}{R} = h(r_l - r_g)g \qquad\qquad 14$$

pc   capillary pressure [Pa]
pl   pressure in the liquid [Pa]
pg   pressure in the gas [Pa]
?l   density of the liquid (wetting fluid) [kg/m3]
?g   density of the gas [non wetting fluid) [kg/m3]
g   gravity constant [m/s²]
h   raising height of the wetting liquid [m]

In a porous medium the capillary tube diameter R represents the actual pore size of a porous media. Comparing such a porous network to a bundle of capillary tubes of different diameters is common practice in soil mechanics, reservoir engineering and petrophysics in order to develop numerical approaches, even though this model is a strong simplification. [45, 38]
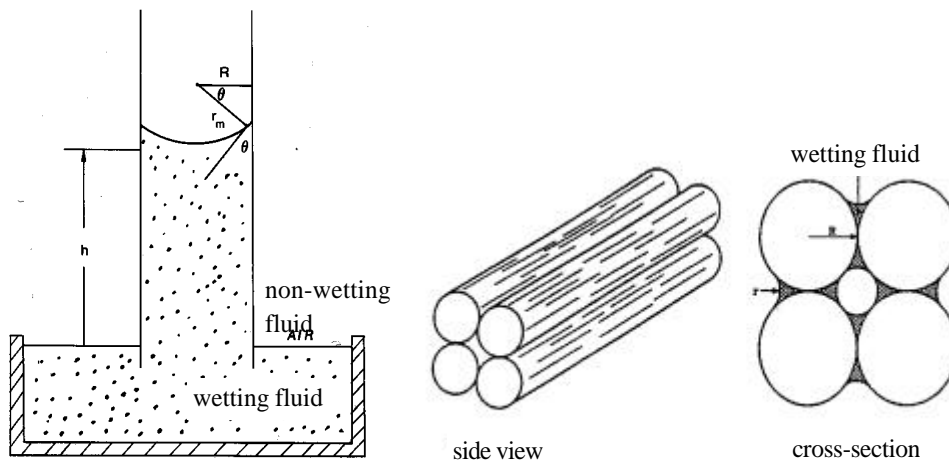
Figure 38: capillary tube and bundle of capillary tubes to model a porous media (Heinemann 1995)

From equation 14 it appears that the highest capillary pressures will be found in very fine grained rocks with very small pore throat radii.

An interfacial tension of water of 72 10^{-3} N/m in a capillary tube of 1 nm diameter with a total wettability of cos?=1 results in a pressure difference of 145 MPa according to equation 14. The pore size distribution of the clays of Est start in a range of 0,01 μm to 0,1 μm.

With air at atmospheric pressure, equation 14 implies that the pressure in the water is negative. This negative pressure, known as capillary suction is one of the main causes of water retention in granular material, fostering adsorption in the case of porous materials.
The term negative pressure leads the term pressure somehow ad absurdum and can be explained by the stronger adhesive forces between the capillary wall and the water compared to the cohesive forces between the water molecules, thus putting the liquid under a kind of tension.

Capillary Suction

The relation between the saturation degree of the material and the capillary suction is usually represented by using the so called retention curve (cf figure 39). This curve is characterized by a hysteresis phenomenon of the capillary pressure versus the saturation degree, which means that the path of the drainage (dehydration) curve doesn't correspond with the imbibition (hydration) curve.

In the case of drainage the big pores are the first to be drained as they have a rather small capillary pressure compared to the small pores. On the other hand these big pores are the last to be filled with liquid in the case of imbibition. The same applies vice versa for the smallest pores.

The hysteresis is such that a certain amount of pressure needs to be applied to start the drainage of a completely saturated sample and to allow the non wetting fluid to enter the sample. This so called threshold pressure corresponds to the lowest capillary pressure of the largest pore radii in the system - which are the first to be drained. The capillary suction, at which a material starts to dehydrate, (threshold pressure) therefore characterizes the material in terms of it's largest pore radii.

In the case of imbibition there is no threshold value that has to be overcome and the process takes place immediately when the dry sample is in contact with a wetting fluid.
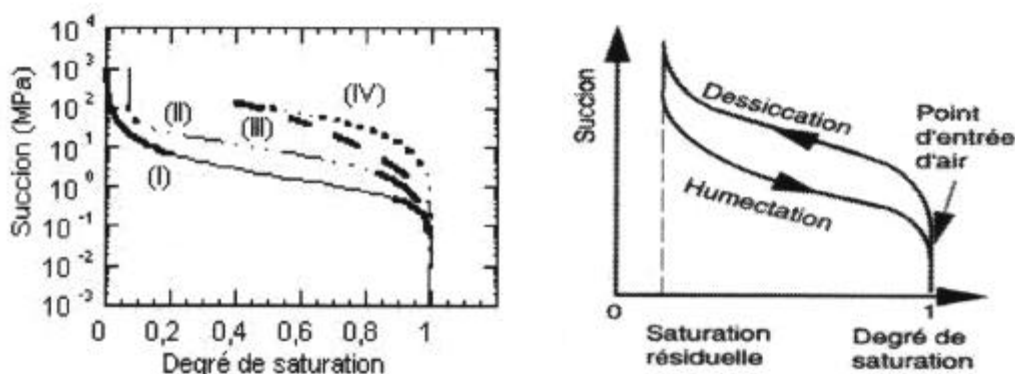
Figure 39: A capillary pressure curve for bentonite (I), clay of mol (II), shale of haute Marne (III), silite of marcoule (IV). The theoretical illustration on the right side shows the threshold pressure which corresponds to the air entry point and the difference in drainage (desiccation) and imbibition (humectation). [mécanique des roches 2000]

The capillary suction curve doesn't give any indication about the swelling or shrinking phenomenon of shale but indicates the irreversibility of hydration and dehydration.

The various kinds of methods used for measurement are all based on the principle of drainage. A certain constant pressure is applied to the non wetting fluid for it to enter the porous material until the system is in equilibrium with the capillary pressure and generates a certain saturation. The applied pressure consequently counterbalances the capillary pressure which corresponds to a certain saturation. Mercury is normally used as the non wetting fluid as its properties are stable in a wide pressure range and its high superficial tension assures ideal non wetting comportment and therefore allows the imbibition into relatively small pores. Nevertheless, this method is limited by pores in the nm range. Alternatively He can be used for this pore size.

The most common testing devices are the classical Welge/Bruce and Purcell tests as well as the centrifuge method where the saturation depends on the rotation speed. [28, 24, 45],

In the science of pedologie the capillary pressure is very often seen as a confining stress between the soil grains. Dry sand, for example, does not exhibit cohesive forces between the grains and does not show any resistance if an external load is applied. If the sand is wet it exhibits a certain mechanical stability which led to the assumption that the capillary pressure acts like a confining stress that holds the loose grains together.

In clayish material it seems to be the opposite, as the decrease of strength is due to an increase of saturation. The difference is very likely to be found in the chemical activity of the clay. i.e. The reduction in resistance due to the change of the chemical bonding between the clay minerals can't be compensated by the capillary forces

The relation of the different parameters in the Laplace equation to calculate the capillary pressure is fairly clear. The problem is their accurate quantitative evaluation. The contact angle can be measured by special devices under stable conditions using optical technologies. In clay systems we don't have stable conditions due to the solid liquid interaction. The fluid brought into contact with a special clay might therefore have a different superficial tension respective contact angle than the initial one leading to a different pressure drop.

We also have to be aware that it's very likely that the free pore liquid is not in contact with the clay particles as the particle is covered with adsorbed water. According to the double layer theory the capillary could thus be covered with a film of water and we would have cohesive forces between the adsorbed water and the free pore liquid rather than adhesive forces as is the normal case between the solid and the liquid phase (cf figure 40). This would of course change the interfacial tensions of the system and therefore the contact angle, resulting in a different capillary pressure in the pore than that calculated.
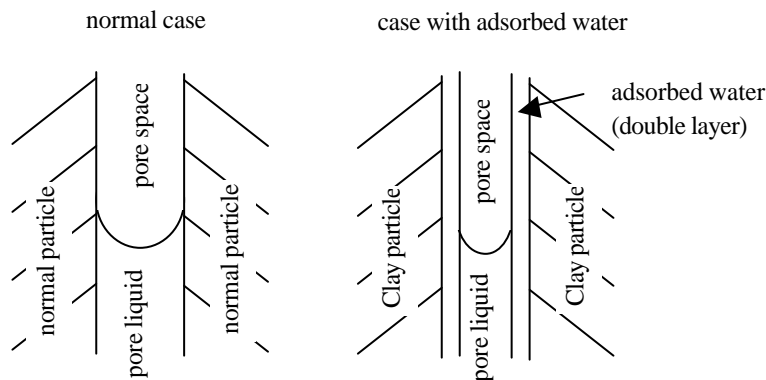

Figure 40: Schematic coexistence of adsorbed water and capillarity in a clay capillary (vertical bedding plane)

The adsorbed particle water should also be taken into consideration when the capillary suction is evaluated by mercury injection. The development of the thickness of the adsorbed water layer on

the particle surface is of a chemical nature, as explained in chapter 2.3.2, and defines the remaining effective pore space. i.e. the effective remaining free pore space depends on the clay particle - pore liquid interaction. Therefore if we inject mercury into a dry clay sample we measure a capillary suction for a pore space configuration that doesn't exist in a partially saturated shale with adsorbed particle water. The conclusion is such that the path of the saturation suction curve obtained by mercury injection does not reflect the real behaviour of the clay as it does not take the fluid liquid interaction into consideration.

In the next chapter we discuss the phenomenon of osmosis and it will be clearly shown that the pressure or suction "anomalies" due to clay liquid interaction must not be neglected.

2.3.5   Osmosis

The phenomena of osmosis may either lead to shrinking or to swelling of partially saturated or even saturated materials and we therefore try to give a detailed analyse about this phenomenon later.

Osmosis has been cited as a mechanism for explaining anomalously high pore fluid pressures in clayish materials [47]. This pressure (up to 2 MPa) is normally higher than the external advective (hydraulic) pressure due to incorporation of water into the already physically saturated clay material. As the existence of osmotic mechanisms in shale is very controversial, this chapter tries to deliver a sound basis for understanding the theory leading into the following discussion.

Osmosis occurs when a semi-permeable membrane separates two solutions of different concentrations and thus of different solvent activity at isothermal and isobaric conditions. The semi-permeable membrane permits only the transfer of some components of the solution and is impermeable to others. The result is a different pressure on both sides of the membrane, due to solvent flow from the side of low solute concentration to the side of high solute concentration (cf figure 41). In the case of aqueous solutions the water molecules will pass the membrane but the hydrated ions will be retarded. Semi-permeable membranes can exclude components on the basis of size and/or electrical restrictions. [60, 62]

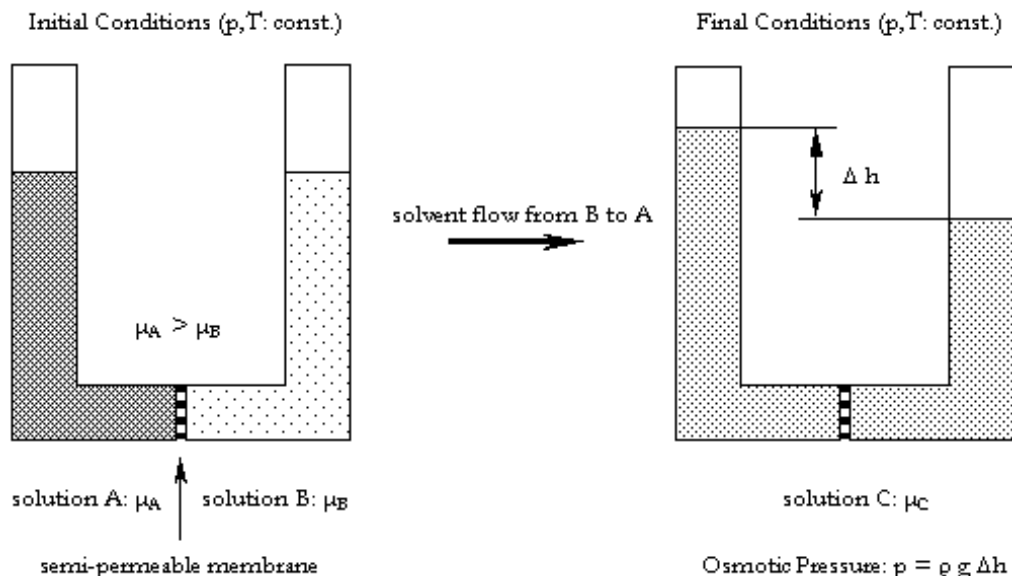Figure 41: A semi-permeable membrane separates two solutions (A and B) of different chemical potential ($\mu_A \neq \mu_B$). The semi-permeable membrane permits only the transfer of solvent but not of solute components. The result is a pressure difference (osmotic pressure) between both sides of the membrane due to solvent flow from the side of low solute concentration to the side of high solute concentration

Any chemical potential gradient at the membrane thus causes migration of solvent (water) to the site with the lower chemical activity. The system is in equilibrium when the osmotic pressure is counterbalanced by a corresponding hydrostatic pressure and no solvent migration occurs.

If an additional external pressure higher than this hydrostatic pressure on the initial solvent influx side A is applied, the result is a reversed solvent flow through the membrane. The back-flow into side B is thus increasing the solute concentration on the out-flow side A and vice versa. This process is called Hyperfiltration or Inverse Osmosis and shows that Osmosis is a reversible process. To be exact we have to talk about a reversible thermodynamic process, as an external force controls the direction and the rate of change of a parameter in the system.

Nevertheless Diffusion is often held as the responsible mechanism for Osmosis in literature. The fact that for example the dissolution of ionic compounds in a solvent can't be reversed by an external applied pressure shows clearly that diffusion is an irreversible thermodynamic process and therefore not responsible for Osmosis.

The explanation for the Osmotic pressure can be given by the motion theory of Brown and the transfer of the microscopical kinetic energy due to the thermal speed of the molecules, into macroscopical work, which results in the osmotic pressure. The pressure itself is counterbalancing the different energy levels on both sides of the membrane.

The preliminary mentioned contradiction about osmosis is such that some researchers [87, 46, 94, 69] couldn't observe any osmotic phenomena during their shale testing and others [18, 39, 97, 102] concluded that osmosis plays an important role and explains the pore pressure anomalies and thus mechanical "anomalies". The point is: we have to carefully distinguish between both the different shale types used for the tests, as well as the different testing procedures themselves.

The question is whether or not a clay can act as a semi-permeable membrane and if a chemical potential gradient is given. Regarding the classical Osmometer test done by several scientists it seems to be quite realistic that Osmosis takes place in clays. In the cases where an ion transfer through a shale could be observed, the existence of osmosis was denied by some scientists which is indeed too simple a conclusion, as will be shown.

A consistent comprehensive theory about osmosis was stated by Wendell et al. [32], which explains and quantifies the phenomenon. In the following paragraph we apply this theory for two different case studies of clay hydration and how and why a clay can act as a semi permeable membrane.

The two cases are illustrated in figure 42. In the first case, the clay is initially dry and later hydrated by a liquid with a given chemical potential. The second case describes an already saturated clay sample, that is brought into contact with a liquid having a different chemical potential to that of the pore liquid of the material.

In case 1 the liquid entering the dry pores because of capillarity will be adsorbed by the clay particle surface with a solute distribution according to the double layer theory as explained in the chapter of 'adsorption'. This ion distribution in the adsorbed layer results in a chemical potential difference within the adsorbed layers and between the adsorbed water and the uninfluenced free pore liquid. The system therefore tends to equilibrate the higher solute concentration in the proximity of the particle surface.

As anions are repelled by the high negative charge of the platelet and cations by their own species close to the surface only solvent from the uninfluenced free pore liquid is allowed to approach. i.e. The adsorbed water of the clay particles defines the semi-permeable character of clays due to electrical restrictions of ions and thus causing an osmotic pressure (cf figure 43). [78, 8, 97]

Another membrane effect could be the overlapping of the adsorbed water layers. As the layer thickness of the adsorbed water (0,5nm to 0,1 μm) is comparable to a certain pore size of the material they can overlap to varying degrees between adjacent particles. This overlapping leaves very little, or no, space for pore liquid in the pores that is uninfluenced by the double layers. The predominant ion species in the pores are therefore cations from the double layer. Anions are again

repelled from entering the pore by the negative charge on the clay platelet and cations are repelled by their high concentration of positive charge in the stern layer. This electrical restriction would nevertheless allow the water molecules to be incorporated into the void space.

CASE 1

?V > 0, ?? >0

| initially dry clay sample | contact liquid with μ_1 |

liquid inflow

CASE 2

?V > 0, ?? > 0

?V < 0, ?? < 0

| initially saturated clay sample with pore liquid with $\mu1$ | contact liquid with μ_2 |

liquid inflow or outflow
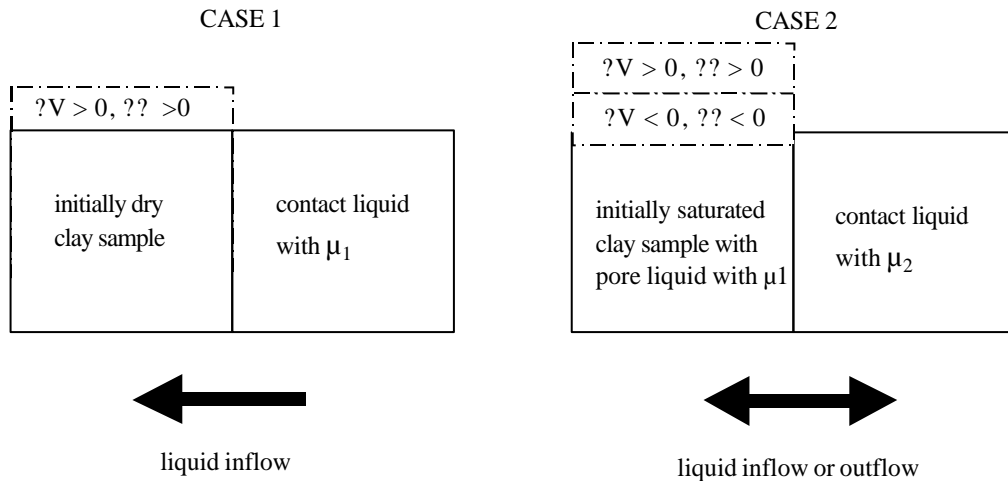
Figure 42: two realistic cases to explain osmosis. In the first case the clay is dry and will be saturated by a liquid with a given chemical potential $\mu1$. In the second case: the clay is already saturated and the sample is brought into contact with a liquid with a different chem. potential μ_2 than the pore liquid of the material μ_1.

Furthermore some clay pore sizes are small enough (0,1 to 0,4 nm) to act as a mechanical semi-permeable membrane and to retard the solutes. However, with reference to the pore size distribution curve of most shale it turns out that the percentage of these sufficiently small pores contributes less to the observed osmotic pressures than the electrostatic restriction of ions.

Derjaguin and Churaev developed the concept of disjoining pressure to describe the phenomena of this kind of pressure anisotropy. The model comprises a solution between two negatively charged plates causing an additional pressure in the direction of the x-axis because of a plate liquid interaction. This pressure anisotropy causes a deformation and stress anisotropy.

$p_2 = p_1 + ??$

double layer with $\mu(f_x)$

x distance

electrostatic distribution y

p_1

inflow

p_1

inflow

contact liquid with μ_1

free pore liquid in reduced pore space

pore width

$p_2 = p_1 + ??$
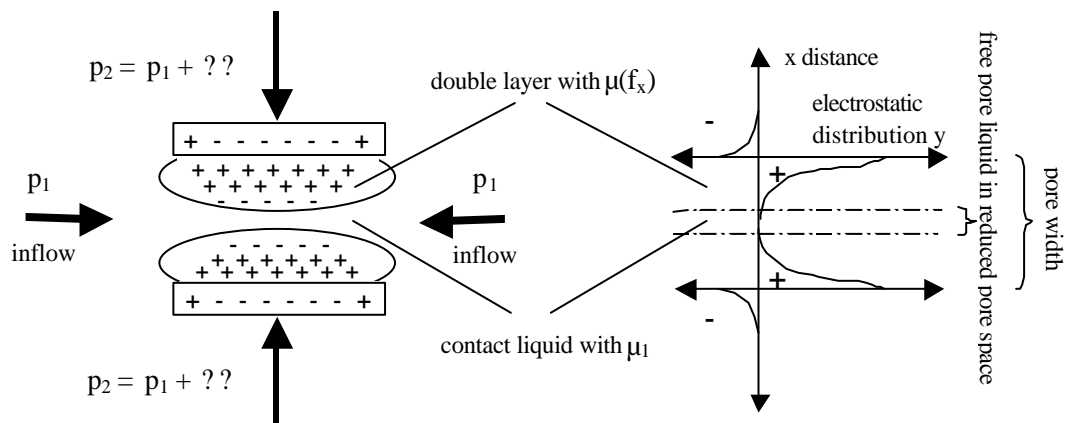
Figure 43: In case 1 an initially dry clay is saturated with a contact liquid with μ_1. The chemical potential difference is within the adsorbed double layer $\mu(f_x)$ of the particle and between the free uninfluenced pore liquid (μ_1) and the adsorbed water $\mu(f_x)$. The membrane effect is given due to electrostatic restriction of the solute. The pressure p_2 is higher than the pressure p_1 because of the osmotic pressure ?? . The case can be described by using the so called disjoining pressure model (pressure anisotropy)

_____

In case 2 the chemical potential difference is already given between the pore liquid of the saturated clay and the contact liquid.

The clay could act as a semi-permeable membrane because of electrostatic and mechanic solute retarding mechanisms as in case 1. The liquid enters the shale pores even though the material is already saturated, purely because of osmotic solvent flow. Another difference to the first case is the additional osmotic effect between the free pore liquid of the clay and the contact liquid.

Depending on the gradient of the chemical potential, an influx into the shale or an outflow into the reservoir of the contact liquid can occur (cf figure 42). If the chemical potential of the contact liquid is higher than that of the pore liquid we have an outflow and vice versa. This results in an increase or decrease of the pore liquid pressure respectively swelling or shrinking.
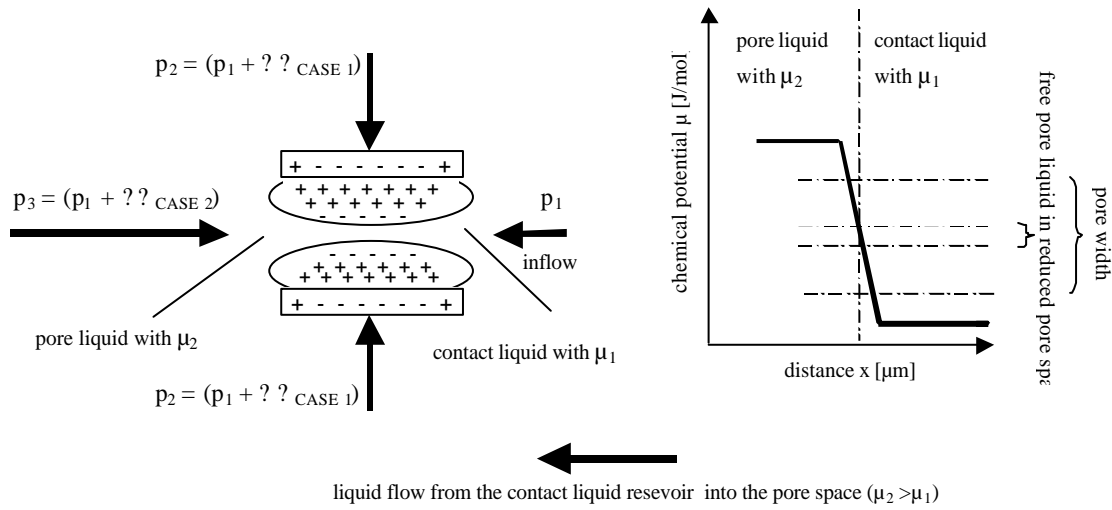
Figure 44: In case 2 the clay initially saturated with pore liquid (μ_2) is in contact with a contact fluid with μ_1. The potential difference is $|\mu_1| - |\mu_2|$. The membrane effect is again mainly because of electrostatic restriction of the solute. The pore pressure inside the shale p_3 is higher than the hydraulic pressure in the contact liquid system p_1 due to liquid influx and a resulting osmotic pressure $??_{Case2}$.

The following paragraphs will give an analytical formulation of the previously explained theories and we'll try to explain the problems we face by using these equations. Let's start with the definition of the chemical potential as it is one of the key parameters of osmosis, which is defined by the Gibbs equation:

$$dU = TdS - pdV + \sum_i \mu_i \, dn_i \qquad\qquad 15$$

U   internal energy [J]
T   temperature [°K]
S   entropy [J/molK]
V   volume [m3]
p   pressure [Pa]
μ_i chemical potential of the component i [J/mol]
n_i molar concentration of the component i [mol]

Alternatively to equation 15 we can relate the chemical potential to differentials of other properties with G as the free Gibbs energy [J]:

$$dG = -SdT + Vdp + \sum_i \mu_i \, dn_i \qquad\qquad 16$$

_____

This leads to the definition of the chemical potential for a pure component, which is the variation of the free Gibbs energy as a function of the concentration of the substance:

$$m_i = \left(\frac{\partial G}{\partial n_i} \right)_{T,p,(n_j)_{j \neq i}} \qquad\qquad 17$$

The subscripts outside the parentheses mean that these variables are held constant during differentiation.

For a non-ideal solution the chemical potential is defined by using the standard potential of the pure solvent (water) related to the activity of the solvent in the presence of solute (solution) and is given by equation 18:

$$\mu_s = \mu_S^0 + RT \ln a_s \qquad\qquad 18$$

μ_S chemical potential of the solution [J/mol]
μ_S^0 standard chemical potential of the pure solvent (water) [J/mol]
R   gas constant [8.3142 J/(mol °K)]
T   temperature [°K]
a_S activity of the solution [ ]

The chemical potential difference at a fixed temperature between the adsorbed water and the uninfluenced free pore liquid of the shale (case 1), or the free pore liquid and the potential of the contact solution (case 2) may be written as (19):

$$\Delta\mu = \mu_S^P - \mu_S^C = \mu_S^0 + RT \ln a_S^P - \mu_S^0 - RT \ln a_S^C = RT \ln \frac{a_S^P}{a_S^C} \qquad\qquad 19$$

μ_S^C = chemical potential of the contact (free) solution [J/mol]
μ_S^P = chemical potential of the shale pore solution [J/mol]
a_S^P = shale pore solution activity [ ]
a_S^C = contact (free) solution activity [ ]

The osmotic pressure difference is related to the chemical potential difference by equation (12) via the volume of solvent that crosses the membrane:

$$\Delta\mu = \overline{V_S}\, \Delta\Pi \qquad\qquad 20$$

? ?   = osmotic pressure difference [Pa]
V_S = partial molar volume of solution [m³/mol]

Equation (19) and (20) lead to the theoretical osmotic pressure difference in the case of an ideal semi-permeable membrane (21). This pressure is proportional to the activity imbalance between the adsorbed layer and the free pore liquid (case1), or the free pore liquid and the contacting fluid (case 2). This potential difference will be counterbalanced by a corresponding hydrostatic pressure (cf figure 41). [94, 60, 43]

$$\Delta\Pi = \frac{RT}{V_S} \ln \frac{a_S^P}{a_S^C} = r_s g \Delta h \qquad\qquad 21$$

$?_s$ density of the diluted solution [kg/m³]

_____

g   gravity constant [m/s²]
? h   liquid level elevation [m]

The activity of a solution can be expressed by using the fugacity ratio as the fugacity reflects the molar free energy of a liquid. For practical purposes a sufficient approximation is the replacement of the fugacity by the vapour pressure that can be easily determined, or even the relative humidity(22). [21, 82, 97]

$$a_s = \frac{f_s}{f_S^0} = \frac{p_s}{p_S^0} = \frac{HR}{100} \qquad\qquad 22$$

f_S fugacity of solution [ ]
f_s^0 standard fugacity of pure solvent (water) [ ]
p_s pressure of solution vapour [Pa]
p_s^0 standard pressure of solvent vapour [Pa]
HR   Relative humidity [%]

If we follow the preliminary theory given, shale can act as a semi-permeable membrane leading to either shale shrinkage or swelling and therefore a change of the stress-strain state of the rock. Argillaceous rocks can therefore theoretically exhibit high levels of osmotic suction (even if they are saturated) that can be treated as a negative chemical pore pressure. It is remarkable that they can have a liquid in their pores that exhibits an osmotic 'negative pressure' and also have a positive hydraulic pore pressure at the same time (proven by classic osmotic cell experiments of Pfeffer 1877). The aqueous chemical potential theory shows that the water in the shale is in a state of chemical tensile stress, which can be treated as a negative pore pressure.[21]

Because shale normally does not exhibit ideal membrane properties, and ions may be transferred, the real observed osmotic pressure will be less than the predicted theoretical by equation (21). To characterize the efficiency of the shale membrane the membrane reflection coefficient was introduced (23). [39]

$$K = \frac{-(n_s - n_w)}{n_w} \quad ; \quad \frac{n_s}{n_w} = 1 - K \quad ; \quad K = \frac{\Delta\Pi_{obs}}{\Delta\Pi_{theo}} \qquad\qquad 23$$

K = reflection coefficient [ ]
v_s = velocity of ion (solute) [ms^{-1}]
v_w = velocity of water (solvent) [ms^{-1}]
? $_{obs}$ = observed (measured) osmotic pressure difference [Pa]
? $_{theo}$ = theoretical osmotic pressure difference [Pa]

An ideal semi-permeable membrane system is characterized by K =1, indicating v_s=0, and all solute is reflected by the membrane and only solvent molecules can pass. Between 0<K<1presents solute(ion) flow through the membrane system and is usually in accordance with a shale membrane and is referred to as leaky membrane system. Introducing this reflection coefficient, equation (21) becomes:

$$\Delta\Pi = K\frac{RT}{V_S}\ln\frac{a_S^P}{a_S^C} \qquad\qquad 24$$

The problem we face, if we want to apply these equations, is the estimation of each parameter. The determination of the exact initial chemical potential of the pore liquid is difficult as it's not a simple

_____

issue to extract the liquid without influencing it, or to introduce a gauge into the material to measure it.

In the case of the estimation of the potential gradient within the double layers of adsorbed water of the clay particles (case 1) the experimental approach is unrealistic and Graham therefore formulated the relation between the negative surface charge of the particle and the solute distribution with equation 25. This equation is based on a distribution of the ions in the water layer of a particle according to the Boltzman statistic. Only electrostatic forces between the ions are taken into consideration. The interaction between the solute and the solvent like Van der Waals forces or Brown motion are neglected and the molecules are considered ideally shaped.

$$U_s = e\,e_0 \mathrm{K} j_{(0)} \qquad\qquad 25$$

U_s negative electrical surface charge of the particle [C/m²]
e dielectric constant of the pore liquid [As/Vm]
e_0 dielectric constant under vacuum [ ]
K   1/K Debye length of the solution [ ]
$j_{(0)}$ electrostatic potential at the surface [V/m²]

The factor 1/K is the so called Debye length which depends only on the chemical properties of the solution. The higher the solute concentration of the liquid the shorter this length and the shorter the interaction radius of the platelet. K takes the different ion species, their valence and their concentration in the pore liquid into consideration (26):

$$K = \sqrt{\sum_{i}^{n} \frac{c_{i(\infty)} e^2 z_i^2}{e\,e_0 k T}} \qquad\qquad 26$$

i…n   number of ion species [ ]
c   ion concentration [mol/l]
e   elementary charge [C]
z   valency of the ion [ ]
k   constant of Boltzman [J/K]
T   temperature [K]

This relation between the ion concentration gradient in the double layer and a resulting chemical potential difference within the layer. It is a purely theoretical approach and shows the problem of estimating the parameter in order to calculate the osmotic pressure of shale.

The next problematic parameter is the membrane itself. It could be observed in tests [60] that the membrane efficiency of shale depends, in general, on the stress state of the rock. Changes in the confining pressure and the axial load in triaxial tests alter the results in terms of osmotic pressure in a wide range.[7, 14]

In the case of micro-crack induction in the rock (for example due to high hydrational or osmotic stresses) the effect of osmosis is completely overshadowed (leaky membrane due to cracks) by the strength reducing effect of cracks.[47]. If we remember the dynamic behaviour of the double layer thickness and the effective porosity - (chapter 2.3.2) - with reference to temperature, pressure and ion concentration in the pore liquid, it's easy to get an idea about the complexity of this phenomenon (27):

$$\Delta\Pi = f(\Delta m, s) \qquad \Delta\mu = f(\mu_1, \mu_2, p, T, e) \qquad s = f(p, T, k, \Phi) \qquad\qquad 27$$

_____

Furthermore we have to take possible dissolution processes between the shale and the liquid into consideration as well as the mineralogical properties of the shale.

Another interesting question is whether or not we should consider the osmotic pressure as a transient problem over time. It seems to be very unlikely that an initially built up osmotic pressure will exist for a long time interval. The dynamic of changes within the clay is too high to look at it as a static pressure anisotropy problem.

However, despite all the contradictions and divergences about Osmosis, the recent drilling mud technology is widely based on the coupling of osmosis ("balanced activity concept") and advection (hydraulic gradient to describe and predict the shale mechanics of the well [21, 23].

In daily practice the specimen is exposed to several controlled environments with different relative humidity. According to equation 22 we can estimate the overall activity of the shale by finding the relative humidity value where the shale neither gains nor looses weight due to water hydration or dehydration, as a function of external stress. Once the shale activity is estimated it's easy to calculate the theoretical osmotic pressure when in contact with another fluid with defined activity (eq. 21). The measured osmotic pressure from a lab test is afterwards compared with the calculated one to define the membrane efficiency R. This purely empirical approach does not allow for any interpretations about the how and why and is only applicable for the short term well stability problems in the petroleum industry.

To predict the behaviour of clay under the influence of osmosis over a longer time period the theory seems to be insufficient as we lack the quantitative estimation and qualitative formulation of the previously described parameters.

2.3.6   Entrapment and pressurization of air bubbles

If a shale dehydrates, it may pass the air entry point, which allows air or any other gas to enter the pores. When the partially saturated material is in contact with an aqueous solution, hydration by capillary imbibition and other mechanisms occurs. This hydration process can theoretically lead to the entrapment and pressurization of air bubbles and might be responsible for causing tensile cracks in the shale (cf figure 45). This would mean that hydration and dehydration under the presence of air cause irreversible damage of the material.

This theory is denied by some scientists, who assume that the gas is not pressurized, but gas diffusion of the small bubbles is thought to happen. This means that the bubbles are in energetic equilibrium with the fluid. The diffusion model therefore denies the possibility of crack induction.

The question about the role of gas inside a shale during rehydration is of interest, as we might deal with partially saturated shale in the labs and in the underground construction site.

In the EDZ zone of the construction site, for example, shale may easily dehydrate beneath the air entry point during the excavation works. After the site is refilled, there is a strong likelihood that the material will be rehydrated. Also specimens used in lab tests may be dehydrated due to insufficient sample preservation and later rehydrated in tests.

Another theory supposes, that the relaxation of the material during sampling could lead to cavitation phenomena as the pore space increases. The pore liquid could thus be depressurised beneath the bubble point pressure, which results in the evasion of the dissolved gas.

Let's first consider the capillary pressure in a capillary tube of 1 nm diameter. An interfacial tension of water of $72 \cdot 10^{-3}$ N/m combined with a total wettability of $\cos? = 1$ results in a pressure difference of 145 MPa according to the equation of Laplace. As the shale from the site of Est comprises nano sized pores, the consequence could theoretically be a damage in the form of micro cracking in the shale, as the tensile strength is between 0.9 and 5.4 MPa.

_____
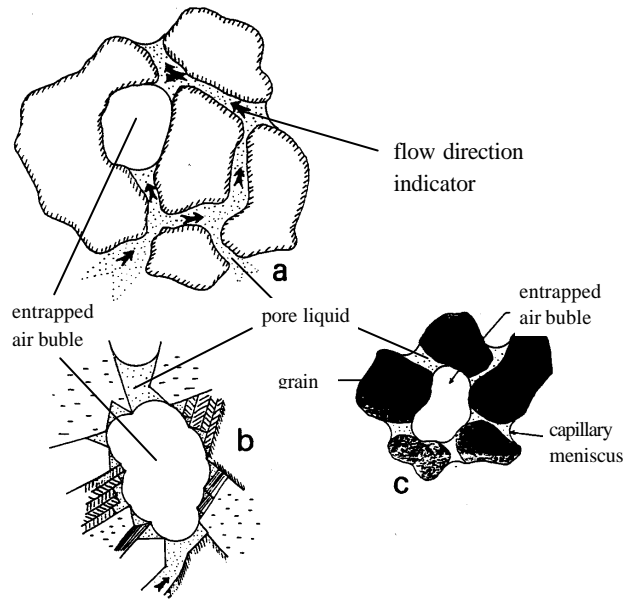
Figure 45: Possible air entrapment in a porous system caused by a short circuit in a macro pore (a),
in a rough macro pore (b), and by condensation of water in pore accesses (Schmitt et al 1994)

According to Mariotte's law (28), pressure is inversely proportional to the occupied volume. A reduction by 5 times of the volume of gas under atmospheric conditions leads to a pressure of 5 MPa, which corresponds approximately to the tensile strength of the shale.

$$p_{gas} = \frac{p_{atm} V_p}{V_{gas}} \quad \vee \quad p_{gas} = \frac{p_{atm} V_p}{V_p - V_{water}} \qquad\qquad 28$$

p_{gas} = gas pressure in the pores [Pa]
V_{gas} = volume occupied by the gas [m^3]
p_{atm} = initial gas pressure (atmospheric) [Pa]
V_p = initial pore volume occupied by gas [m^3]
V_{water} = volume invaded by water [m3]

If we introduce the law of Laplace into the law of Mariotte, we can express the relation between the gas pressure of spherical shaped entrapped gas bubbles and the existing pore volume of the material (29):

$$p_{atm} V_p = \frac{32 s^3 p}{3 p_{gas}} = \frac{8}{3} s p \ r^2 \qquad\qquad 29$$

r = radius of entrapped gas bubbles

Schmitt et al. as well as Santarelli et al. concluded after tests, that swelling and destruction is mainly caused by capillary phenomena (for unsaturated samples) and therefore not representative for onsite material behaviour. They state that shale reaction is mostly due to lab artefacts .

In contradiction to that, Santos et al concluded, that the pore water content, the amount and distribution of the water controls shale reactivity, and not the presence of air in the material.

_____

2.4   Swelling and shrinking of shale

As explained in the previous chapter, a change of the moisture content may alter the specific volume of the material. This means, when in contact with a hydrous solution (or polar molecules in general), some shales either swell or shrink under certain circumstances. The swelling/shrinking rate depends on the composition, concentration and pressure of the pore-liquid and the type, stress state and initial saturation of the shale. If the volume change is constrained, a swelling pressure is developed which acts against the constraint. This pressure can reach values up to 8 MPa. [5, 54]

The micro-scale processes adsorption, absorption, osmosis and probably capillarity are in summary responsible for these macro-scale behaviour patterns, due to changing moisture contents.

$$e_v = \frac{V_v}{V_s} \quad e_w = \frac{V_w}{V_s} \qquad 30$$

e_V void space ratio [ ]
e_W water content (vol. ratio) [ ]
V_S volume of the solid [m^3]
V_P pore volume [m^3]
V_W water volume [m^3]
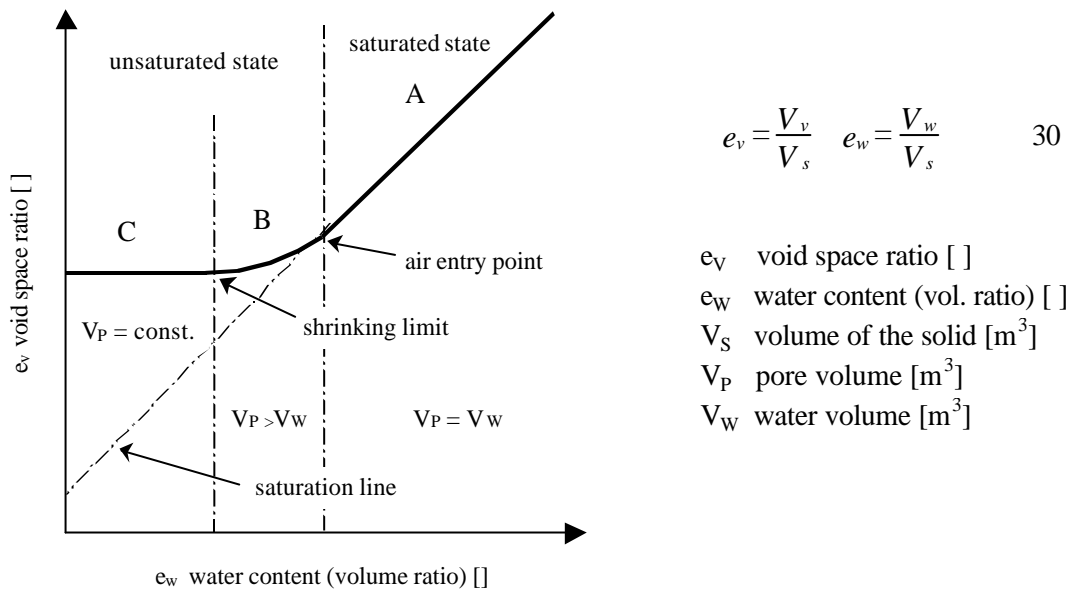
Figure 46: schematic drying curve of a shale that represents the volume change due to a change in water content

The general shrinkage curve of a shale (cf figure 46) can be described by three phases:

Region A: every change in the water volume corresponds to the same change in shale volume, i.e. water content and volume have a linear relation as the shale structure compensates the drainage and stays saturated. This saturated region of the shale ends when air is allowed to enter the specimen (air entry point).

Region B: the volume change of the shale sample is smaller than the drained volume of water. The shale can not compensate the liquid loss any longer. Air enters the shale in this phase (drainage by imbibition). The sample is already in an unsaturated state and the region ends at the shrinkage limit.

Region C: no variation of the shale volume can be observed, although the drainage processes continues i.e. liquid loss continues. The shale is stabilised due to inter-granular contact when the water content falls under the value corresponding to the shrinkage limit point. [29]

The expression of the volume change with changing water content is very helpful and a common procedure in characterizing shale. Figure 47 represents the shrinkage curve of a Callovo Oxfordian shale from the site of Est.

_____

Figure 47: drying curve of the shale from the
site of Est (ANDRA 1997)

The relation of each of the three regions of the shrinkage curve to the corresponding hydration mechanism is still not exactly defined. But there i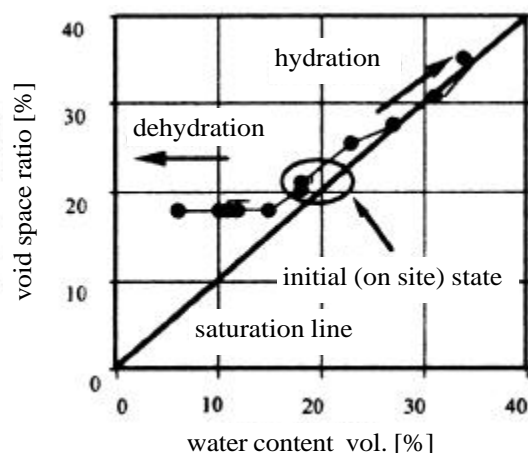s general agreement that capillarity, adsorption and absorption play a major role for unsaturated shale, whereas osmosis is often denied.

In conventional practice , maximum swelling pressure is defined as the pressure applied to the shale to prevent any volume increase when the shale is exposed to water. There are commonly three types of oedometer tests used: the free swelling test, the constant volume test and the Huder-Amberg test. [4, 54, 74, 91]

The constant volume test consists of a rigid cell where the volume of the sample is held constant, and the stress generated by the shale due to swelling is measured. To simulate onsite conditions, the sample is normally also pre-stressed in the cell prior to the test. This test allows the evaluation of the maximum possible swelling stress of a material

Alternatively, the free swelling test allows the shale to produce a certain swell-strain. Once the limit of this strain increment - which is not standardized - is reached, the volume is reduced to the initial sample volume by applying an external force. The force necessary for this volume reset is thought to correspond to the swelling stress.

Another possibility is the Huder –Amberg testing method. The sample is pre-stressed according to the onsite stress and then put it into contact with the fluid. Afterwards the external load is released step by step and the swell heave according to each load state is documented.

All these three tests are performed by using liquids and they only take the axial deformation into consideration. Several different triaxial strain methods including radial strain measurement were developed recently, but are not yet common practice.

With reference to the conditions in the underground site, the possible influence of hygrometry on the behaviour of the shale should be analysed. i.e. it requires a testing procedure that evaluates the influence of different moisture degrees in the air on the swelling/strain behaviour of the sample. An isotropic lateral confinement pressure is not necessarily required, as the EDZ in the gallery no longer exhibits initial stress conditions.

In the practical part of the thesis we present an appropriate sample holder as well as an air conditioning system. This equipment permits the realisation of different hygrometry swelling/strain tests with the shale under uniaxial load.

_____

2.5　　The potential of the pore liquid and total suction

As introduced, a change of the saturation state of shale may change its physical characteristics. This change relies on migration of fluid into, or out of the shale system. We therefore examine a short discussion of the concept of potential in this chapter, as it is a common approach to describe the mechanics of liquid movement in shale.

A potential is defined as a physical quantity, capable of measurement, whose properties are such that flow always occurs from regions in which the quantity has higher values to those of lower values. This applies regardless of the direction in space of the migration.

The international committee on soil science redefined the total potential of the constituent water at a point in a soil at temperature: It is the amount of useful work per unit mass of soil water that must be done by externally applied forces, to transfer reversibly and isothermally an infinitesimal amount of water from the standard state to the soil liquid phase at the point under consideration.

The total potential of a pore liquid therefore represents its energetic state. No fluid migration occurs if the shale liquid system is energetically balanced. In the case where this system is not equilibrated fluid migration happens in order to re-establish balanced conditions.

In the chapter of osmosis we noted that the chemical potential is expressed in Joule par molar substance [J/mol]. It can be interpreted as the energetic state of a certain number of molecules of a species. In soil sciences potential is often expressed in terms of energy per unit mass of groundwater [J/kg]. Alternatively it can be expressed as energy per unit of volume [J/m^3], which has the unit of pressure [Pa]. If we divide this form by the product of the water density and the gravity, the potential quantity has units of length [m] and is referred to as head, similar to a hydraulic head, which is widely used in hydrogeology. The logarithmic expression of this height equivalent is the so called pF scale in [cm], which is commonly used in agriculture. The correlation of the different units as well as their relation to the total suction is given in table 3. [29]

The total potential of a pore liquid (31) has a number of components that influence its actual state. It is considered as the sum of different particular potential, whereby this additivity is hypothetical.

$$\psi_{tot} = \psi_{grav} + \psi_p + \psi_\Pi \qquad\qquad 31$$

ψ_{tot}　　total potential
ψ_{grav}　　gravitational potential
ψ_p　　pressure potential
$\psi_?$　　osmotic potential

The gravitational potential represents the work necessary to transfer the liquid under the influence of the gravitational field of the earth. It is the work done per unit mass in raising the water isothermally and isobar to elevation z.

$$\psi_{grav} = \rho_w g z \qquad\qquad 32$$

ρ_w　　density of the pore water [kg/m^3]
g　　gravity [m/s^2]
z　　elevation [m]

The pressure potential refers to the work necessary to change the pressure of the pore liquid and is expressed by equation 33, which describes a hydro static pressure head equivalent:

$$\psi_p = \rho_w g h \qquad\qquad 33$$

_____

h   pressure head [m]

The pressure potential itself is the sum of several other potential as given in equation (34):

$$\psi_p = \psi_a + \psi_{pc} + \psi_{pn} \qquad\qquad 34$$

ψ_p pressure potential
ψ_a adsorption potential
ψ_{pc} capillary potential
ψ_{pn} pneumatic potential

The sum of the adsorption and capillary potential are also referred to as matric potential. Matric potential arises from the interaction of pore water with the matrix of solid particles that influence the pressure state of the pore liquid. The nature of the capillary pressure drop and the adsorption mechanism are described in chapter 2.3.2 and 2.3.4. The pneumatic potential is the pressure in the gas phase (atmospheric in the lab).

The gravitational and pressure potential can also be expressed by using the equation of Bernoulli and neglecting the velocity term in it, as the migration speed in shale is considered to be very slow. Hence this approach doesn't take any liquid-solid interaction into account, and reflects only the mechanical part of the pressure potential.

Finally the total potential of a pore liquid in shale can be expressed as the sum of all these different potentials:

$$\psi_{tot} = \psi_{grav} + \psi_a + \psi_{pc} + \psi_{pn} + \psi_\Pi \qquad\qquad 35$$

As mentioned the potential can be expressed by several different units. One possibility is the expression of the potential by using pressure units. We also examined in the chapter of capillarity that the pore liquid can be in a state of tension and therefore exhibit a negative pressure which can be seen as suction (capillary pressure curves). For a shale system the total suction has to take the liquid solid interaction into consideration and thus comprises matric suction and osmotic suction.

If the atmospheric pressure is taken as zero, the matric suction is the absolute sub-atmospheric pore water pressure and is equal to the capillary pressure. The application of Kelvin's relation (cf chapter 2.3.5) for the osmotic pressure and the capillary pressure leads to the total suction:

$$S_t = \frac{RT\rho_w}{M_w}\ln\left(\frac{p_S^A}{p_S^0}\right) = \frac{RT\rho_w}{M_w}\ln RH \qquad\qquad 36$$

S_t total suction [Pa]
p_S^A partial vapour pressure of water within the air [Pa]
p_S^0 partial standard vapour pressure of the solution [Pa]
M_w molar mass of the solvent [kg/mol]
ρ_w density of the solvent [kg/m³]

The interpretation of equation (36) is such, that the humidity, to which a shale is exposed, creates a certain suction (cf table 3). Consequently the shale either takes in water or looses it. However, the shale will neither gain nor loose any weight, after a certain period of time, in a constant environment. This means the water content won't change any further and the material is equilibrated. This relation is the basis for several methods of measuring the total suction, acting in a clay medium, under laboratory conditions.

_____

hygrométrie	succion (MPa)	hauteur d'eau équivalente (m)	pF
100%	0,00	0	−∞
99%	1,31	131	4,12
98%	2,64	264	4,42
97%	3,98	398	4,60
96%	5,34	534	4,73
95%	6,70	670	4,83
90%	13,8	1377	5,14
85%	21,2	2124	5,33
80%	29,2	2917	5,46
70%	46,6	4662	5,67
60%	66,8	6677	5,82
50%	90,6	9060	5,96
40%	120	11977	6,08
30%	157	15738	6,20
10%	301	30098	6,48
0%	+∞	+∞	+∞

table 3: the different units of succion and their relation, using the law of Kelvin
to calculate the total suction of a corresponding humidity [Rambambasoa 2000]

In practice, the total suction is determined by performing a multi stage experiment, in which a clay sample with a known initial water content is exposed to air at various controlled relative humidity levels at a constant temperature. By weighing the sample at each equilibrium stage, a graph can be plotted showing gravimetric water content against relative humidity (cf figure 48). This relation is renown as the water retention curve or adsorption-desorption isotherms. These curves are characteristic for each shale as they represent their affinity for water in terms of suction for certain degrees of saturation. To calculate the volumetric water content, the change of the volume of the material must be measured, which is not a simple issue regarding the precision required.
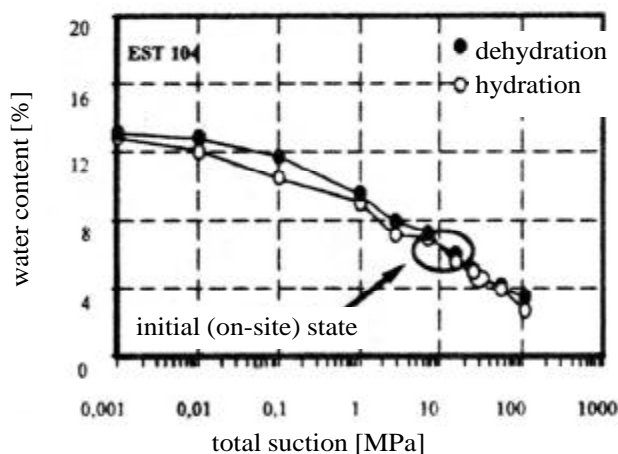
Figure 48: result of hydration and dehydration
of shale from the site of Est [Andra 1997]

The difference to the classical capillary pressure curves presented in the chapter 'capilarity' is such: the adsorption-desorption isotherms take the physico-chemical solid liquid interaction into account which corresponds to the total suction.
But as the water retention curves are measured on unconfined samples they don't represent the on-site behaviour of shale, whose initial stress state is different due to the acting overburden pressure.

The creation of controlled humidity environments is normally realised by using different types of saturated salt solutions. These salt solutions create a certain humidity under constant temperature conditions. The sample is therefore placed in different vacuum desiccators with different solutions and thus different humidity conditions. Table 4 represents the humidity values created by these different salt solutions.

Solutions salines saturées	Humidité relative (%) à 30 °C
$CuSO_4,5H_2O$	98*
$Na_2SO_3,7H_2O$	95*
KCl	83,62
NaCl	75,09
$NaNO_2$	73,14
NaBr	56,03
$CaCl_2,6H_2O$	36,5*
LiCl	11,28

Table 4: the different relative humidities created by different saturated
salt solution in desicators according to Daupley 1997

The limited volume of the desiccators is a disadvantage, as it limits the installation of any measuring gauges. Another possible procedure is the use of a climate box which allows the variation of humidity and temperature in a wide range without displacing the sample several times. Such a computer controlled air conditioning system will be presented in the practical part of this thesis, as it was used to conduct the tests in our lab.

_____

2.6   Conclusion

A description of the general shale structure and the most important clay minerals of the shale from the site of Est was presented. The fluid clay interaction mechanisms were introduced and show clearly that shale can be very reactive when in contact with a wetting polar liquid.

Some of the physical, mechanical and chemical parameters of shale have to be considered as state variables, rather than static parameters. Permeability, porosity, mechanical strength, pore liquid pressure and the electrochemical properties of the clay platelets may vary in a wide range. These alterations are mainly related to the saturation of the shale, it's pore liquid composition and concentration as well as the physical conditions such as stress state and temperature.

Concerning the distinct physico-chemical mechanisms it can be concluded that:

Adsorption is believed to influence the properties of shale more than thought. The thickness of the adsorbed water layers varies from some nm to μm, mainly depending on the character of the pore liquid and the clay species. Considering the enormous specific surface of shale it is easy to imagine that the thickness of the covering water layers of the clay particles influence the strength and transport properties. This assumption is strengthened by the theory that plasticity and creep mechanism can result from clay particle/sheet slipping and sliding of dislocations.

Furthermore the adsorbed water exhibits an internal gradient of the ion concentration, which also gives the shale it's semi-permeable characteristic and fosters osmosis. We therefore conclude that osmosis is very likely to occur in shale, and yes, shale can act as a semi-permeable membrane. The disjoined pressure and pressure overheads can thus be partially explained by the combination of osmosis and adsorbed water.

Absorption of water produces the highest swelling or shrinking strains in Smectite rich materials. This mechanism governs the mechanical connection of the Smectite sheet layers. Depending on the chemical character of the pore fluid it can lead to complete dispersion, cracking or mineralogical transformation of the material. The mineralogical transformation normally requires a change of temperature, but can also take place under constant temperature conditions, as for example the Smectite transformation by K^+ ions. Absorbed water can have a very dramatic effect on the overall characteristic of Smectite rich shale.

The superposition of the capillary meniscus and the adsorbed water layer in a shale pore requires a new reflection of capillarity for this material. There is a likelihood that entrapped air bubbles in shale may be pressurized due to capillary mechanisms and lead to damage of the material. Capillarity is not the only mechanism held responsible for the material's high affinity for polar wetting fluids.

Concerning the shale from the site of East, the mineralogical composition indicates, that the material could be very reactive to water based solutions. As the composition of the material varies over depth, this statement is only valid for materials, which contain Smectite minerals and a high clay content combined with a small calcite percentage.

The general problem of modelling a shale system is the micro-macro transfer, where the micro mechanisms cause a certain macro comportment of the shale. The macro behaviour of a shale-liquid system is the superposition and summary of the micro mechanism. Unfortunately it is not yet possible to quantify and separate the influence of each mechanisms. The message is clear: we have to address the physico-chemical clay liquid interaction when modelling shale.

Finally we conclude that anisotropic damage of the clay matrix due to solid fluid interaction is very likely. These damages would not be the result of an external applied force, but related to the internal micro mechanisms in shale. The deterioration could have the form of micro cracks.

3   Micro cracks in shale

As one of the primary requirements of a waste disposal facility is to avoid migration of the contaminants into the biosphere under all circumstances, any possible change of the fluid transport mechanism has to be investigated. Furthermore the mechanical stability of the underground construction has to be guaranteed. Micro cracks are likely to influence the transport and diffusion properties as well as the mechanical characteristics of shale.

In this chapter we therefore highlight the importance of micro-cracks, and how they can be detected using X-ray microfocus technology.

3.a   Résumé sur la micro fissuration

Les micro-fissures influencent probablement les propriétés de transport des liquides et de leur diffusion ainsi que les caractéristiques mécaniques de l'ardoise.

La zone de perturbation due au creusement dans des formations argileuses montre souvent des macro fissures et des micro fissures provenant de la modification de l'état des contraintes initiales et des conditions de saturation. Les micro fissures peuvent être provoquées par le changement de l'état des contraintes initiales et du degré de saturation dans le matériau ainsi que par les réactions chimiques entre les minéraux argileux et le liquide interstitiel.

Ces fissures peuvent être d'une nature structurelle ou intrinsèque. Les fissures intrinsèques sont associées aux propriétés des matériaux. En revanche les fissures structurelles sont le résultat des conditions d'appui mécanique.

La plus grande difficulté est de détecter les micro-fissures. La méthode la plus courante est de préparer des lames minces du matériau et de les analyser en utilisant un microscope électronique à balayage. La préparation de ces lames minces est très difficile car le broyage est une méthode plutôt inadéquate pour analyser les micro-fissures. Dans l'ardoise on rencontre des micro fissures surtout sur des surfaces stratifiées. C'est à dire, que si nous voulons les visualiser nous devons broyer le matériau perpendiculairement aux surfaces stratifiées ce qui risque d'obstruer les fissures existantes ou de créer de nouvelles fissures. De plus, comme l'échantillon est détruit après la préparation nous ne saurons jamais comment les fissures se seraient développées sous d'autres conditions.

La tomographie et la radiographie aux rayons X à haute résolution rend possible la visualisation non destructive à deux ou trois dimensions des structures intérieures d'un objet ce qui n'est pas visible à la lumière du jour mais uniquement sous les rayons X. Le principe de la tomographie consiste dans l'irradiation de l'échantillon avec des rayons X sous différents angles afin de créer un ensemble de données 2D des caractéristiques intérieures de l'objet. Un algorithme de reconstruction utilise l'ensemble des données 2D pour reconstruire le modèle de l'objet en 3D.

En traitant l'objet aux rayons X, la radiation est ralentie et l'intensité permanente des photons est enregistrée par le détecteur. L'interaction des photons de rayons X et des atomes du matériau provoquent le ralentissement de la radiation. Ces mécanismes interactifs sont surtout l'absorption des photons et la dispersion. Le ralentissement est une fonction du numéro atomique des éléments à l'intérieur de l'échantillon et de la densité des matériaux. Plus la densité de l'objet est élevé et le nombre atomique des éléments existants augmentent, plus la radiation ralentit.

La technologie aux rayons X est un outil approprié pour visualiser la structure intérieure de l'ardoise. La différence dans le ralentissement des rayons X entre les fissures et les composants de l'ardoise permet une visualisation nette des micro-fissures et des caractéristiques intérieures de l'ardoise. Une résolution maximale de 2μm (taille du pixel de l'image) est possible. La technologie utilisée par l'Institut Fraunhofer a rendu possible une résolution de 20μm pour des échantillons cylindriques (16 mm diamètre, 30mm hauteur).

_____

3.1   Introduction into micro cracks

The term micro crack refers to fissures with an aperture of some micrometer and a length of up to some millimetres (cf figure 49). Even though the distinction between fissures and cracks is not clearly defined in literature, the term micro-crack is probably best applied to the more indurated rocks which exhibit brittle failure, whereas the term micro fissures should be used for plastical clays.
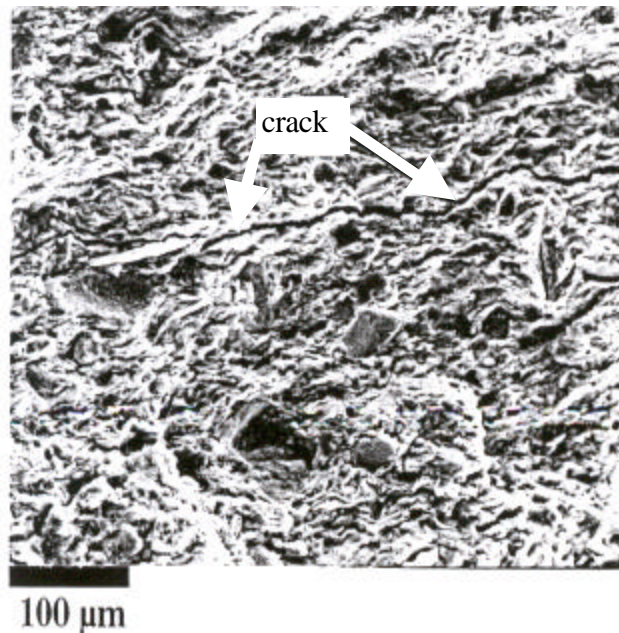

Figure 49: Scanner electron microscopy image of a small micro crack
with a very weak aperture in the shale of Tournemire [Daupley 1997]

Shale may initially have existing onsite cracks and post-initial cracks, which were induced by an alteration of the onsite pressure and saturation conditions.

Initial cracks are generated when the pore fluid pressure approaches the lithostatic pressure of the formation, leading to micro cracking of the shale, which is possible under certain geological conditions. These micro cracks are thought to support the pore liquid expulsion and thus the migration of fluid. This theory describes one of the main mechanisms of hydrocarbon migration from the mother rock to the reservoir rock.

Post-initial cracks are induced due to a change in the original stress and saturation state of the material. Altered stress conditions, changed moisture contents as well as chemical reactions due to fluid shale interaction are generated in the excavation damage zone due to the construction works.

Capuano [17] tried to give evidence that initial micro cracks exist and that they support fluid flow through shale. She performed a number of scooping calculations on the possible effect of micro-cracks on the permeability by introducing a crack surface factor into the so called cubic law for flow in a fracture (cf equation 37). Her calculation resulted in a strong increase of the hydraulic conductivity of the shale due to micro cracks by 8 to 9 orders of magnitude larger than the typical matrix permeability of the compacted shale.

_____

$$K_{cr} = \frac{N r_w g d^3}{12 h_w f}$$

37

K_{cr}	effective hydraulic conductivity [m²s⁻¹]
N	number of parallel microcracks per unit width across a plane normal to the flow ( )
$?_w$	density of fluid [kg/m³]
g	gravity constant [m/s²]
d	aperture of the micro cracks [m]
$?_w$	dynamic viscosity [Ns/m²]
f	crack surface caracteristic factor [ ]

If the ideas of Capuano about the influence of micro cracks are correct, they have to be taken into consideration of fluid flow models.

Chiarelli et al. [26] concluded that the induction and propagation of orientated micro cracks is responsible for induced anisotropic damage of the material. Induced anisotropic damage is defined as the deterioration of the elastical parameters of the material. Many shale exhibit a very low plasticity threshold value hence irreversible deformations already appear under small loads. The message is clear: micro cracks are very likely to be related to time dependent behaviour like creep and the general failure mechanism of shale, as well as to strains with a large irreversible portion.

The excavation damage zone in shale formations often exhibits macro-cracks and micro cracks due to changes of the initial stress and saturation conditions. These cracks can be of a structural nature or of an intrinsic nature. Intrinsic cracks are related to the material properties, whereas structural cracks are the result of the mechanical support conditions.

An explanation is given in figure 50. The bar in case 1 is not allowed to expand or contract in any direction due to the fixed support conditions. Any treatment which normally results in a volume change of the material causes stress, which can create micro-cracks if the stress state approaches the mechanical strength of the material. These cracks are so called structural cracks as they also depend on the structure of the support system.

In case 2 the material is allowed to dilate completely free in any direction. Any treatment leading to a volume change of the material also alters the stress state, but the stress is only related to the intrinsic material properties and not to the support conditions as in the first case. That's why cracks generated under such conditions are so called intrinsic cracks.

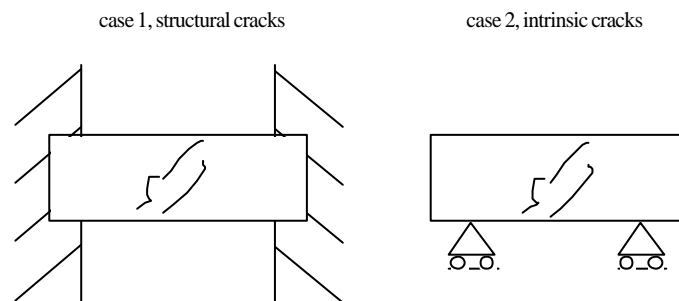case 1, structural cracks   case 2, intrinsic cracks

Figure 50: Schematic difference between structural and intrinsic cracks. Intrinsic cracks are related to the material properties, whereas structural cracks also depend on the support conditions of the system

In the case of waste repository both types of cracks are of interest, structural and intrinsic cracks in the EDZ and intrinsic cracks in the uninfluenced barrier formation. The question is whether or not shale from the site of Est exhibits the property of intrinsic cracking.

Some investigations of thin cross sections concluded that a decreasing water content of the shale matrix leads to shrinking and thus to cracking around imbedded quartz grains. These cracks refer to as intrinsic cracks.

Should intrinsic cracking exist, the matter of interest are the conditions which foster or inhibit the micro cracking of shale. Conditions, such as stress, chemistry and pressure of the pore fluid, saturation and temperature.

3.2 The detection of micro cracks

The biggest problem we face when we deal with micro cracks is their detection. How can we detect them under conditions which don't close existing cracks or create new cracks?

The most commonly used technology is to prepare thin cross sections of the material and to analyse them by using scanner electron microscopy or tunnel electron microscopy. The preparation of the thin cross section is quite difficult, as the grinding of the material is a rather inappropriate method concerning micro cracks. In shale the micro cracks occur mostly within the bedding planes. This means if we want to visualize them we have to grind the material perpendicular to the bedding plane which might close existing cracks or create new cracks.

In literature we find cases where theories about micro cracks have been challenged due to the preparation techniques used for thin cross sections. Miliken and Land [58] for example disagreed with Capuano [17] about her results, as they thought it possible that at least some of the crack features seen in thin sections are artefacts of specimen preparation.

A similar situation concerned the saturation of Smectite rich shale with a solution containing Potassium. The result is often a shrunken shale combined with an increased permeability by the factor of two [47]. The theory suggested that the increase of permeability is very probably due to micro cracking in the shale. No evidence was brought to support the theory, as an appropriate technology to detect the micro cracks was lacking.

Thin cross sections deliver only in two-dimensional images of the crack system. Attempts were made to prepare a big number of cross sections of a sample and to reconstruct a three-dimensional model by using special software. The effort necessary to reconstruct a relatively small volume of a sample is in no relation to the accuracy of the pictures, from the authors point of view. Furthermore the sample is destroyed after the preparation and we will therefore never know how the cracks would have developed under changing conditions.

The conclusion is that we were looking for a non destructive three-dimensional detection of micro cracks in shale, that allows us to observe the cracks under different conditions. A possible technology is the two dimensional computer microfocus X-ray radiography (2D µCR) and the three-dimensional computer microfocus X-ray tomography (3D µCT), as will be introduced in the next chapter.

3.2.1 The microfocus X-ray radiography and tomography

Computer X-ray tomography (CT) enables the non destructive three-dimensional visualisation of the inner structures of an object, which may be not transparent to visual light but to X-rays. The technology was initially developed in the 1970's for medical purposes. In the late 1980's the technology found it's introduction into other disciplines, such as material and geological sciences. The problem with this technology in the early days was it's limited resolution of about 0,5 mm within the slice and 1mm slice thickness. In the 1990's the resolution could be enhanced by the use

of new microfocus X-ray tubes [93]. Recent technology at the European Synchrotron Radiation Facility institute permits a resolution less than 2 μm.

X-rays are electromagnetic radiations comprising photons, exhibiting dualistic properties of wave and mass. The commonly used x-ray radiation for μCT exhibits a radiation energy between 20 and 200 keV, with a spectrum of wave length from 0,06 to 0,6 ? .

The principle of tomography is the irradiation of the sample with x-rays under many different angles, in order to produce a 2D dataset of the inner features of the object corresponding to the different angles. A reconstruction algorithm uses the 2D data to reconstruct the 3 D model revealing the inner structures of the object (cf figure 51). In practice the sample is positioned on a rotating table between the x-ray source and a detector. (cf figure 52)
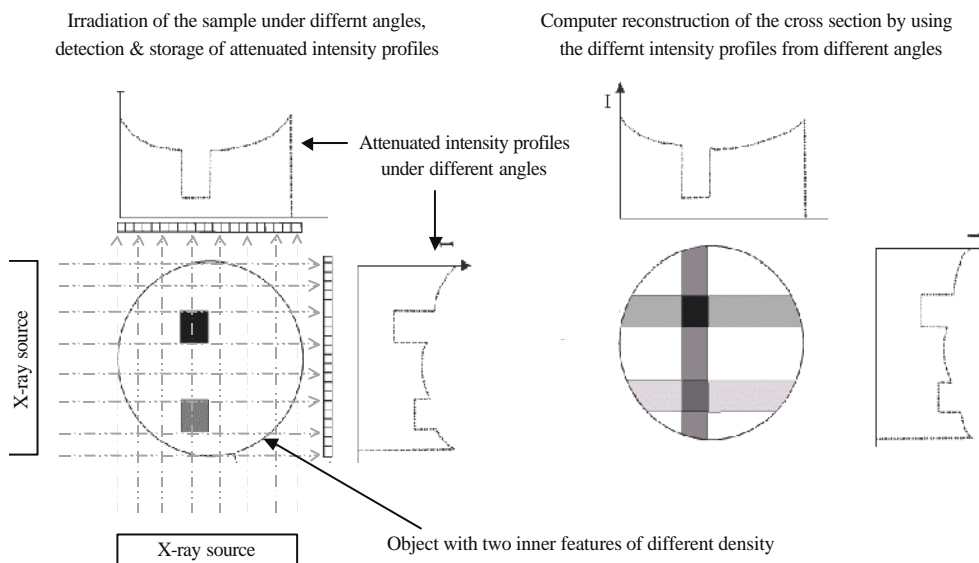
Irradiation of the sample under differnt angles, detection & storage of attenuated intensity profiles

Computer reconstruction of the cross section by using the differnt intensity profiles from different angles

Attenuated intensity profiles under different angles

X-ray source

X-ray source

Object with two inner features of different density

Figure 51: scheme of the μCT with the irradiation of the sample under different angles and the following reconstruction of the intensity profiles to obtain the cross section [Van Geet 2001]

When the object is irradiated with the x-rays, the passing radiation is attenuated and the remaining intensity of the photons registered by the detector. Attenuation of the radiation is caused by an interaction of the x-ray photons and the atoms of the material. These interaction mechanisms are mainly photon absorption and scattering. Absorption is the complete removal of a photon from the radiation beam, whereas scattering addresses the deflection of a photon into a random course.
Attenuation is a function of the atomic number of elements inside the sample and the materials density. The higher the density of the object and the atomic number of it's comprising elements, the higher the attenuation of the x-ray beam.
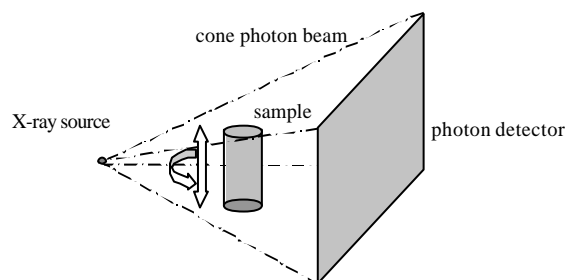
cone photon beam

X-ray source

sample

photon detector

Figure 52: μCT, sample on a rotating table between the source and the detector

In the case of a crack in the material, the attenuation will be much smaller than in the undisturbed material, due to a lower density and atomic number inside the crack.

Van Geet [93] used μCT to study the exploration and production possibilities of coalbed methan extraction by visualizing the 3D fracture patterns inside the material. He developed an algorithm that also allows the measurement of the fracture aperture including a statistical evaluation of the fractures in each CT slide. He concludes that μCT has a high potential of being an additional tool to for characterizing fluid flow behaviour and reservoir characteristics of porous media.

Besides all it's advantages, μCT also has a problem in reproducing 100% identical images. These are so called artefacts in the image due to second radiation emitted by the sample, beam hardening and others. i.e. reconstructed images can contain randomly orientated small lines, rings, stars and others. The use of special hardware filters and software tools can minimize the artefacts in the reconstructed images. We discovered some line and ring artefacts in our CT images, but they didn't impair the identification of cracks in our samples.

3.2.2   The first results

For realizing the first X-ray tests we had to find an institution, which could conduct these measurements for us. It was not predictable whether or not we would see any internal structural features in the shale, as the atomic number of the main elements in the shale are very similar and the shale has a rather homogenous density. No case about the use of μCT or μCR for shale was found in the literature. In terms of the micro cracks we were not sure about their aperture and size and therefore if the resolution would be fine enough to visualize them.

The following institutions were contacted and invited to submit their quotation and technical possibilities in order to meet our requirements:

- Laboratoire Contrôle Non Destructif par Rayonnements Ionisant (CNDRI)
  Bât. Antoine de Saint Exupéry 25, avenue Jean Capelle
  69 621 Villeurbanne Cedex
  M. Peix Gilles
  résolution max. 20 μm
  offre cf.: III Appendice page 26

- Fraunhofer Institut für Zerstörungsfreie Prüfverfahren
  Universitätsgebäude 37
  D-66123 Saarbrücken
  M. Gondrom Sven
  résolution max. 10 μm
  offre cf.: III Appendice page 26

- ID19 Topography & Tomography Group
  European Synchrotron Radiation Facility
  6, rue Jules Horowitz
  F-38043 Grenoble Cedex
  Mme. Boller Elodie
  résolution max. 1,6 μm
  offre cf.: III Appendice page 26

From the technical point of view, the ID19 Tomography group offers far the highest resolution and precision. By the same token, a high resolution reduces the analysed volume, which then maybe too small to be representative for the over all properties of the sample. High resolutions are also more costly than lower resolutions. We chose the Fraunhofer Institut für Zerstörungsfreie

Prüfverfahren, as they had the best price performance ratio. The strategy was too use the lowest possible resolution, which allows us to visualize cracks inside the sample. In the case we wouldn't find what we were looking for, we still had the possibility to increase the resolution by using the facilities of the ID19 Group.

The following pictures show 2D µCR images of cylindrical samples (diam. 16 mm, height 50mm) of shale from the site of Est. The material is from a depth of 482 m in the Callovo Oxfordian formation and was sampled through the well number 205. The resolution of these pictures is about 20µm. High attenuation is dark in the radiographic pictures and bright in the reconstructed tomography images. I.e. cracks appear white at 2D µCR pictures (cf figutr 53, 54, 55) and dark in the 3D µCT (for the 2D slides of the reconstructed 3D volume cf figure 56, 57)

The represented 2D µCR images and 3D µCT slides unfortunately exhibit an inferior printed quality in this document than they do if they are visualized by using a computer with a good screen. We therefore suggest to use the dataset from the attached CD of appendix x for further analysis of the pictures.

The sampling technology as well as the preservation technologies are presented in the practical shale testing program.
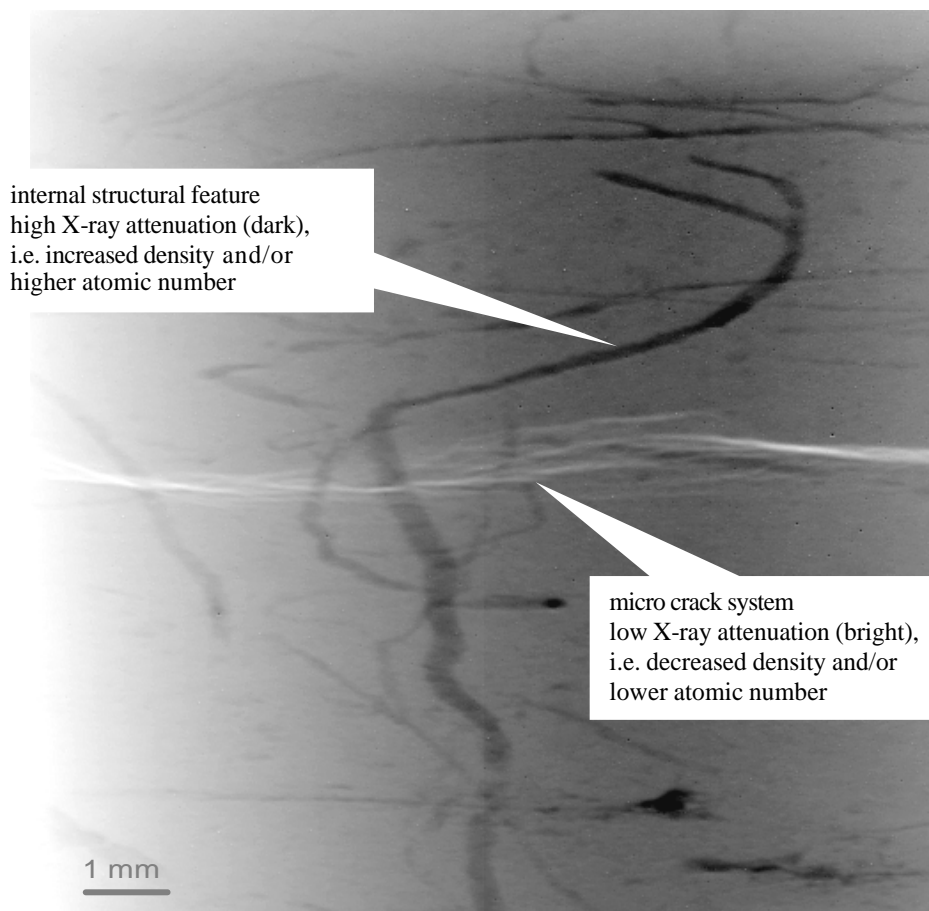

internal structural feature
high X-ray attenuation (dark),
i.e. increased density and/or
higher atomic number

micro crack system
low X-ray attenuation (bright),
i.e. decreased density and/or
lower atomic number

1 mm

Figure 53: 2D µCR picture of shale from the site of Est, sample # 11, untreated but exposed to air for several days and therefore probably desaturated. The image exhibits a resolution of 20µm.
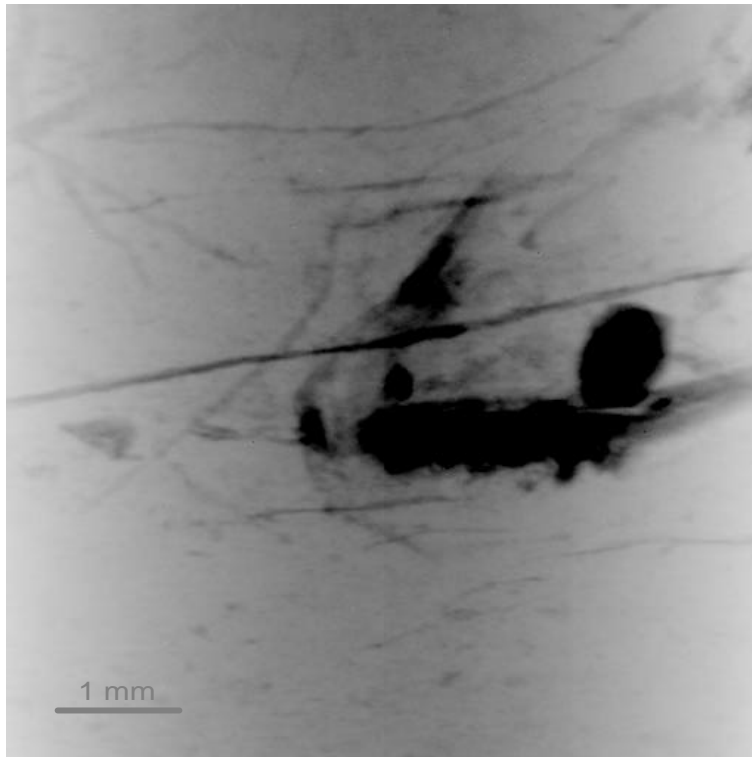
Figure 54: 2D µCR image from sample # 8, untreated but exposed to air for several days and probably desaturated. The image reveals an inclusion of higher density and/or higher atomic number (dark) (resolution of 20µm)
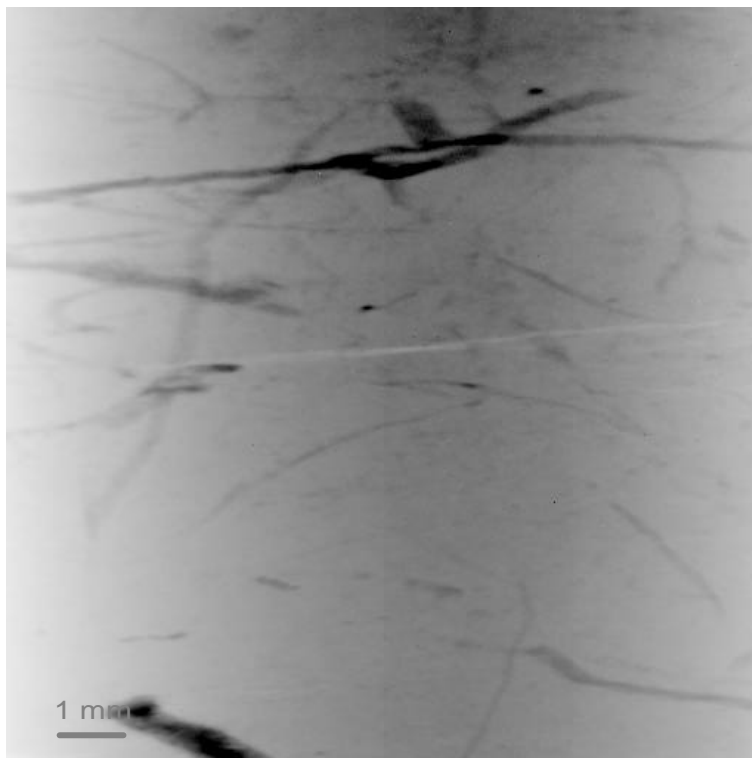

Figure 55: 2D µCR image from sample # 8, untreated but exposed to air for several days and probably desaturated. The image reveals a small micro crack (bright) at medium height from the right to the left side (resolution of 20µm)
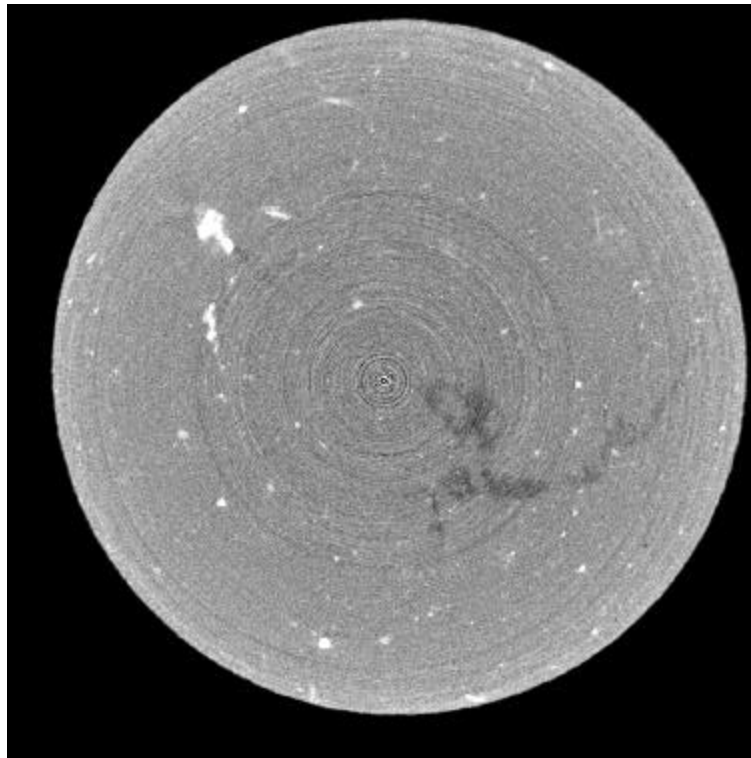
_____

Figure 56: 2D image of a slide of the reconstructed 3DµCT of ample # 8 , view of the x-y plane. At about "3 o'clock" a shade is clearly recognizable, which is a micro crack in the bedding plane (dark)
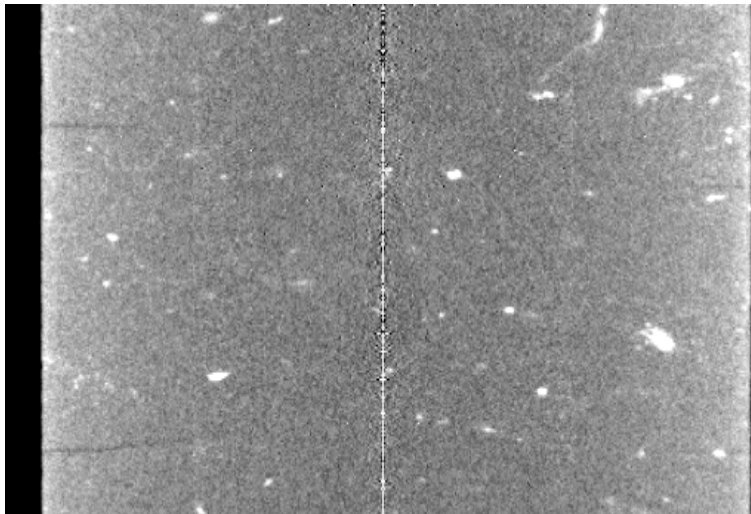
Figure 57: 2D image of a slide of the reconstructed 3DµCT of ample # 8 , view of the x-z plane. On the left side two micro cracks - one in the upper third and a longer one underneath – were detected (dark)

Considering the required computer performance to animate the whole reconstructed 3D volume of the sample, a good processor combined with at least 500 MB RAM is sufficient.
The tomographical data set was animated using a time licensed version of the "Volume player 3.0" software developed by Fraunhofer Germany.

_____

3.3   Conclusion

It could be demonstrated that that the X-ray microfocus technology is an appropriate tool to visualize the internal structure of shale. Even though artefacts such as rings and lines are visible in the obtained images, we could clearly visualize micro cracks and internal features of the shale. The difference in the X-ray attenuation between the cracks and the shale components allow for the clear visualisation of micro cracks exhibiting a minimum aperture of about 25 to 30 µm.

One of the advantages of the technology is it's non-destructive character as well as the possibilities for three-dimensional visualization. As the cracks in shale occur mostly in the bedding plane it is very helpful to view them in the z direction, orthogonal to the bedding plane.

Nevertheless this technology has limits in representing big enough volumes with a high resolution. The whole sample has to be in the field of view during scanning. i.e. the resolution of the images is limited by the size of the specimen. It therefore requires very small sample geometries for the resolution to be at maximum.

The aim in this test was not only to achieve the highest possible resolution (10 µm), but also to deal with a sample size that is representative for the material. The preparation of the sample through drilling and cutting changes the state of the material in terms of water content and maybe also in terms of preparation induced cracks. If the sample size is too small, an undisturbed zone of the sample will not remain which would therefore not be representative of the material.

The sample size we chose (16mm diameter.), enables a maximum resolution of 20 µm which seems to be a good compromise between resolution and sample size, but is constrained to cracks with an aperture slightly bigger than that pixel size.

4.   Practical shale testing program

This chapter presents all aspects related to the shale tests conducted with material from the site of Est. Beginning with a general introduction about shale testing, how - and most importantly, why the new shale testing program was developed – is described. And finally the test results, analysis and conclusions, which contribute to a new understanding of this material and hopefully to future work in the domain of these kinds of argillaceous materials.

4.a   Résumé sur les essais

L'essai sur la solution a été développé pour observer la réaction en temps réel de l'ardoise dans le site de l'Est au moment où elle entre en contact avec différentes solutions aqueuses. On a défini le degré de friabilité ainsi que la déformation et le comportement général du matériau à l'aide de la technologie des rayons X µRG en immergeant le matériau dans une solution.

Les spécimens furent exposés à une charge uniaxiale de 1,5 MPa sans confinement latéral ainsi que des solutions de $MgCl_2$, $CaCl_2$, NaCl et de KCl d'une concentration de 0,2 et de 1,3 mol. De l'eau pure et un liquide reconditionné ont également été utilisés.

La désintégration, le degré de friabilité et la déformation dépendent en partie de la concentration des ions ainsi que des types des ions de la solution. Ces réactions nettement visibles sont causées par le gonflement ou le dégonflement des minéraux stratifiés du type Illite-Smectique qui sont implantés dans une matrice des carbonates.

La désintégration observée et le développement des micro-fissures peuvent être classifiées en deux groupes : les fissures orientées qui se trouvent dans les plans de la stratification et les fissures sans orientation qui existent dans les autres parties de la structure.

L'eau pure, l'eau reconditionnée et les solutions ayant une concentration de 0,2 mol, ont provoqué plus de micro-fissures sans orientation que les solutions à 1,3 mol. Ces détériorations sont responsables de la plastification du matériau observée en utilisant des solutions de 0,2 mol.

Les conditions d'humidité relative dans le dépôt souterrain peuvent varier et influencer les propriétés du matériau. Lors d'un test cinétique l'ardoise a été exposée à des degrés différents d'humidité relative et à des conditions de pressions uniaxiales. On a utilisé une enceinte climatique électronique contrôlée par un ordinateur pour créer des degrés d'humidité différents et on a transféré directement les résultats de la déformation axiale et des paramètres environnementaux. La relation entre l'humidité environnementale, la déformation axiale, la charge axiale et les micro fissures a été analysé.

La technologie des rayons X a été utilisée pour radiographier des spécimens avant et après les essais. Le matériau a été testé sous une humidité relative de 5% à 99% pour évaluer l'influence de l'humidité sur le comportement des micro-fissures et de la déformation. Un test cyclique a été développé afin de définir le degré de friabilité dans un secteur entre 35% et 75% d'humidité relative.

Finalement, un test combiné a été réalisé afin de comparer la réaction dans l'eau pure d'un matériau saturé dans un environnement humide avec sa réaction dans l'eau en étant dans son état initial de saturation. Le matériau a été d'abord exposé à une humidité relative de 5% et 99% et ensuite immergé dans l'eau pure. Grâce à ce test on a découvert un phénomène d'hydratation qui pourrait être important pour les procédures des essais normalement appliquées.

4.1 Practical problems in shale testing

As shale can be very reactive and irreversibly change its properties, the problem is obvious. During the sampling, storing and specimen preparation, the material is exposed to several different conditions, which may alter its characteristics.
The message is clear: no matter which procedure is used for sampling, or preservation, the material no longer exhibits 100% of its initial onsite properties. The goal is therefore to minimize the disturbances and to preserve the material as much as possible.

Let's start with the sampling. The use of an appropriate drilling mud is very important. The primary aim is to avoid any interaction between the mud and the material and to obtain representative initial samples. Inhibitive, non wetting mud, for example synthetic oil based mud or polymer mud is highly recommended. In general, ion containing fluids may be considered as suitable with reference to wellbore stability, but must not be used for shale sampling. (See chapter 2.4, pp. 47) Furthermore the rate of penetration and the application of overbalanced or underbalanced drilling is applied may effect the material characteristics.

In any case, after the sample has been cored, its initial stress state has changed, which may cause an expansion of the pore volume and/or a change of the pore size. A change of the pore size can result in the induction of micro cracks. Both mechanisms may in turn foster cavitation phenomena or other micro structural mechanisms. The consequence could be an irreversible deterioration of the material, before it even reaches the surface. By the same token, pore volume expansion could also cause a "negative" pressure inside the material, which could increase the apparent resistance of the material (non drained or weakly confined sample).

Once the sample arrives at the surface the specimen should immediately be sealed to avoid the risk of desaturation. The material should therefore be either immersed in synthetic oil or wrapped in an impermeable plastic jacket to avoid dehydration. An external applied load on the sample, to simulate on site stress conditions, is also strongly recommended. This re-loading is recommended even though the de-loading may already have caused irreversible damage. Proven facts about the consequences of initial de-loading do not exist.

The specimen preparation itself is also critical, as each cutting or drilling phase may disturb the material. As an excavation damage zone is created during the underground construction works, so too a preparation damage zone is created due to the specimen preparation. Water or water oil emulsions must not be used to cool the cutting or drilling tools due to the reactivity of the clay minerals to water. Instead, water, air or synthetic oil must be used. In any case the material close to the machining surface will be altered and partially destroyed, due to pore liquid loss in the form of vapour.

Another problem causing phenomenon is the so called scale problem. Depending on the size of the samples - even though the shape is identical (same ratio of diameter to height)– the same material may produce different results in lab tests. This incompatibility must be regarded with reference to the enormous scale differences between a possible sample size used in lab tests, and the real size conditions of a formation.

Resaturation technologies, sometimes used for shale prior to testing, were already discussed in chapter 1.3.2. We have mentioned them once again, to emphasize the general sensitivity of shale to the testing conditions.

The sampling, preservation and storage technology used by ANDRA is highly efficient from the authors point of view, as it takes all previously mentioned factors into account (cf figure 58). Nevertheless we observed indications of dehydration (cracks and colour inhomogenities) when we opened the coreholder of sample 02517 for example (cf chapter 4.3)

Figures 58 a), b), c), d): Preservation technology used by ANDRA. The specimen is wrapped in a plastic jacket, which is embedded in a casing of concrete. The concrete is moulded in a PVC tube around the core. In the axial direction the sample is charged by a linear compression spring.

_____

4.2   The goal of the testing program

The general goal of the thesis was already stated in chapter 1.4, which also comprises the practical aims of the work. As explained, deterioration due to micro cracks is believed to play a major role in the mechanical comportment of shale. They shall therefore be analysed qualitatively, to determine their development under different circumstances. To facilitate the understanding of the points of interest they are represented again:

> To qualitatively analyse the influence of saturation changes of the shale on the micro fissures and to determine whether the kinetics of dehydration/hydration is of relevance.

> To qualitatively analyse the influence of different water based salt solutions on the micro cracking and the strain of the material.

> To determine whether entrapped air in the material influences the cracking/strain comportment when the material is resaturated.

In order to achieve these goals it was indispensable to install the appropriate equipment, with the following specifications, in the lab:

> A sample holder that allows for the application of various constant loads and the measurement of the strain development during the test. In addition to this, the real time crack detection (X-ray µCT) has to be possible when the sample is in contact with aqueous solutions

> A precise air conditioning system allowing the greatest possible range of controlled temperature and humidity, as well as the application of the sample holder under load with real time data monitoring (temperature, axial strain, humidity).

The description of the tests themselves as well as more detailed information is given in the following chapters 4.6 to 4.8.

4.3   The material used for the tests

Four different cores of material from the site of Est were received and three of them were used for tests. ANDRA uses the preservation technology discussed in chapter 4.1.
The lab from the site of Est is located at Bure, on the border between the district of Meuse and Haute Marne in the north east of France (cf. figure 59). The region belongs to the Parisian Basin and is composed of several distinct sedimentary layers.
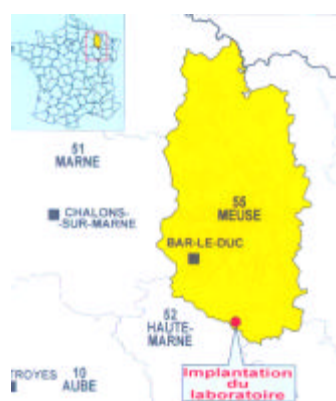

Figure 59: location of the lab in Meuse, North East of France, from where the material originates.

Figure 60: geological 3D model of the underground lab of ANDRA at Bure (ANDRA 2000).

_____

The samples originate from the argillaceous Callovo Oxfordian layer, in which the underground laboratory is installed (cf figure 60, 61). The layer dates back to roughly 150 million years and is about 130 meters thick. The argillaceous Callovo Oxfordian layer is classified by C2, which is divided into the 4 subgroups of a, b, c and d (cf figure 62).
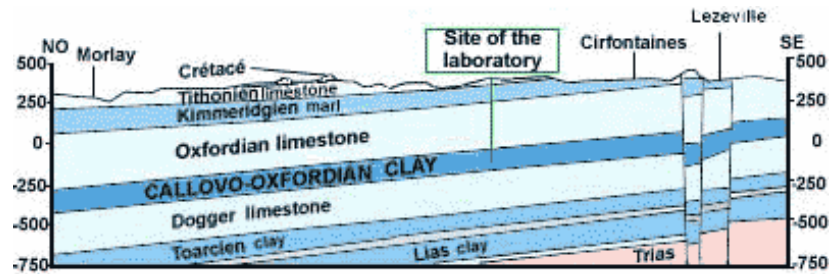

Figure 61: geological cut through the formation of the site of Est from NW to SE (ANDRA 2000)
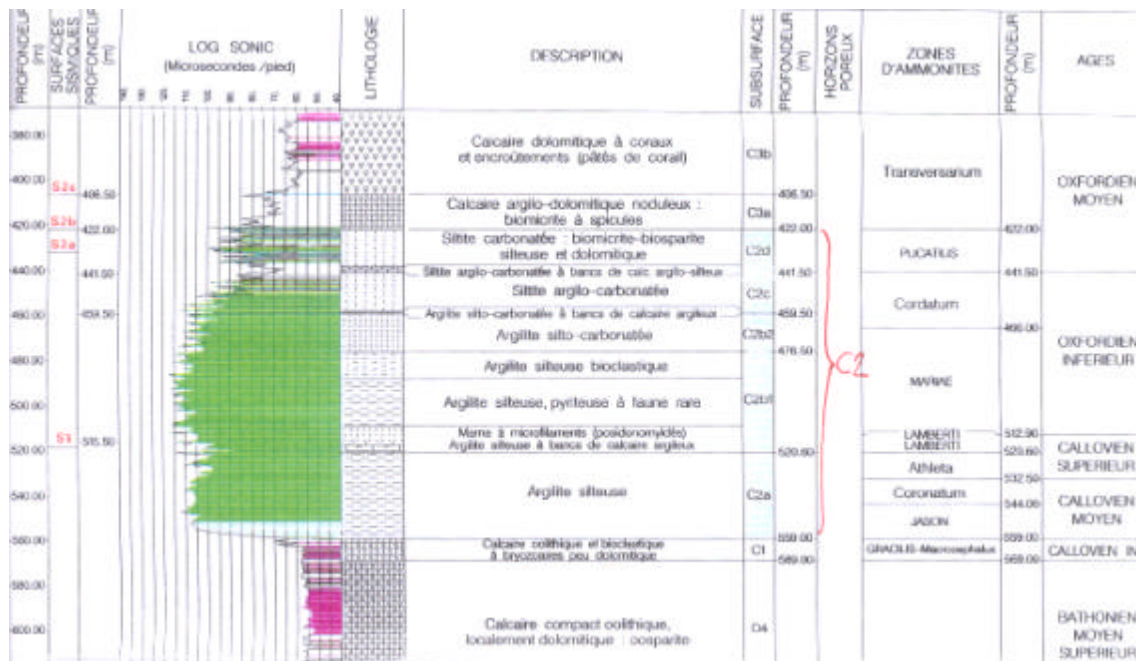

Figure 62: excerpt of the detailed geology of the argillaceous Callovo Oxfordian layer. The layer is indicated C2, which is divided into four subgroup layers a, b , c and d.

With reference to the lithological correlation of the different wells drilled (Andra 2002, [4]), our samples were classified according to the corresponding subgroup. The composition of the material we used was determined by interpolating the values of the two closest already geochemically analysed samples from the same well (Andra 2002, [4]).

Even though there is only a small differences in depth between the analysed samples and the material we used, the values obtained have to be considered as an approximation, as the formation exhibits high variations of composition within very small depth differences (cf figure 63 , table 5).

_____

summary average characterisation of the material received from ANDR.				*perpendicular to stratification	
sample #	[ ]	05514	05664	02153	02517
well #	[ ]	205	205	104	104
depth	[m]	445	482	445	511
coring date	[dd/mm/yy]	15.09.2000	17.09.2000	17.03.1996	20.03.1996
pres. type	[ ]	GTA 4	GTA 4	GTA 4	GTA 4
geol. zone	[ ]	C2c	C2b1	C2c	C2b1
mech. zone	[ ]	A3	C1	A3	C2
Mica/Illite	[%] mass	7	9	12	19
Illite/Smectite	[%] mass	13	31	18	12
Quartz	[%] mass	30	25	31	22
Calcite	[%] mass	51	22	25	38
Dol./Anker.	[%] mass	3	4	3	3
water cont	[%] mass	3,1	8,2	6,6	5,8
wave speed*					
compression	[m/s]	3800	2300	3700	2500
dry vol. mass	[kg/m3]	2500	2400	2400	2300

Table 5: summary of the description of the material received by ANDRA. The values are partially interpolations of measured values as well as measured values.

The samples 05664 and 05514 from well 205 were well preserved and generally in good condition. The colour of 05514 was rather light , compared to sample 05664. This is due to the high portion of carbonates at the corresponding depth, as can be seen in figure 63. The material from sample 05514 was unreactive, contrary to sample 05664, which was very reactive. A three-axial test conducted in our lab with 05514, determined a strength of 150 MPa. The average value of the Callovo Oxfordian shale is normaly about 50 MPa. This increase of shale strength due to a high portion of carbonates, which acts as a strong matrix, conforms to the existing theory.

When sample 02517 from well 104, which had already been stored for more than six years, was opened, macroscopically visible cracks were found on the surface of the material. (cf figure 64) These cracks are thought to arise from desaturation, as the plastic jacket did not exhibit any further elastic properties and was no longer in good condition. Inhomogeneous geological inclusions were found in the material 02517. These inclusions (rare paleontological fauna) correlate well to the geological description of its layer of origin. The colour of the material was very pale, even though the geochemical analysis highlighted a normal content of carbonates. The conclusion is therefore, that the material was partially desaturated during the storage time.

As in the case, where the jacket is not 100% sealed, the suction created by the dry concrete seems to favour dehydration. This could be avoided by either using controlled humidity environments or storing the whole preservation device in synthetic oil.

The sampling of the core 05664 and especially sample 02517 was very difficult, as the samples broke under the slightest manipulation such as sawing or drilling. The inclusions in 02517 favoured mechanical failure during manipulation.

Sample 02153 from well 104 was not opened, as the geological classification was C2c, which corresponds to the zone of sample 05514 from well 205. The results of 05514 were unsatisfactory, as the material showed very modest reactions to the de/rehydration tests and to different aqueous solutions.
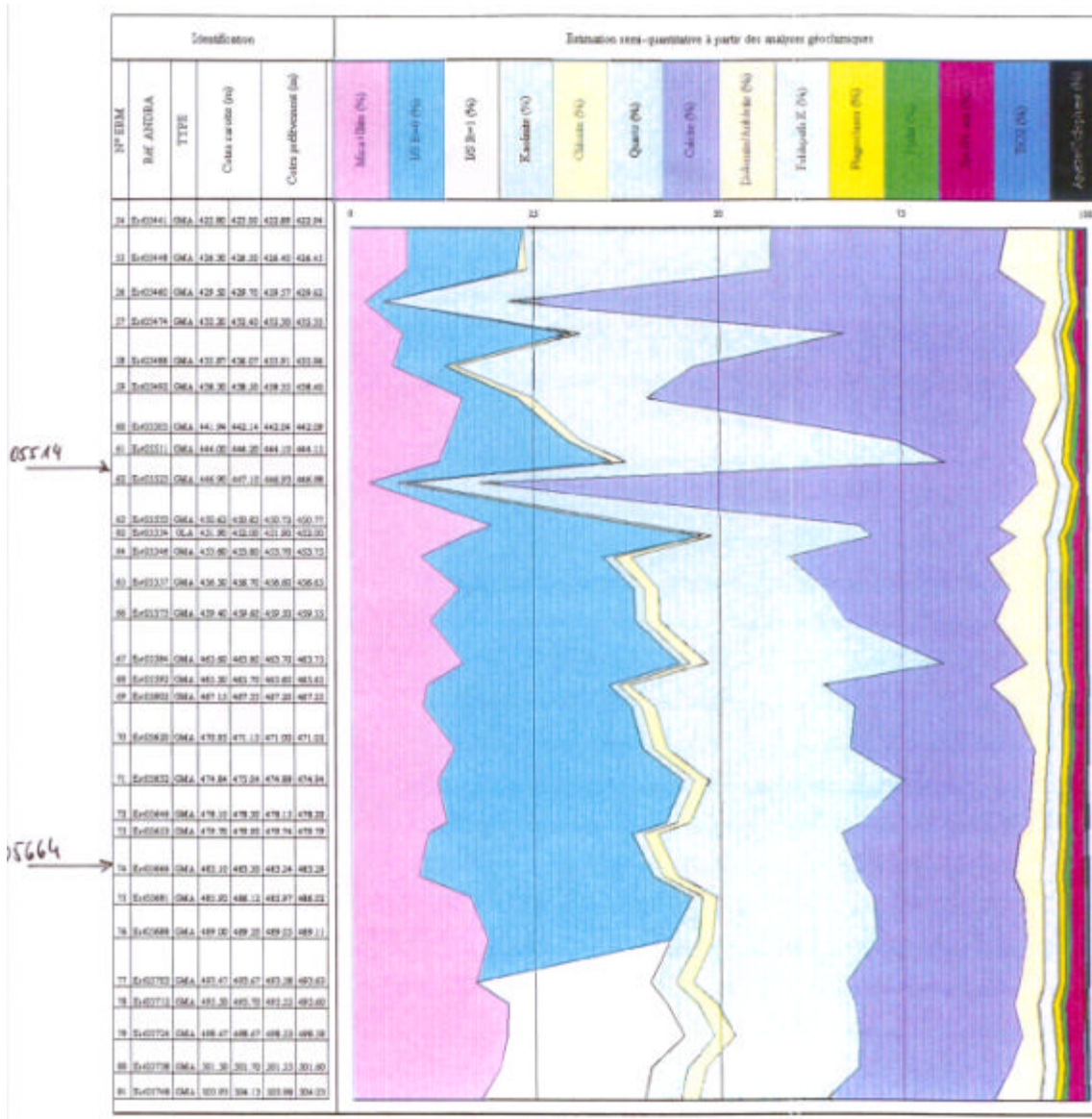
Figure 63: Geochemical composition of the material according to well # 205. The variation in a depth between 426 and 450 m is extraordinarily high. On the left side the samples 05514 and 05664 are indicated. Sample 05514 was unreactive, which is mostly due to the high portion of carbonates combined with a relatively low Smectite Illite content. These variations explain why the samples reacted completely differently – as will be shown in the test results - even though the materials originate from the same geological main formation.

However, after the calculation of the geological interpolation, it nevertheless turned out, that there is a strong likelihood that sample 02153 (well 104) would exhibit a strong reactivity. This assumption is based on the relatively high interstratified Illite/Smectite portion combined with a low content of Carbonates, which is in general, the basis for good reactivity to saturation changes. By the same token the material could be unreactive, as the variation of the composition in the depth between 440m and 460m is extraordinary high.
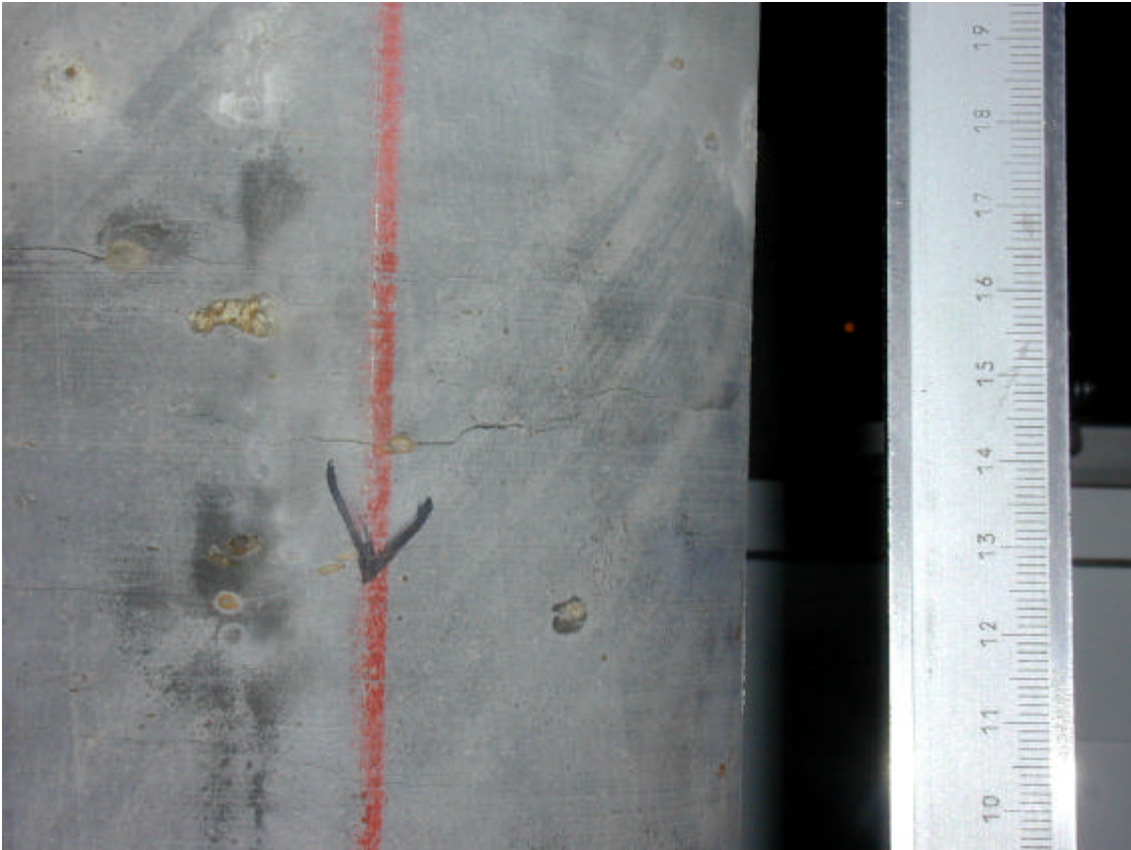
Figure 64: the core sample # 02517 from well 104 immediately after opening the storage device with radially propagated macroscopically visible cracks on the surface – most probably due to dehydration. The inhomogenities are clearly visible. The colour could also be interpreted as an indication of dehydration

4.4   The sampling technology

Figure 65 explains the different steps of the applied sampling procedure. One of the main problems was the previously mentioned fragility of the material. Many cylinder broke even before they were completely drilled. The reasons were either already existing cracks or inclusions in the material.

The use of air cooled cutting and drilling tools slowed down the whole procedure, as we had to be very careful not to overheat the material. Despite a very high drop out rate of samples and the recently mentioned problems, the process of sampling was always finished after a maximum of 90 minutes.

Once stored in the vacuum plastic bags, the samples change their saturation within a negligible range, which can be shown by weighing them before packing them and again after a certain time of storage in the vacuum bags. Immediately after sampling the specimen were sent to the Fraunhofer Institut, where an X-ray micro focus analysis was done, to document the initial state of the specimen.

All specimen are numerized, characterized - including a brief test description - and listed in the Appendix.

1
optical check for external damage

2
de-charge and opening of the preservation cell

3
weighing and optical check of the material
(macro cracks, spots..)

4
dry cutting of the he material into slizes of 30mm thickness
(saw-blade air cooled)

5
dry drilling of cylinders, 16mm diam., 30mm height
(drilling tool air cooled)

6
determination of mass, sound speed (long.), geom. size
and optical features of each specimen

7
packing of the specimen in sealing vaccuum plastic bags
(two bags)

8
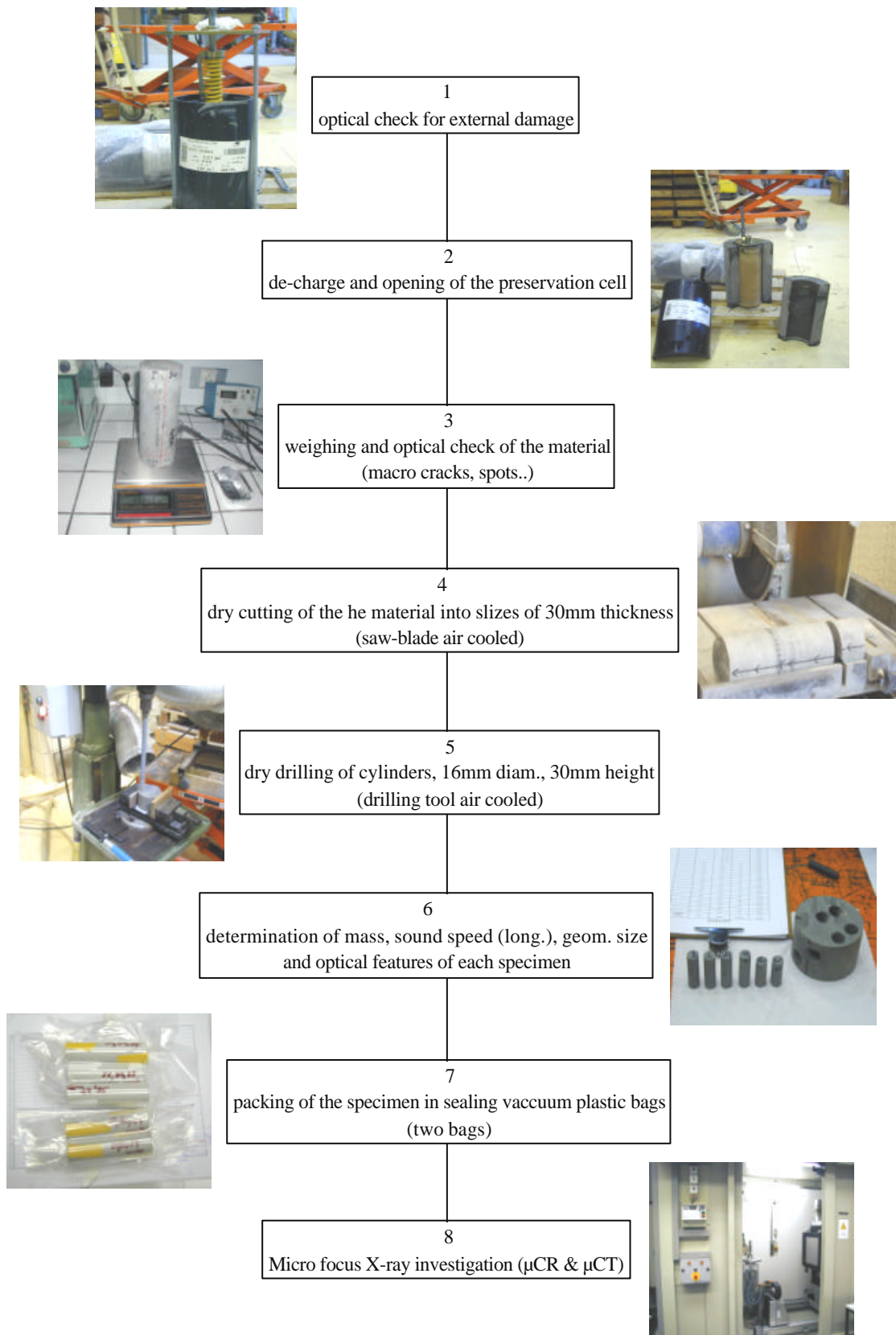Micro focus X-ray investigation (µCR & µCT)

Figure 65: flow chart of the applied sampling procedure to obtain cylindrical specimen of
16 mm diameter and 30 mm height for several distinct tests.

_____

4.5   The sample holding device

Classical swelling tests normally evaluate the swelling stress. In these tests the sample may either be restricted to a constant volume, or it has a variable volume. But in both cases the method is not very representative of on site conditions in a gallery. To conduct a swelling test in which the sample is under a certain constant load and free to change its volume seems to be more appropriate, first of all for the swelling in a controlled humid environment.

The applied stress in the material during the test should be in the elastic range. This range is limited by a maximum of approximately 12 MPa, depending on the composition of the material, according to uniaxial compression tests. The specifications for the device were the following:

> To charge the specimen with a constant uniaxial load
>
> The load has to be variable from (1 MPa < P < 12 MPa)
>
> Three axial volume variations of the specimen during the tests shall be possible
>
> The device must be appropriate for solution tests (liquid reservoir) as well as the climate chamber (access of the conditioned air)
>
> The X-ray µCT & µCR analyse must be possible during the solution test (to observe the development of the deterioration and the µ-cracks during the test)
>
> The axial strains have to be measured electronically or mechanically (mechanically for the measuring during the X-ray µCT& µ CR)
>
> An applicable specimen size range from 10 to 60mm length and 5 to 16mm diameter
>
> The device has to have a rigid frame, to obtain reliable results
>
> The device has to be small enough to fit into the climate chamber, cheap and simple

Figure 66 shows the plan of the sample holder device developed by the author in order to meet the required criteria listed above. The idea was that the sample is connected to the rotating table of the X-ray device (cf chapter 3.2.1) and turns. The sample holding device is fixed and doesn't turn, in order to avoid the two main screwed rods (6) coming between the specimen and the X-ray source, which would cause additional X-ray absorption and therefore produce false images.

This means that the sample (1) is part of the turning "shaft" (3, 2, 5), which is supported by two axial ball bearings (7, 15). The bearings were calculated according to the DIN specification 622 [30].

The two main screwed rods (6) were dimensioned according to the VDI standard 2230 [30] with reference to thread damage. The chosen material is Polyamid 6.6, as it has very low X-ray absorption properties. This would be of advantage in case the specimen (shaft) is blocked and therefore cannot turn. A blockage of the sample could arise because the sample changes its volume and may therefore change shape and position.

The different loads are provided by different linear compression springs (10), which are pre-stressed accoding to the required load. To achieve the highest possible sensitivity of the springs, three different types of springs were chosen for the tests.

The reservoir is a removable (for the climate chamber) plastic tube (12), which is sealed against the device with synthetical fat.

During the tests it turned out that the device is useful and reliable, but that certain changes could be made to ease its handling. The contact between the upper part (11) and the main screwed rods (6) should be guided (to avoid blockage), fully closed bearing should be used (to avoid corrosion and blockage) and the centralizing of the specimen should be eased by a ring at part 2. (better handling).

_____
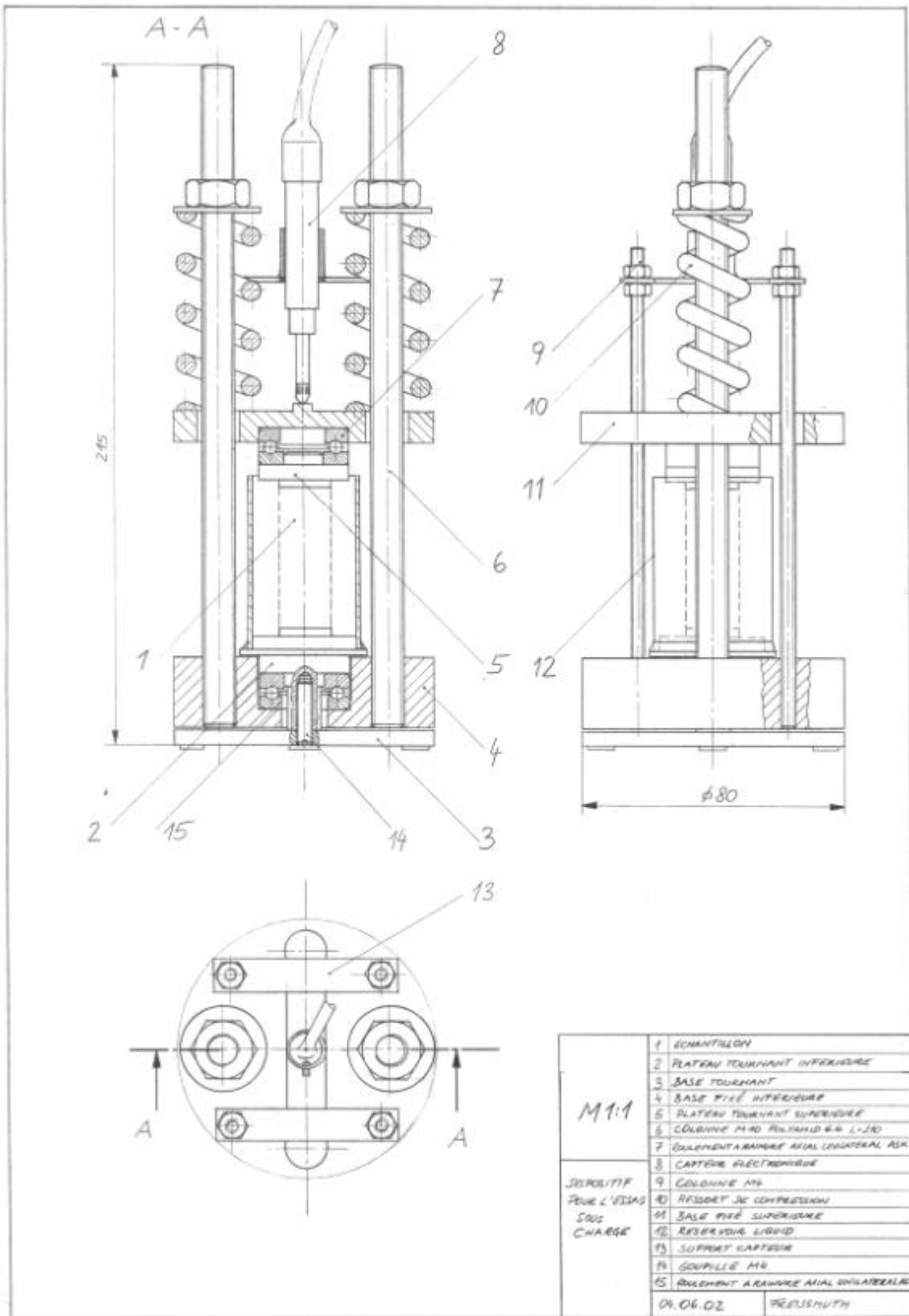
Figure 66: sample holding device for the solution and climate chamber tests, which allows a simultaneous X-ray μCT & μCR analysis under load and when in contact with a liquid.

Figure 67: Sample holding device during a solution test under load in front of the X-ray μ-focus source with a mechanical μ-meter gauge to measure the strain.

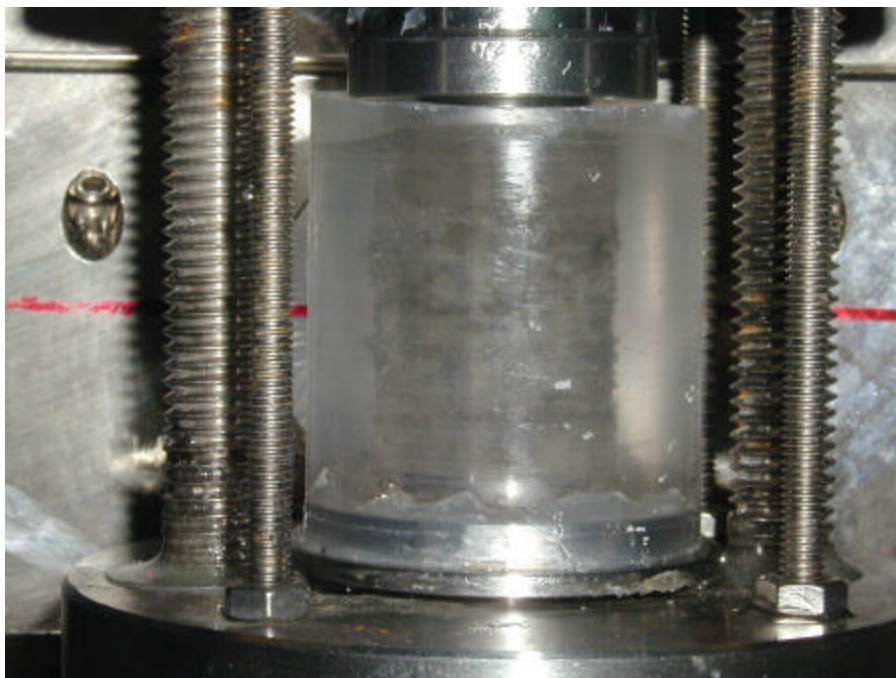Figure 68: Device during preparation before a test with a solution (empty reservoir with sample and upper bearing.

Figure 69: magnified view of the full reservoir (salt solution) with the specimen in the middle during a loaded test in front of the X-ray μ-focus source.

Figure 70: Decharged device with a full reservoir (salt solution) and the specimen in the centre after the test.
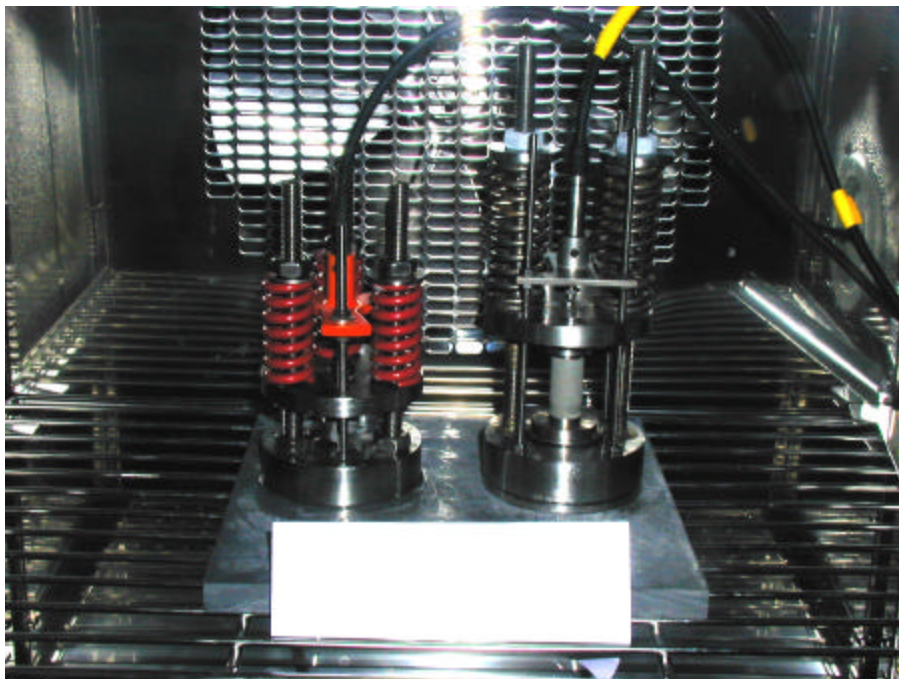

Figure 71: Sample holding device during a kinetic test under load in the climate conditioning chamber (without a liquid reservoir). This device is equipped with electronic online strain measuring sensors.

4.6   The solution test

It was found that the chemical composition of the water within the same construction site varies significantly in the ANDRA laboratory. Water based solutions could also change their migration path within the EDZ and encounter shale which was initially in contact with another solution. The reactions it could provoke are therefore of interest.

The solution test was developed to qualitatively observe the real-time reaction of the shale from the site of Est, when in contact with different aqueous solutions. The crack development as well as the strain and the general behaviour of the material was investigated by using the X-ray µRG technology while the material was immersed in a solution.

Another reason to run the test is the behaviour of some Smectite mineral containing shale when in contact with a Potassium solution (cf chapter 2.3.3). The permeability of the material could increase remarkably. Micro cracks are held responsible for this increase, but they were never previously observed inside. The X-ray µCR allowed us to do so, as the shale of ANDRA contains these clay minerals.

Geomechanical laboratories often use tap water for all different kind of shale tests. But is "water" coming out of a tap in lab A the same as the tap water from lab B? One thing is sure: tap water is not equal to chemically pure water. We wanted to see what happens when the shale is in contact with chemically pure water and if there is a difference to the tap "water" from our lab. Anyway, pure water should be used instead of tap water to standardize the tests. This would make results more comparable.

The solutions used contained Ca, Na, Mg and K, as these ion species are commonly encountered in natural water. It was of interest whether or not the material would react differently to each salt.

Reconditioned pore liquid was also used. The term reconditioned pore liquid refers to a solution that is theoretically similar to the initial pore liquid. It is a common technique to use such a liquid to resaturate shale. This liquid is thought to cause no chemical reaction with the material as it is of the same nature as the initial pore liquid of the material. This would mean that only physical mechanisms like capillarity would occur when a shale is in contact with its reconditioned pore liquid. We wanted to "see" this.

At the beginning of the tests it was not sure if the material we received from ANDRA would react at all to the different solutions. It was also unknown how long such a reaction could take. Neither could the successful measurement of a possible strain be taken for granted as a new sample holding device was used in combination with unknown material.

4.6.1   Testing procedure and solutions

The X-ray tests were conducted in Germany, Saarbrücken at the Fraunhofer Institut for Non Destructive Material Testing. The cylindrical specimen were transported in vacuum plastic bags and only unpacked immediately prior to starting the tests.

The specimen were first X-ray µ-focus analysed in their initial and unstressed state, to document the reference condition of the material.

In the second step the material was positioned in the sample holding device and charged with a load of 1.5 MPa and another X-ray µRG image was taken. To make sure that the springs were pre-stressed with the same load in each test, 2 pairs of counter screw nuts were installed at each screwing rod.

Following this, the liquid reservoir of the sample holding device was filled with a solution through a small flexible plastic tubule. Straight after the filling the next image was taken.

_____

Finally a picture was taken every two minutes until the sample failed or a maximum testing time of 45 minutes had passed.

The solutions used are given in table 6 and table 7. Their concentration was chosen according to reactivity tests described in literature with similar material [55, 85]. The aim was to qualitatively analyse the influence of the different chemical species on the material, as well as the influence of their concentration. Two different concentrations of each solution, with relatively high differences in concentration, were therefore used.

the different solution concentrations for V = 75 ml

species	molar mass	conc.	salt content	mass conc.
[]	[g/mol]	[mol/lit]	[g]	[%]
KCL	74,55	0,2	1,12	1,5
	74,55	1,3	7,27	9,7
NaCl	57,50	0,2	0,86	1,2
	57,50	1,3	5,61	7,5
MgCl2	95,20	0,2	1,43	1,9
	95,20	1,3	9,28	12,4
CaCl2	111,00	0,2	1,67	2,2
	111,00	1,3	10,82	14,4

Table 6: the different salt solutions (chemically pure water G=56nS enriched with distinct salt species)

In addition to the salt solutions chemically pure water with an electrical conductivity of G=56 nS and reconditioned pore liquid (crushed shale is immersed in water until a chemical equilibrium is reached) of the sample #05664 from well 205 were used (cf table 7).

Mesures de terrain	T° en °C	21,5
	pH	7,4
	Cond en mS	2,9
Anions en mg/L	HCO3-	nm
	F-	<2,5
	Cl-	61,4
	NO2-	<0,01
	Br-	<0,01
	NO3-	<0,01
	SO4--	1288,4
Cations en mg/L	Li^+	<0,02
	Na^+	463,7
	NH_4^+	1,7
	K^+	46,7
	Mg^{++}	55,3
	Ca^{++}	151,7
Total ANIONS [méq/L]		28,6
Total CATIONS [méq/L]		33,6
Ecart Anion/Cation		5,0

Table 7: analysis of the reconditioned liquid (chemically pure water with G=56nS enriched with shale powder from the site of Est, sample # 05664, well 205 (75h at 60°C)

_____

The reconditioned pore liquid was produced by crushing some of the testing shale and pulverizing it in a mortar, to obtain the largest possible specific surface. Afterwards 400 g of the shale powder were mixed with 600 g of pure water. This mud was heated to 60°C and held in constant movement by a magnetic stirrer. After 75 h on the stove, the solid particles were separated from the liquid phase in a centrifuge at approximately 4000 rot/min for a period of 45 min. A chemical analysis of the reconditioned liquid was then prepared.

Before running the tests in Germany, some simple immersion tests were done, as it was not known whether the material would react at all. Small pieces of material were put into pure water, tap water and different other solutions.

4.6.2   Results

As more than 300 2D µCR images were acquired during the tests, only a small portion of them are presented in this chapter. The images unfortunately exhibit an inferior printed quality in this document than they do if they are visualized by using a computer with a good screen.
As the resolution of the pictures is quite good, they can be strongly magnified and therefore more clearly analysed by using a computer. Micro cracks with a minimum aperture of about 30 µm can be clearly identified. (pixel size between 18 and 22 µm). Figure 72 shows a magnified section of a small image, which highlights features that cannot be seen in the small image.
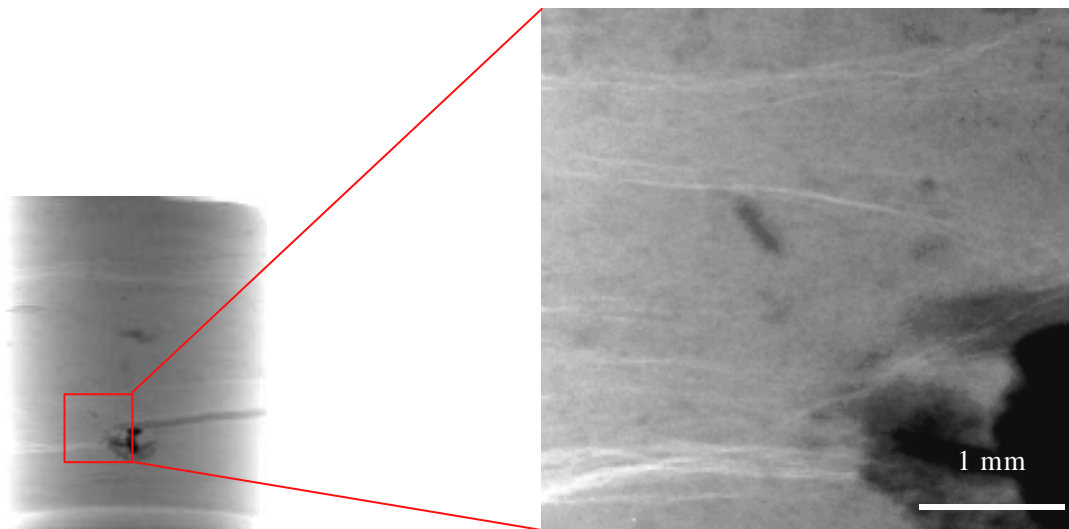

Figure 72: image of material from sample #05517 well 205 #78. In the magnification small micro cracks are visible, which cannot be seen in the small image (µCR =22µm).

Picture 73 and 74 show the reaction of pieces of shale from sample #05564, well 205 immersed in pure water and a 1,3 molar solution of Potassium. The pieces were fragments, left from the sampling and were immersed immediately after the opening of the preservation device.

The pieces reacted strongly immediately on being put in contact with the water. The swell heave was very strong (strain ~ 30%), the piece changed its shape, lost its solid character and fell finally apart. The shale dispersed completely within 20 min (cf figure 73).

The material in the KCl solution showed no dispersion, stayed in shape an kept its solid character. Macroscopically visible cracks could be observed at the surface after 10 minutes. The sample as well as the glass cylinder were covered with little gas bubbles. These bubbles were not observed when the material was immersed in water. An explication of this phenomenon was not found.
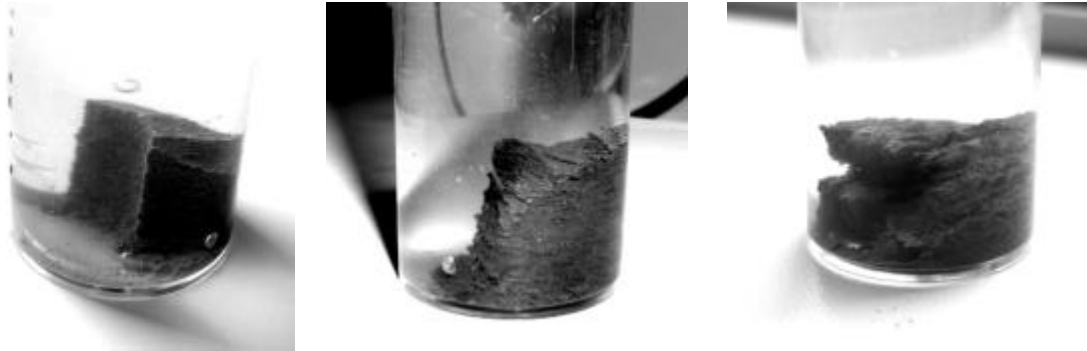
Figure 73 a), b), c): a) after immersion of the shale in pure water, b) after 10 minutes, c) the material dispersed completely after 20 minutes. The deterioration started in the stratification plane (sample #05564 well 205)

Figure 74 a), b): The left glass contains a 1.3 molar KCL solution. The other cylinder is filled with pure water G=56 nS. The KCL glass is completely covered with small gas bubbles and the sample does not disperse but cracked. Both glasses contain material from sample #05564, well 205.

The reaction of the material to tap water was similar to that of pure water, but the dispersion took longer and was not that strong.

As the deterioration and the cracking seems to take place mainly in the bedding plane, cylindrical samples were taken under different angles to the stratification plane from sample #05564 well 205. The angles were 90° for #1, 0° for #3 and 45° for #5, relatively to the drilling (z) axis. The specimen 1, 3 and 5 were immersed in a 2 molar KCl solution. The result is given in figure 75. The cracking occurred in all three cases in the direction of the stratification plane.

Figure 75: from left to right: specimen #1, #3 and #5, after immersion in a 2 molar KCl solution. The cracks in all three cases are in the direction of the bedding plane: 90° for #1, 0° for #3 and 45° for #5.

To verify whether the deterioration and cracking in pure water also takes place in the bedding plane, an unloaded free swelling µRG analysis was done with specimen #34. The image series number 1 shows the comportment of shale during a 16 minutes period in contact with pure water.
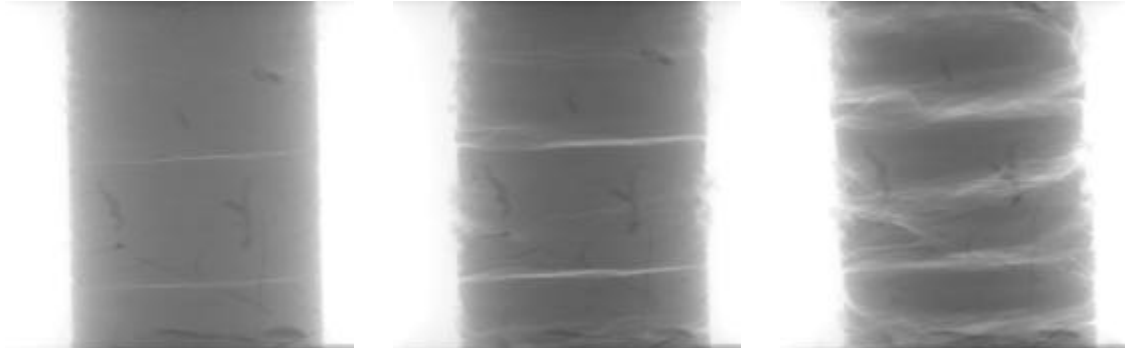
Series 1: cylindrical specimen 16 x 30 mm (#34 from sample #05564 well 205) during an unloaded free swelling test in pure water with G=56nS. Image a) after 2 minutes, b) after 8 min and c) after 16 min.

The test with #34 was stopped after 16 minutes, because the material started to disperse completely and the cracks were no longer visible as the sample fell apart. The strong swelling heave is obvious, as the black spots in image a are located lower than those in image c.

The tests with samples #1, #3, #5 and #34 clearly showed that the cracking and deterioration of the material mainly takes place in the bedding plane, with pure water and a KCl solution.

Finally the solution test, under load, as previously described, was conducted. The results present four images of each specimen in contact with a liquid and under load. Even though many more images were taken we have only presented a series of three, to keep the chapter clearly arranged.

The first image of each series represents the situation immediately after the reservoir of the sample holding device was filled. The second shows the state after 16 minutes had passed. The last image illustrates either the condition after 45 minutes, or is the last picture taken before the sample failed.

The pictures exhibit a resolution of 20 to 23µm and the tested specimens are the described standard cylinders with a diameter of 16mm, a height of 30mm and drilled perpendicularly to the bedding plane. The outer vertical borders of the picture correspond to the diameter of 16mm and can be used as scale. All tests were conducted with material from sample #05564, well 205 (482 m depth)

The first series (cf series 2) illustrates the behavior of specimen #23 in contact with pure water. The material deteriorates slower than without load, but in the same manner.
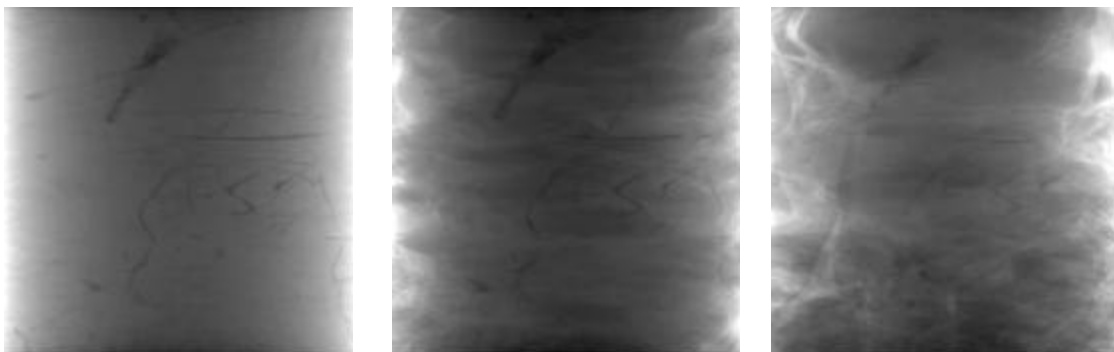
Series 2: specimen #23 in pure water (G=56nS) immediately after the filling, after 16 minutes and before the sample failed after 38 minutes. Load =1.5 MPa, T =25°C, picture width = 16mm, µCR=22µm.

The solid character of the material was completely lost after the test and the material had characteristics more similar to wet soil than to indurated sediment.

Series 3 shows specimen #18 and its behavior when in contact with the reconditioned pore liquid. Contrary to the expected unreactive behavior, the material reacted powerfully to the liquid and after 20 minutes started to deform plastically before failing after 30 minutes. The reaction was very similar to the one that was observed with pure water.
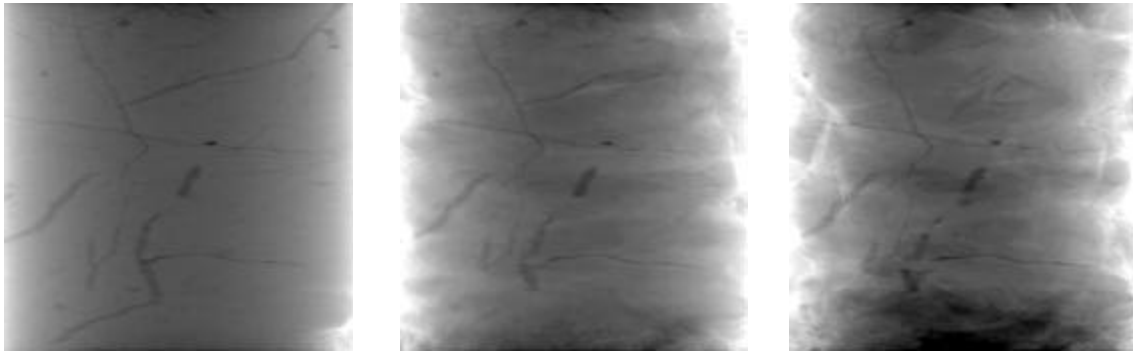
Series 3: specimen #22 in reconditioned pore liquid immediately after the filling, after 16 minutes and before the sample failed after 30 minutes. It showed plastification after 20 minutes. The reaction was not consistent with the theory about reconditioned liquid. Load =1.5 MPa, T =25°C, picture width = 16mm, μCR=22μm.

When specimen #26 was in contact with a 1,3 molar KCl solution, the reaction was as expected (cf series 4). The material didn't get plastified or deteriorate as in the case of water and reconditioned liquid. One of the most noticeable effects was the stable surface of the material. In the other two cases the deterioration started by destroying the surface. The lower concentration in combination with the load seems to suppress a very strong fissuration within the first 30 minutes, as happened during the 2 molar unloaded immersion test. Only two main crack systems and a few smaller cracks above the higher main crack could be detected. This inhibitive character of Potassium on the behaviour of shale validates the theory presented and described in chapter 2.3.3. The discussed increase of the permeability due to cracks also fits into the concept.

Series 4: specimen #26 in a 1,3 molar KCl solution, immediately after the filling, after 16 minutes and after 40 minutes. Horizontal main crack systems are visible, as well as a few smaller cracks above the upper main crack. Load =1.5 Mpa, T =25°C, picture width = 16mm, μCR=22μm.

The same test was performed with 0,2 molar solution and specimen #24. In this series (cf series 5) the specimen was not positioned exactly centrically in front of the X-ray source, to better observe

the reaction of the surface. The reaction was very similar to that 1,3 molar reaction, but seemed to be a little bit stronger in terms of the main cracks and the surface deterioration. One main crack could be observed and a bigger system of many smaller cracks above the main crack. These small cracks were at the height of the small deteriorated piece at the edge.
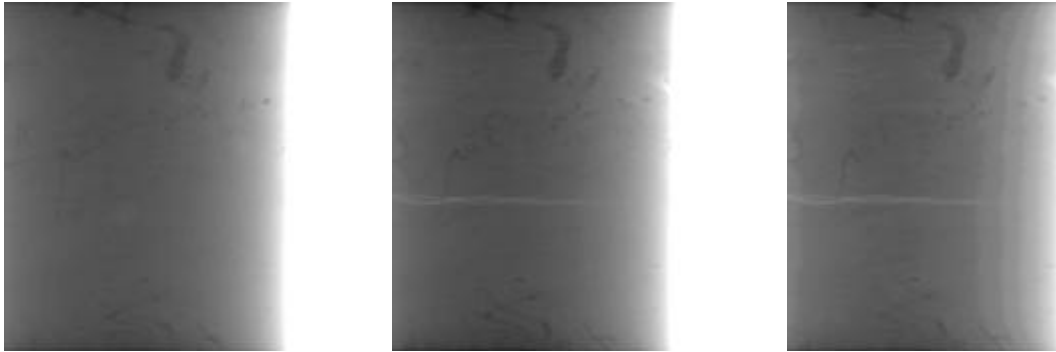
Series 5: specimen #24 in a 0,2 molar KCl solution, immediately after the filling, after 16 minutes and after 40 minutes. One horizontal main crack system is visible, as well many smaller cracks above the main crack. Load =1.5 MPa, T =25°C, picture width = 14mm, µCR=22µm.

Series 6 documents specimen #19 in contact with a 1,3 molar NaCl solution. The quality of the images is slightly inferior concerning the contrast. As the adjustment of the X-ray device was identical in all the other cases, an explanation could be a higher X-ray attenuation of the NaCl solution. The reaction clearly shows the deterioration in the bedding plane between the layers starting from the surface moving towards the middle of the cylinder. The cracks grow from the surface into the material. One horizontal main crack passing the sample was observed. The material did not show a strong plastification before it failed after 45 min. (cf figure 76) All the other sample, which broke during the test, showed plastification comparable to creep. It also did not deteriorate as much as the samples in contact with pure water or reconditioned liquid.
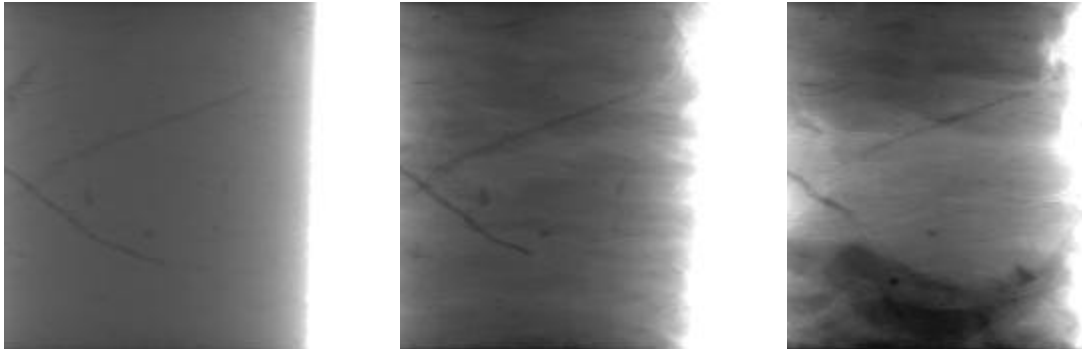

Series 6: specimen #19 in a 1,3 molar NaCl solution, immediately after the filling, after 16 minutes and before the sample failed after 45 minutes. The whole sample is full of many cracks, growing from the surface towards the centre of the sample. Load =1.5 MPa, T =25°C, picture width = 16mm, µCR=22µm.

A NaCl solution with a 0,2 molar concentration was put in contact with specimen #21 (cf series 7). The reaction was extremely strong and started immediately after the filling of the reservoir of the sample holding device. The speed of deterioration was astonishing and the sample failed after 30 min. After only 12 minutes the first signs of plastification were observed (cf figure 76). The failure itself was comparable to strong creep rather than to a rupture of an indurated sediment. Many small

and bigger cracks could be determined. The diameter of the specimen was already very much reduced when the sample failed. The swelling heave is very low and similar to specimen #22, which was in contact with reconditioned liquid (cf figure 76). The mechanism of deterioration is of the same nature as the mechanism observed with the 1,3 molar NaCl solution of sample #19. The difference is, that the deterioration of the surface is much stronger, which is comparable to the reaction caused by the pure water and the reconditioned pore liquid.

The dark region at the bottom of the last image is caused by material, which disconnected from the surface of the specimen and settled at the bottom of the reservoir.


Series 7: specimen #21 in a 0,2 molar NaCl solution, immediately after the filling, after 16 minutes and before the sample failed after 30 minutes. The whole sample is full of many cracks, growing from the surface towards the centre of the sample. Load =1.5 MPa, T =25°C, picture width = 14mm, µCR=22µm

The next test was done with a 1,3 molar $MgCl_2$ solution and specimen #20 (cf series 8). The deterioration of the surface progressed quickly at the beginning but seemed to slow down after 15 minutes. Contrary to that, the specimen was completely interstratified with many smaller and bigger cracks and had a relatively high swelling heave (cf figure 76) The sample neither lost its solid character nor dispersed. As the sample did not fail, the test was stopped after 45 min. Interesting was the development of the cracks. Their growth from the outside to the centre could not be observed as was the case with NaCl. It's very alike that the aperture of the cracks was too small to be detected at the beginning of the reaction and that they opened later.
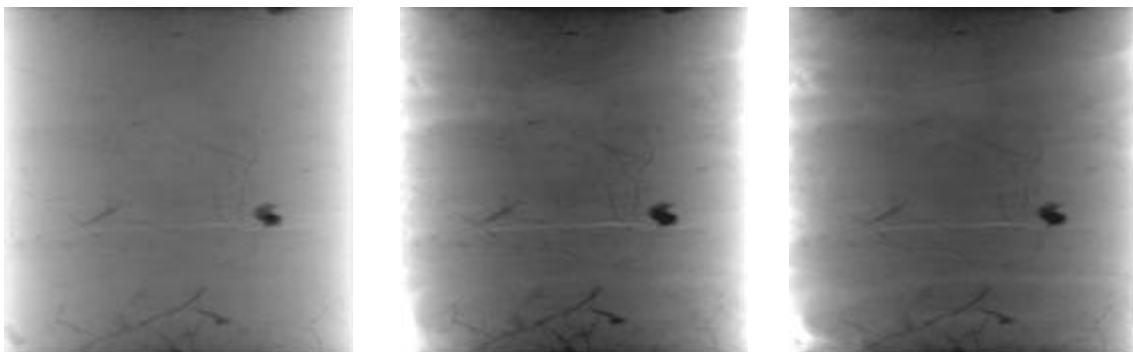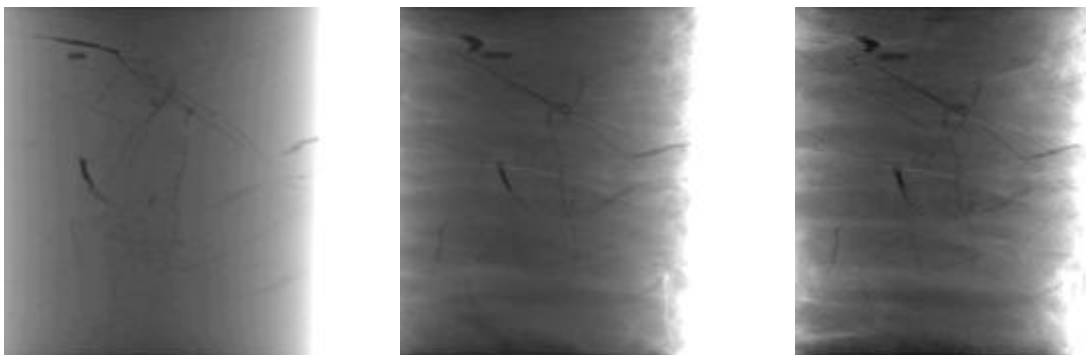

Series 8: specimen #20 in a 1,3 molar $MgCl_2$ solution, immediately after the filling, after 16 minutes and after 45 minutes. The whole sample is full of many small and bigger cracks. The growth from the surface towards the centre could not be observed. Load =1.5 MPa, T =25°C, picture width = 16mm, µCR=22µm

Series 9 presents the images of specimen #28 in contact with a 1,3 molar CaCl₂ solution. The surface reaction was slightly stronger than in the case of the MgCl₂ solution. The material kept its solid character and did not fail after 45 minutes. Two main crack systems developed in the upper region and many smaller cracks close to the bottom. The swelling heave was relatively strong and in the magnitude of the MgCl₂ growth. (cf figure 76).
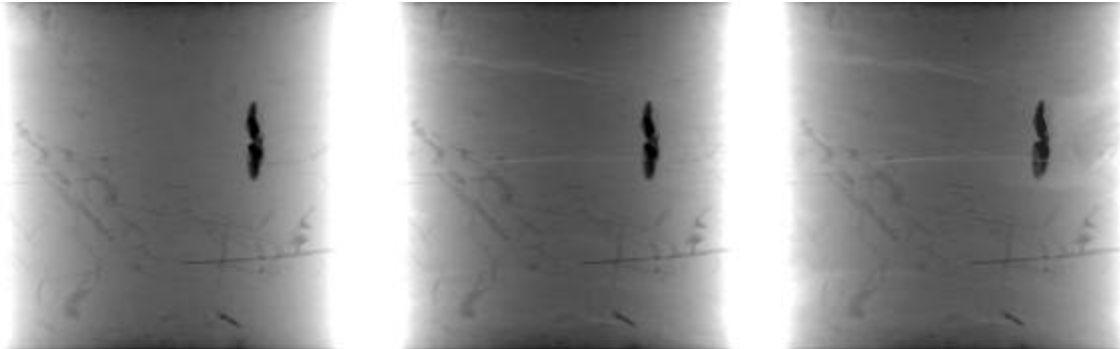
Series 9: specimen #28 in a 1,3 molar CaCl₂ solution, immediately after the filling, after 16 minutes and after 45 minutes. The last image shows two main crack systems and many smaller cracks close to the bottom. Load =1.5 MPa, T =25°C, picture width = 16mm, µCR=22µm

The last series (10) illustrates the comportment of specimen #29 in contact with a 0,2 molar CaCl₂ solution. The reaction was in general stronger than the reaction caused by the Calcium solution with a concentration of 1,3 mol. The material started to creep after 20 minutes and failed after 31 minutes. The horizontal crack density is higher compared to the density in series 9 (NaCl 1,3 mol).

Series 10: specimen #29 in a 0,2 molar CaCl₂ solution, immediately after the filling, after 16 minutes and after 31 minutes before it failled. The deterioration of the surface was rather strong and the whole sample was interstratified with small and bigger cracks. Load =1.5 MPa, T =25°C, picture width = 14mm, µCR=22µm

The sample holding device was equipped with a mechanical micrometer gauge (+- 2 µm precision) to measure the axial strain during the test. This was possible as the X-ray chamber at the Fraunhofer institute is equipped with a security window in the door, which allows the reading of the gauge. The results of the axial strain are given in figure 76.

As it was interesting whether or not it is possible to visualize a liquid front entering the material, medical tomography injection fluid, which is used for humans was tested. The X-ray attenuation was too strong and the image did not show the sample, but only a big gray spot – the liquid reservoir. The main components of the liquid were Na, Ca, Cl, I, and Ethanol as the solvent.

axial deformation of shale from Est, well #205/482 m when in contact with distinct aqeous solutions
axial stress = 1,5 Mpa, Temp. = 25 °C, sample size = 16 mm diam. & 30 mm height
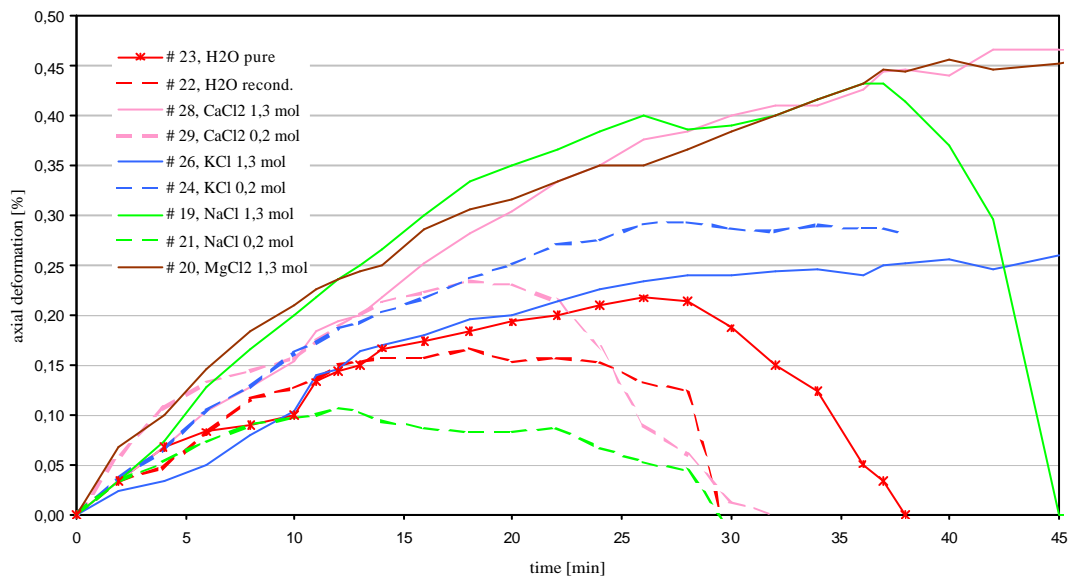
Figure 76: the different swelling heaves measured with a mechanical gauge during the solution test.

Some µRG pictures were also taken after the test when the sample was in an unstressed state but still in the sample holding device, which was still filled with solution. It was observed that many cracks enlarged their aperture and the sample sometimes broke. New cracks also appeared in some cases due to the deloading.

The macroscopical difference of some samples caused by the different solutions is given in figure 77. The pictures were taken when the samples were in a dry and unstressed state and therefore very fragile and brittle. The only sample that stayed completely intact after drying was #26, which was in contact with 1,3 molar KCl solution.

Figure 77: some samples after the solution test in dry conditions (sample 05664, well 205: #26 KCl 1,3 mol; #24 KCl 0,2 mol; #20 MgCl2 1,3 mol; #19 NaCl 1,3 mol,

As the swelling curves presented in figure 76 were measured by using a mechanical gauge and only one or two test series for each solution were done, these curves have to be carefully interpreted.

Except the Potassium solutions, the solutions of 1,3 molar concentration produced higher swelling strain values than the sol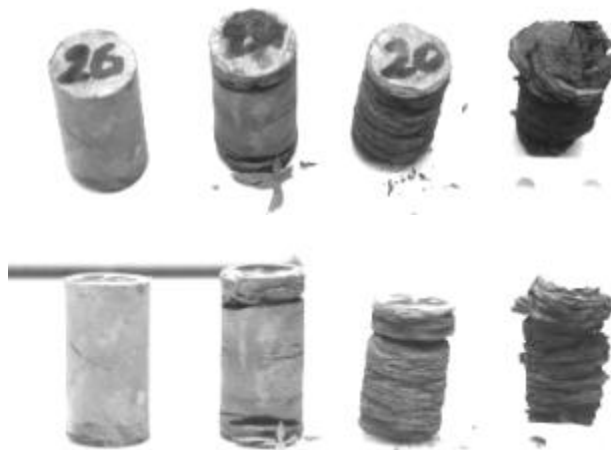utions of 0,2 molar concentration. At a first glance this seems to be contrary to the theory, which predicates the highest swelling strains and swelling pressures for pure water and low concentrated solutions. Only the reaction of the material to the potassium solutions can be immediately recognized according to the theory, as the lower concentration produces a higher swelling strain, and the solution has a very inhibitive effect.

This apparent inconsistency can be explained by analyzing the X-ray images in combination with the obvious plastification of the material when exposed to the 0,2 molar solutions, the water and the reconditioned liquid.

The X-ray 2D μRG images clearly show that there is a difference in the deterioration of the material between the 1,3 molar and the 0,2 molar solutions. The deterioration of the material caused by the 0,2 molar solutions is in general greater than the damage of the 1,3 molar solution.

The horizontal crack density is higher and the regions near the surface are more damaged by the solutions with low concentration. Furthermore these solutions generated more cracks, which are not orientated in the bedding plane of the material (cracks without orientation). These cracks develop between the different stratification layers and cross them in various directions. In summary it can be stated that the 0,2 molar solutions caused a remarkably higher reaction than the 1,3 molar solutions – which is consistent to the theory (cf figure 78). These stronger reactions seem to disrupt the clay particles perpendicular to the bedding plane, which results in the development of cracks without orientation.
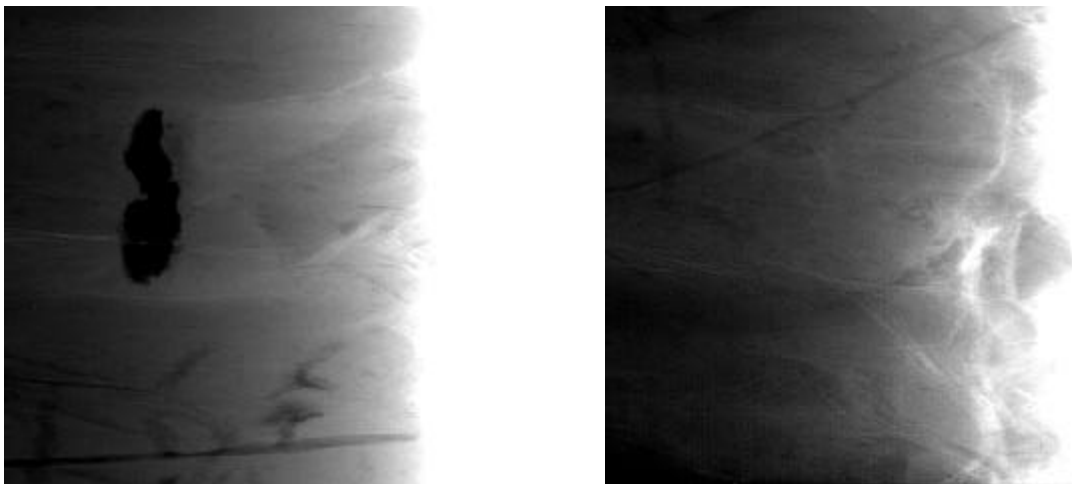
Figure 78: a), b):difference of the surface deterioration, crack orientation and crack density. a) specimen #28 in a 1,3 molar CaCl$_2$ solution after 31 minutes. b) #29 in a 0,2 molar CaCl$_2$ solution after 30 minutes. Load =1.5 MPa, T =25°C, picture width = 7 mm, μCR=22μm

The lower swelling heaves for the lower concentration result from the radially unconfined testing conditions. They allow the lateral movement of the material, which loses its cohesive strength due to the reaction with the liquid. This strength reduction is partially caused by micro cracks, and the swell comportment in general. Cracks without orientation, which exist in various directions, strongly support this lateral movement.

Each time the swelling pressure exceeds the equilibrium between the load and the strength of the material, the specimen deforms. This means the material loses its resistance step by step, which is reflected by the plastification we observed.

In the case of the 1,3 molar solution the material did not deteriorate as much and the cracks are, in general, more parallel to the bedding plane (orientated cracks), i.e. rather perpendicular to the direction of the load and the swelling pressure. The crack density is also lower. This is why the material could support the swelling stress and "grow" vertically.

The same material would produce higher swelling heaves with 0,2 molar compared to 1,3 molar solutions in a classical rigid odeometer cell, which also confines the specimen radially. Even if the material lost its mechanical strength during the test, it would swell in the direction of the z axis, as this is the only possible direction of expansion.

The distinct reaction provoked by the different solutions can be explained by the existing theory with reference to the mineralogical composition of the material. All specimens in these tests originate from sample 05664, well205/482m. The material contains a high proportion of interstratified Illite/Smectite (40%) in combination with a relatively modest percentage of carbonates (26%). The observed reactions result from this high content of swelling minerals, imbedded in a relatively weak matrix.

This conclusion is supported by the results of the chemical analysis of the reconditioned liquid. The relation of the dissolved quantity of cations is $Na^+ : Ca^{++} : Mg^{++} = 9 : 3 : 1$. The common compensator and interlayer cations of Smectite are mainly Na^+, Ca^{++} and Mg^{++}. Obviously the Smectite/Illite minerals reacted to pure water. The ions were dissolved, which leads to the loss of bonding forces between the mineral layers, and an increase in the over all net negative charge of clay particles. The consequence is inter–particle and inter-layer swelling. This means more adsorbed water, because the double layers expand due to the higher negative charge, and the incorporation of water and water complexes into the interlayer spacing. Finally the material deteriorates completely, as the swelling pressure of the clay particles exceeds the strength of the matrix.

A solution with a lower concentration has a higher remaining dissolving potential than a solution with a higher concentration. It therefore dissolves more exchangeable compensator or interlayer cations and/or hydrates more interlayer ions of the Smectite particles. The higher dielectric constant in combination with the increased net negative charge – (because some compensator cations dissolve) – leads to the expansion of the double layer. This explains the weaker reaction of the 1,3 molar solutions

The swelling curves of the $MgCl_2$, $CaCl_2$ and the NaCl solutions are very similar. Mg and Ca are both divalent with nearly the same large Stoke radii of 307 pm and 345 pm. The incorporation of these large water complexes causes strong swelling. But their high charge and small ionic radii also result in a small remaining dissolving potential – i.e. less reactivity. The deterioration and the crack density they generate is the lowest apart from the Potassium solutions.

The deterioration and the horizontal crack density of the Na solution is higher than that of the Mg and Ca solution. Even though the Stoke radii of the Na complex is only 180pm, the result is a high swelling strain. The density of the horizontal cracks indicates a higher reactivity - Na is monovalent - that compensates the smaller dimensions of the hydrated ion. The inter particle swelling is also greater for Na than for Mg and Ca, due to the higher dielectric constant of the solution.

The reaction of the KCl solution is caused by the incorporation of the unhydrated Potassium cations into the hexagonal shaped holes of the mineral layers. Their small radii and their relatively high charge, compared to the hydrated ions, reduce the interlayer spacing between the particles and lead to local shrinkage. The over all swelling arises from inter - particle swelling, which seems to be higher than the shrinkage. The locally inhomogeneous composition of the material most likely results in different local stress conditions, which foster the cracking.

The difference between the reaction of pure water and reconditioned pore liquid is not entirely explainable. One thing is clear, reconditioned pore liquid deteriorates the material a lot, and is not useful for resaturating shale. The test was repeated three times with two independently prepared reconditioned solutions. The result was always the same- a remarkable deterioration of the material. The concentration of the ions in the reconditioned pore liquid is much lower than in the 0,2 molar solutions, which explains the reactivity.

The summary of the micro crack orientation, the crack density and general deterioration as well as the surface deterioration, is schematically presented in figure 79 for the different solutions.

The gray rectangle above the specimen represents the relation of the measured maximum positive strain among the specimen. The distance of the vertical lines, which are parallel to the vertical specimen surface, reflects the depth and intensity of the surface deterioration. The upper horizontal line in the specimen means that the cracks were mainly orientated parallel to the bedding plane. A star indicates the existence of cracks without orientation. The size of the star represents the degree of these cracks. The lower horizontal line stack inside the specimen indicates the crack density as well as the intensity of the general deterioration of the material.

KCl 1,3 mol   MgCl$_2$ 1,3 mol   CaCl$_2$ 1,3 mol   NaCl 1,3 mol   water G = 56 nS

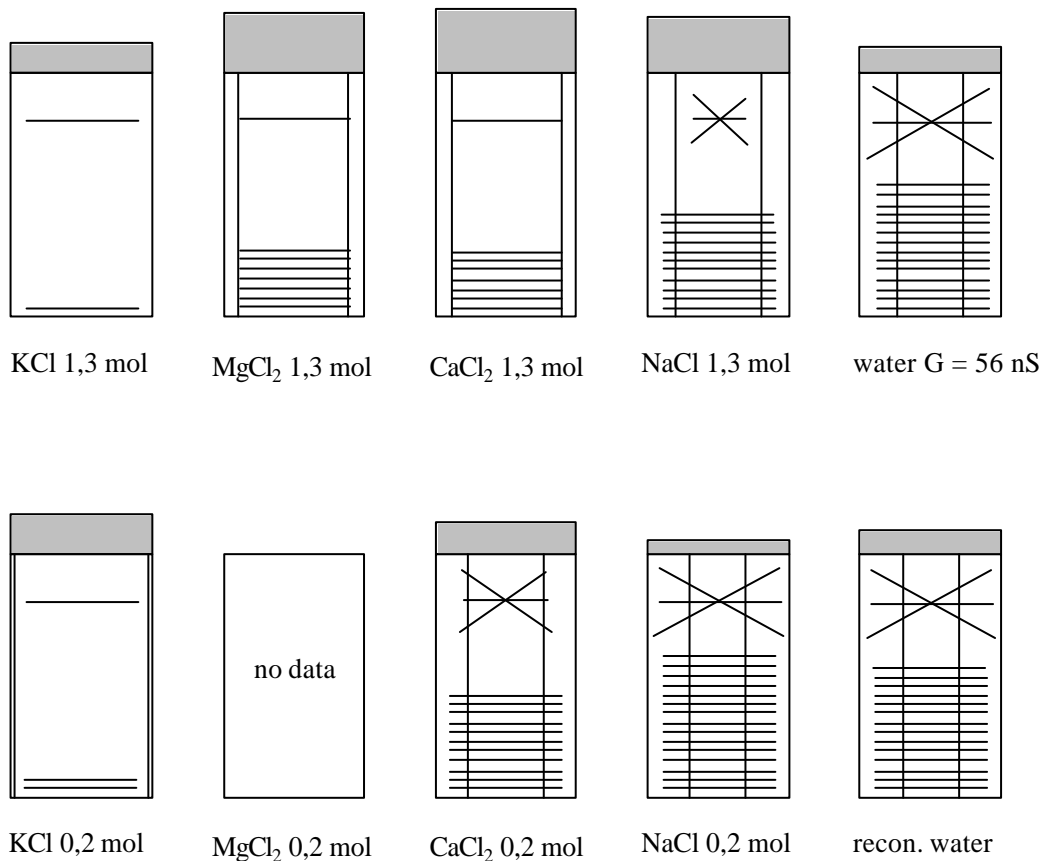KCl 0,2 mol   MgCl$_2$ 0,2 mol   CaCl$_2$ 0,2 mol   NaCl 0,2 mol   recon. water

Figure 79: Figure: schematic representation of the observed material comportment when in contact with different solutions.

4.6.3   Conclusion

The real time comportment of shale from sample 05664, well 205/482m, under the influence of distinct aqueous solutions was analyzed by using X-ray microfocus technology. The test arrangement, which comprises the sample holding device and the X-ray microfocus apparatus of the Fraunhofer Institut, enabled, for the first time, a nondestructive real-time observation of material deterioration and the development of micro cracks.

The specimen were exposed to uniaxial load conditions of 1,5 MPa without a lateral confinement $MgCl_2$, $CaCl_2$, NaCl and KCl solutions with a 0,2 molar and 1,3 molar concentration, as well as pure water and reconditioned pore liquid were tested.

It was clearly shown, that the deterioration, the development of micro cracks and the strain are partially governed by the ion concentration and the ion species of the solution. The distinct observed reactions are caused by the swelling or shrinkage of the interstratified Smectite/Illite clay minerals, which are imbedded into a relatively weak matrix of Carbonates

The observed deterioration and micro crack development can be classified into two main groups. Oriented cracks, which are almost parallel to the stratification plane and cracks without orientation, which exist not only in the bedding plane, but also in any other direction.

The solutions of 0,2 molar concentration, water and reconditioned water caused more cracks without orientation than the 1,3 molar solutions. These cracks are held responsible for the observed plastificatin of the material with the 0,2 molar solutions.

The 1,3 molar solutions containing Mg and Ca did not exhibit plastification, which corresponds to the fact that they developed mostly orientated cracks.

With reference to the crack density, the solutions with high concentrations produced a lower density than the solutions with low concentrations. Mg and Ca solutions effected the material in a very similar way and besides the Potassium, had the lowest cracking/deteriorating influence. The clay particles seem to be more sensitive to Na.

The deterioration and plastification of the material through pure water and the reconditioned pore liquid was enormous. Reconditioned liquid was not appropriate to resaturate argillaceous materials without a reaction.

As the Potassium solution has an inhibitive character, both solutions led to a very small amount of damage in the form of a few micro cracks.

Finally it can be concluded, that the existing theory about clay liquid interaction is in general very consistent to the observed behavior of the material in this test, as well as very helpful in interpreting this behavior.

4.7 The kinetic test

The consideration, which led to the test is the fact that the relative humidity conditions in the underground repository may change and effect the properties of the material. Another strong argument was, that no tests had ever been conducted, that exposed argillaceous material to controlled humidity changing conditions under load, accompanied by a constant measurement of the deformation and followed by a X-ray µRG analysis.
No information was found about the effect this could have on the general comportment of the shale and on the micro cracking. Many desiccator tests of the past led to very helpful results, but this testing technique is limited and not useful for this kind of test, as will be explained later.

The term kinetic is used with reference to the saturation gradient over time – the speed of hydration or dehydration, the material is exposed to. If a saturated sample is put in a very dry environment, a strong suction is created, which causes a fast dehydration and thus a high saturation/time gradient. This means a high saturation change per time unit. The same applies for the hydration of a dry sample – in the opposite way.

The previously presented solution test for example, creates the highest possible saturation/time gradient for hydration – the rather brutal consequences were already examined. Contrary to this, the kinetic test was designed to expose the material to different saturation/time gradients and different values of humidity (suction). Tests with a constantly held humidity and with cyclical changing humidity were conducted.

The facility must thus enable swelling tests under load in controlled environmental conditions, which create a certain suction. The only problem is that the sample holding device equipped with the strain measuring gauge is too big for classical desiccator tests. Furthermore it's not very practical to change the salt solution in the desiccator each time another humidity is required. The sample would also be exposed to uncontrolled conditions during each change and a constant change of the saturation/time gradient is not possible.

A precise computer controlled air conditioning system (ACS), which allows the greatest possible range of controlled humidity was installed. This ACS has a big enough test chamber, which allows the simultaneous application of two sample holding devices, equipped with the electronic online strain measuring sensors. The data of humidity, temperature, axial strain and testing time were processed and stored by using the Lab View software package.

The tests were very exiting, as for the first time the axial strain and fissurisation of shale under load and different humidity conditions could be recorded.

4.7.1 Testing procedure and air conditioning system

All samples used were standard cylindrical samples, with a diameter of 16 mm and a height of 30 mm. The bedding plane of the material is perpendicular to the z axis of the cylinder.

The first step of each test was a 2D µCR analysis of the specimens in their initial and unstressed state, to document the reference condition of the material.

In the second step the specimens were positioned in the sample holding devices and charged with a load of 1,5 MPa and 4 MPa. The chosen load was again in the elastic range of the material as in the solution test. To make sure that the compression springs are prestressed with the same load, 2 pairs of counter screw nuts were installed at each screwing rod.

Subsequently, the sample holding devices were placed in the prepared air conditioning system (ACS) chamber and the electronic sensors were mounted on the devices. Once the chamber was closed, the data recording started, by using a prepared file in the Lab View software, and the ACS chamber program was started.

Finally the specimens were packed in plastic vacuum bags after the test and 2D μCR images were taken to analyse the material with reference to micro cracks and deterioration.

The entire preparation of the samples and the devices, including the start of the program took between 30 and 40 minutes. During this time the sample was exposed to the environmental conditions of the lab, which are about 20°C to 25°C and a relative humidity of about 55% to 65%.

The installed ACS chamber is the Vötsch VCN100 system, which is fully programmable. It can operate in a humidity range of 5%RH to 99% RH and at a temperature interval of –30°C to 130°C. A precision of +- 2%RH for the set up humidity values is guaranteed by the manufacturer in a temperature range of 25°C to 90°C. These guaranteed humidity values cover a range from 10% RH to 98% RH, which are given in figure 80. According to this humidity range chart a minimum temperature of 40°C has to be adjusted, in order to obtain 98%RH.
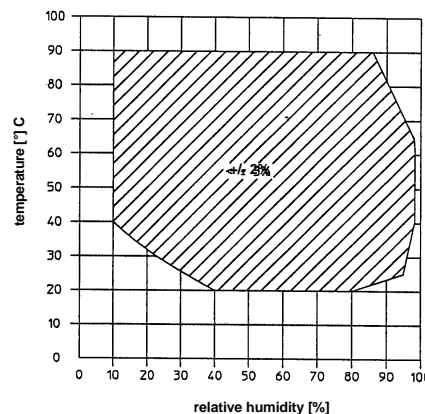

Figure 80: guaranteed temperature and relative humidity range of the
Vötsch VCN 100 air conditioning system (manual Vötsch)

During the tests the measured humidity values always reached 99% RH at a temperature of 40°C. This value has to be interpreted according to the precision of the system - the measured value of 99%RH could also reflect real conditions of 97%RH in the chamber. Values higher than 99%RH inside the chamber were never reached, as no condensed liquid water was found, neither on the sample holding devices nor on the samples. The dew point was therefore not reached or exceeded.

The system is equipped with a security system in case the measured values do not correspond to the programmed values. The tolerance range (difference between the set up and the measured value) can be defined by the user. If the measured value is out of the tolerance range the system stops automatically and an acoustic alert goes of. This was very helpful, as some of the tests had a duration of several weeks. It helped avoid the loss of time and specimens.

Demineralized water with an electrical conductivity of G=0,1 μS is required for the ACS chamber. An appropriate deionisation cell with a conductivity control gauge was installed in the lab, to provide the required water supply to the system.

In general, the Vötsch ACS chamber worked without any problems worth mentioning.

Before starting the test program, the electronic strain measurement sensors were calibrated and a reference curve of the charged sample holding device was recorded. The reference curve was used to evaluate the maximum strain variation of the charged sample holding device due to changing humidity conditions. The curve also takes the influence of changing humidity on the precision of the sensors into account, as they were in use during this reference test.

The reference curves were recorded, while the sample holding devices were charged with a cylindrical reference specimen under a load of 2 MPa and 4 MPa. The reference specimen have the same size as the shale specimen and are of the same material as the holding device.

The reference curves are given in figure 81. The periodic peaks, appearing for both devices, are due to vibrations caused by the fan inside the chamber, which turned on and off automatically from time to time, in order to regulate the air conditions. Otherwise no influence of a changing humidity on the sample holding device system can be recognized.

axial deformation of the sample holding devices and the elecric strain measuring sensors under changing relative humidity (5%/99%) at a constant temperature of 41 °C
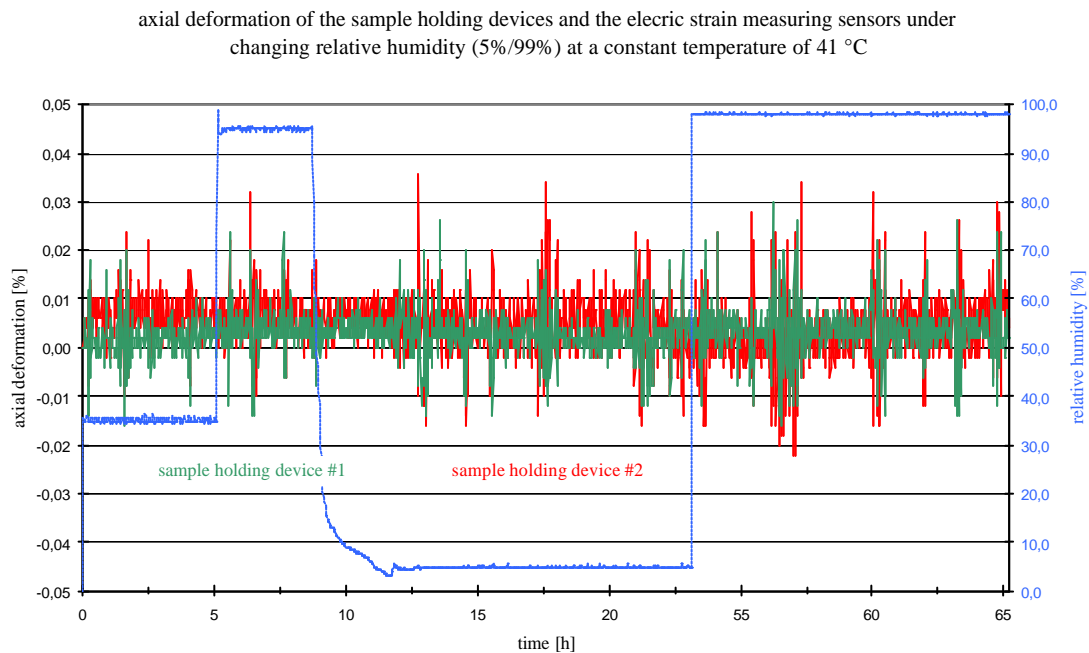

Figure 81: reference curve of the two sample holding devices to evaluate the influence of changing humidity

As the sample holding devices and the electronic sensors consist of metal, a temperature variation influences the measured strain of the system due to dilation of the gauge and the device. This deformation is about 0,03% to 0,04% for a temperature increment of 10°C. This strain was measured in a range between 10°C and 50°C.

According to figure 80, it was necessary to heat the chamber to 40°C, to realize a maximum humidity of 98%RH. Even though the strain (~ 0,05%) caused by a difference of about 15°C between room temperature and the required test temperature is rather negligible, the chamber was preheated to 40°C before the tests were started, to stabilize the whole system.

The sensors made by Phi Mesure exhibit a precision of +- 2,5 µm and were calibrated with a special high precision micrometer (+- 2µm) device. They provide an electric potential as output signal, which is converted into a corresponding length unit by the Lab View 6.0 software. The sensor signal was processed each minute, providing representative curves without any interpolation.

The precision of the measured strain values during test conditions are in the magnitude of +- 12% (relative error fro strain values bigger than 0,2%), which is the sum of the sensor precision the calibration precision and the maximum variation of the sample holding device in use. This means that a measured value of for example 0,3% axial deformation during a test represents approximately, a real value between 0,27% and 0,33% strain.

4.7.2   Results

The first test was a dehydration test with material from sample 05664, well 205/482 m. Specimen #32 and #33 were exposed to a humidity of 5% relative humidity and a temperature of 25°C. A temperature of 25°C was chosen in order to achieve the highest possible suction and therefore a strong saturation/time gradient (cf figure 82).

The specimen started to contract immediately after the start and stabilized after about 24 hours. Sample #33, which was charged with of 4 MPa stabilized at –0,85% strain and sample # 32 under 1,5 MPa at -0,7%. The contraction is partially due to the load and partially due to the desaturation in the dry environment.

Unfortunately it is not easily possible to separate the two influencing factors of suction and load.. A prestressing of the sample before puting it into the ACS chamber until the specimen stabilizes does not make sense without knowing the exact saturation of the material. The reason is, that the sample would be exposed to the humidity of the lab environment. This humidity is not necessarily equal to the initial saturation of the material. The consequence would be a suction. Meaning the two components would again act.

A possible solution would be to evaluate the exact initial saturation of the sample and to expose the sample to humidity, which corresponds to that saturation, which would not cause a suction, with the consequence of zero water transfer between the two systems. The contraction would only be caused by the mechanical effect of the load.

axial deformation of shale from Est, well #205/482 m in 5 % relative humidity,
sample #32/33, axial stress =1,5 MPa and 4MPa, Temp.= 25°C
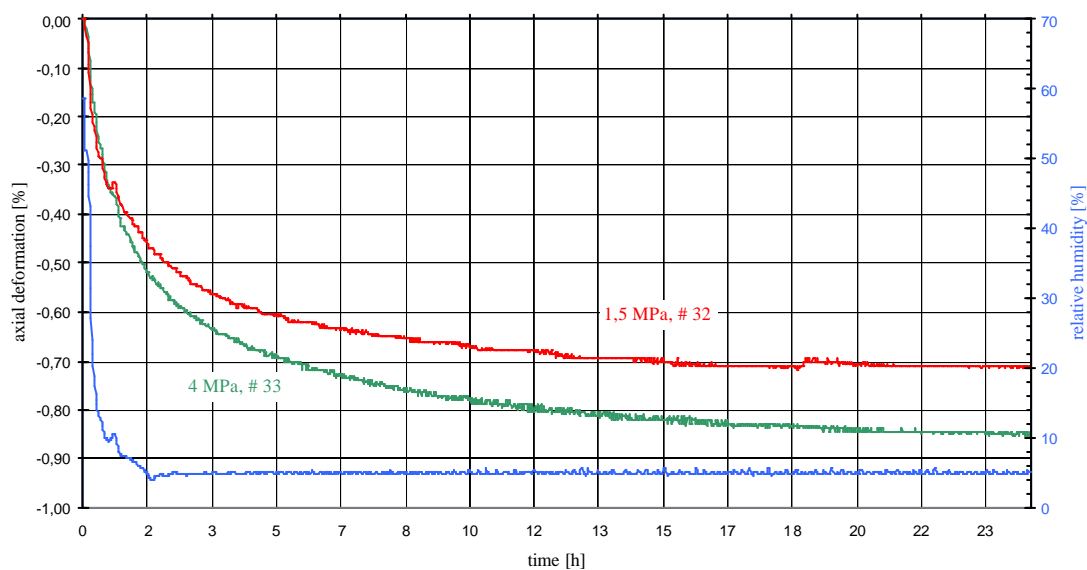
Figure 82: axial strain of #32 and #33 under different stress, exposed to a relative humidity of 5%.

The horizontal part of the curves represents an equilibrium of the sample between the stress and the saturation state of the material.

The relation of the higher strain to the higher load is not completely clear. The higher load could also stabilize the material and make it more resistant to humidity changes. The maximum strain could be smaller or the curve flatter due to a weaker saturation/time gradient. As there is no

evidence of this, the reason is probably that the specimen was not pre-stressed before the test. The mechanical stabilization therefore happened during the test.

If the additional strain is only because of the higher load, another option to separate the mechanical and saturation component would be possible. The desaturation of an unloaded sample would create a strain purely because of the influence of the saturation change. Each additional strain difference of a loaded specimen would be caused by the mechanical component. But this theory requires a constant influence of the saturation change on the strain, no matter what load is applied.

The reaction of the material to the small humidity derogation after 1 hour is remarkable. Both specimen reacted immediately to the small humidity change.

The comparison of the 2D µCR images (cf figure 83) showed a small difference between the condition of the material before and after the test for #32. Two micro crack systems were visible before and after the test. Their aperture and length was slightly increased after the test. This difference could be identified by using the maximum magnification on the screen.

Figure 83 a), b), c): 2D X-ray µCR from specimen #32. a) middle part before the test, c) lower part after the test and c) upper part of the specimen after the test. The material was exposed to a relative humidity of 5% and a charge of 1,5 MPa. T = 25°C, picture width = 16mm, µCR=22µm

Contrary to this, the comportment of the initial crack in the upper region of specimen #33 is obvious (cf figure 84). The crack system grew, passed the whole cross section of the specimen and increased its aperture. At the end of the crack a fine micro crack system developed. Several very small new cracks could be observed at the edge of the lower part.
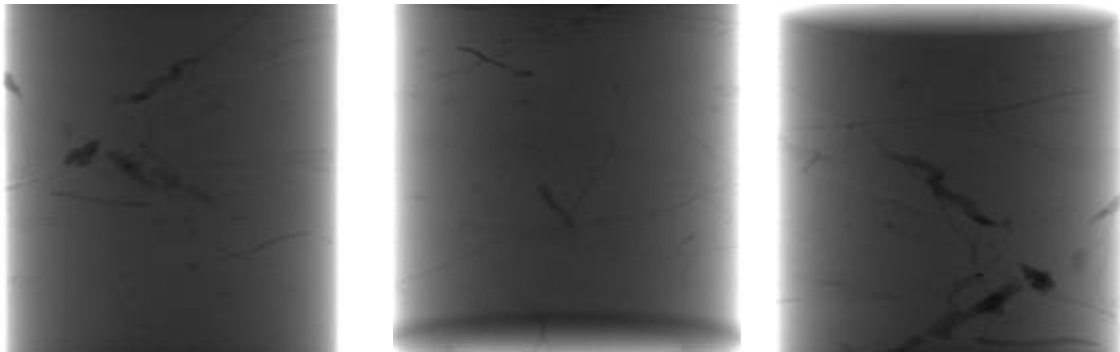

Figure 84: a), b), c): 2D X-ray µCR from specimen #33. a) middle part before the test, c) lower part after the test and c) upper part of the specimen after the test. The material was exposed to a relative humidity of 5% and a charge of 4 MPa. T = 25°C, picture width = 16mm, µCR=22µm

The next test was a hydration test in an environment of 99% RH with material from sample 05664, well 205/482 m #. Specimen #35 was charged with 4 MPa and #35 with 1,5 MPa (cf figure 85).

The specimen shrank a little initially and swelled continuously thereafter. The initial negative strain is due to the relative humidity at this time. The ACS chamber initially needs some time to achieve the set up value. In addition to this the ACS control system had a small delay in achieving the 99%RH, which is reflected by the up and down of the blue humidity curve in the diagram within the first 10 minutes of the test.

Specimen #35 showed the first indications of failure after just over three hours and broke completely 40 minutes later at 0,6% strain. Contrary to that #37 grew within the first 18 hours and stabilized afterwards at 2% strain. The horizontal part of the curve of #37 can be interpreted as an equilibrium between the applied mechanical stress and the saturation of the material.

axial deformation of shale from Est, well 205/482 m, exposed to 99 % relative humidity,
sample # 35/37, axial stress = 1,5 MPa and 4 MPa, Temp.= 41°C
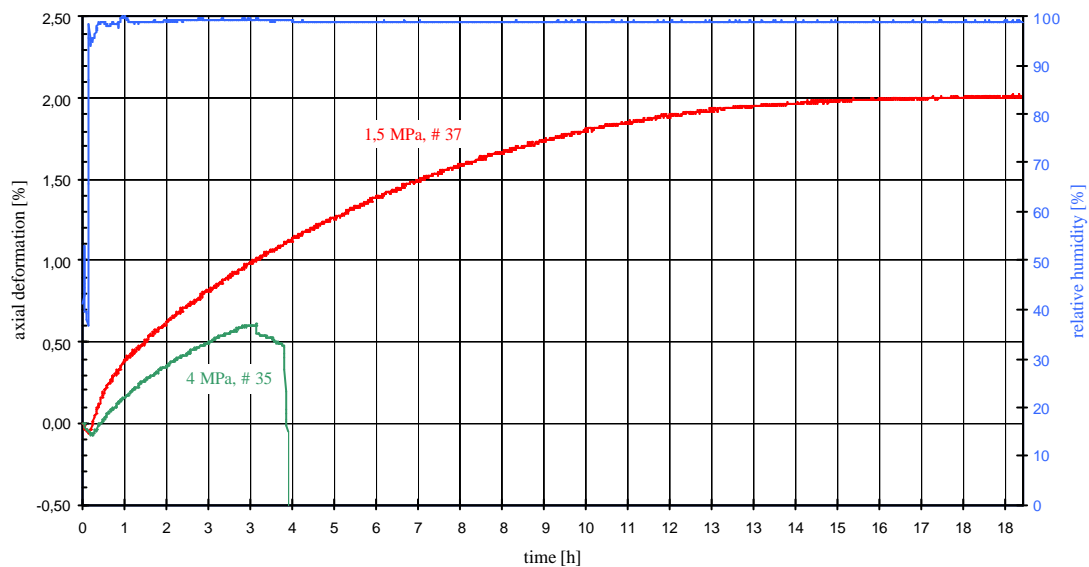
Figure 85: axial strain of #35 and #37 under different stress, exposed to a relative humidity of 99%.

The initial 2D X-ray image did not show any micro cracks in #37. After the test the whole specimen was completely interstratified with big and smaller micro crack systems (cf figure 86)
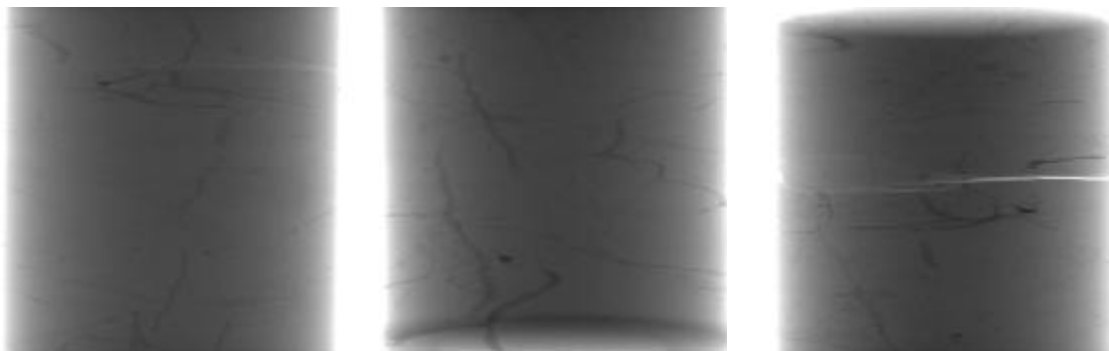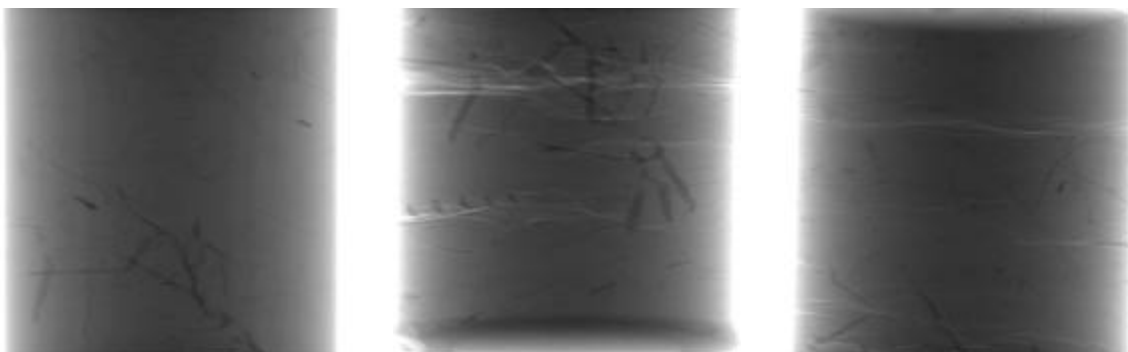

Figure 86 a), b), c): 2D X-ray μCR from specimen #37. a) middle part before the test, b) lower part after the test and c)upper part of the specimen after the test. The material was exposed to a humidity of 99% and a charge of 1,5 MPa. T =41°C, picture width = 16mm, μCR=22μm

Initially, the failure of #35 was thought to arise from the existing micro cracks in the material. The 2D X-ray image taken before the test highlighted a very tiny micro crack system close to the bottom and in the middle part of the specimen (cf figure 87).

Instead, the 2D X-ray analysis after the test clearly shows that the specimen failed in the top part, where no indication of cracks or other deterioration could be found before the test. The initially existing cracks were thus not responsible for the failure, but increased their aperture remarkably during the test. New crack systems appeared and the whole specimen was interstratified by them.
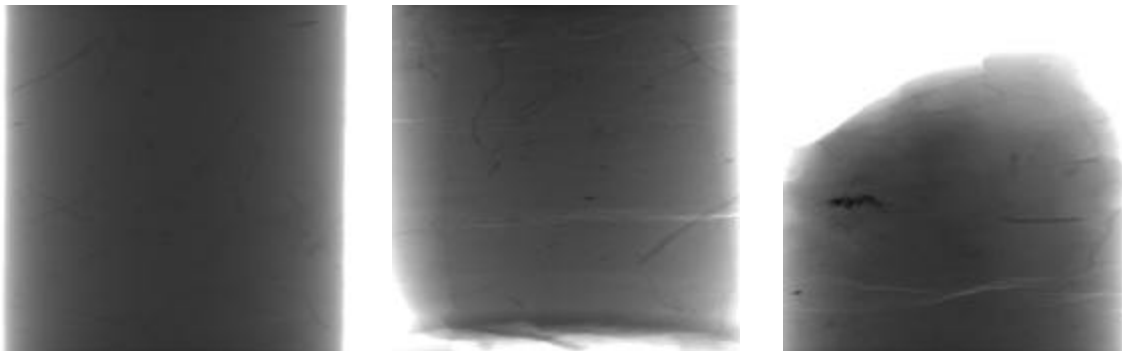
Figure 87 a), b), c): 2D X-ray µCR from specimen #35. a) middle part before the test, b) lower part after the test and c)upper part of the specimen after the test. The material was exposed to a humidity of 99% and a charge of 4 MPa. T =41°C, picture width = 16mm, µCR=22µm

The test with specimen #38 and #41, which originate from sample 05664, well 205/482 m, determined the maximum possible axial strain in a range from 5% RH to 99%RH (cf figure 88). Specimen #41 was charged with 4 MPa and #38 with 1,5 MPa.


Figure 88: axial strain of #38 and #41 under different stress, exposed to a relative humidity of 5% and 99%.

Both samples shrank immediately after the test was started, when exposed to 5% RH. They stabilized after 19 hours. Specimen #41 at a strain of –0,8 % and #38 at –0,6% (almost the values of #35 and #37. When the humidity was increased to 99% the material reacted instantly and grew. As in the last test, the material charged with 4 MPa failed, though a little later. The other specimen with 1,5 MPa stabilized at 1,9% strain after 32 hours.

The behaviour of the material in this test was in accordance to the previously described tests. The strain values as well as the fissuration of the material due to the subsequent hydration was very similar.

The next test was conducted to determine the most sensitive range of humidity in terms of axial deformation (sample 05664, well 205/482m). The relative humidity was constantly varied from 30% to 99%. The samples #30 and # 31 were charged with 4 MPa and 1,5 MPa (cf figure 89).
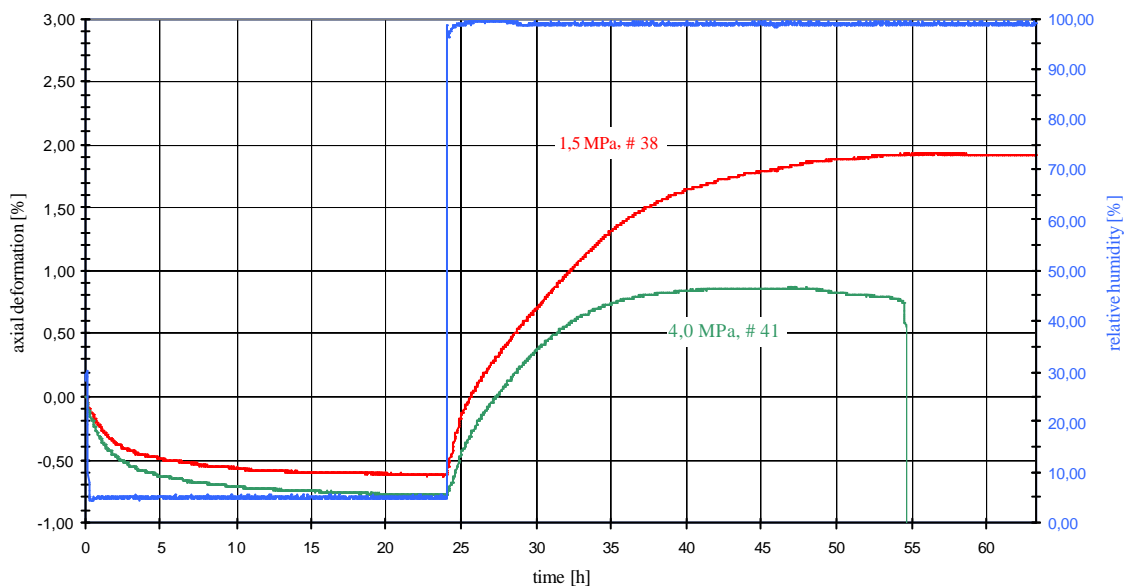
Initially the material shrank although started to grow constantly when the humidity passed about 40%. Both curves show a perfectly parallel growth comportment between 40% and 90% at different strain levels. Between 40% and 70% the growth rate was linear (could be linear under 40% without initial equilibrium). Subsequently between 70% and 90% the growth was still nearly constant, but with an increased gradient. After the humidity had passed 90% the growth rate was again increased for both specimen. #31 reached its maximum gradient after passing approximately 95% relative humidity, whereas #30 had an almost constant growth rate of between 90% and 99%.

Unfortunately an error occurred when the ACS system reached the 99% relative humidity value and the test had to be stopped. Nevertheless it could be shown that the highest growth gradient is reached at a relative humidity higher than 90% for #30 and with a maximum between 95% and 99% for #31.

axial deformation of shale from Est, well #205/482 m, exposed to a varying relative humidity from 30% to 99%, sample # 30/31, axial stress = 1,5 MPa and 4 MPa, Temp. = 41°C

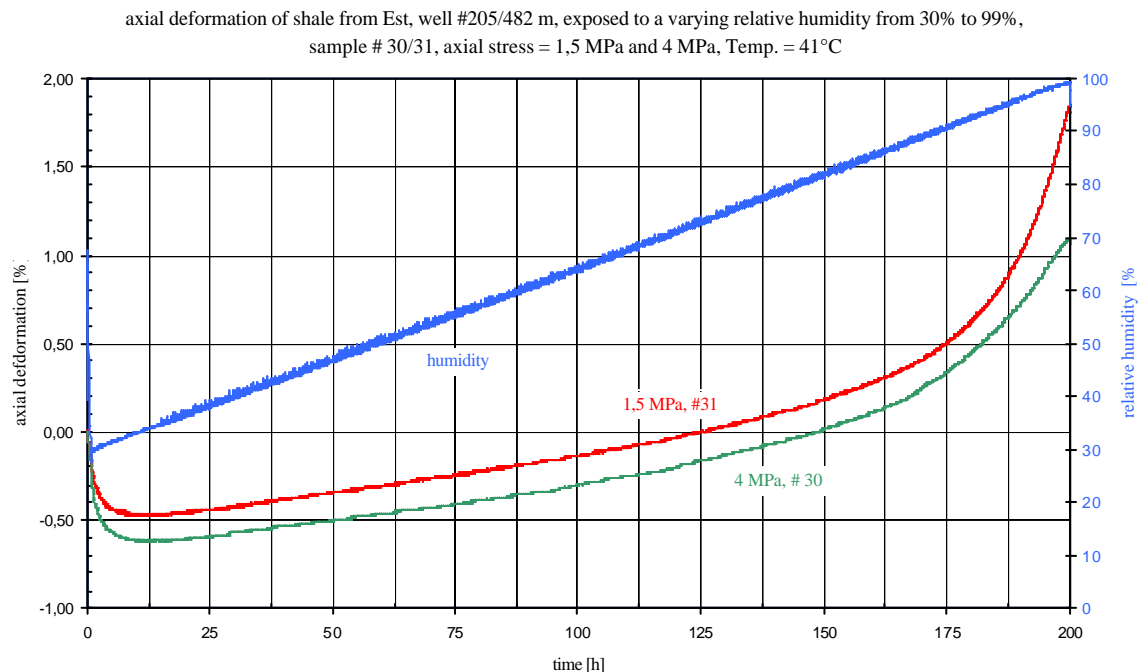Figure 89: axial strain of #30 and #31 under different stress, exposed to a constantly varying relative humidity between 30% and 99%.

Even though the specimens were slowly hydrated for a period of 188 hours, and only exposed to a relative humidity of 99% for some minutes, the 2D X-ray µCR detected micro cracks after the test, which didn't initially exist. The micro cracks had in general a weaker aperture than the cracks

generated in the test where the material was exposed to 99% relative humidity from the beginning and for a longer time. But the distribution of the cracks is similar. One big crack system, which passed the whole cross section of the sample, and many small cracks were detected in specimen #31 (cf figure 90).

With reference to the growth rate it is very likely that the highest saturation increase of the material is in the range of 90% to 99% relative humidity, which triggers the cracking.
The total strain during the whole test was 2,4% for specimen #31 and 1,7% for #30 which corresponds to the previously obtained results.
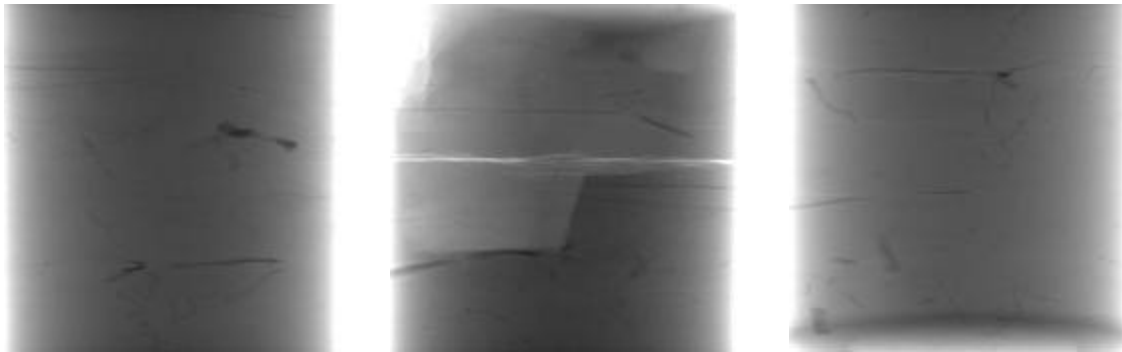

Figure 90: a), b), c): 2D X-ray µCR from specimen #31. a) middle part before the test, b) lower part after the test and c) upper part of the specimen after the test. The material was exposed to a constantly varying humidity between 30% and 99% and a charge of 1,5 MPa. T =41°C, picture width = 16mm, µCR=22µm

The following cyclical test was conducted with specimen #39 and #40 from sample 05664, well 205/482 m. The standard stress of 4 MPa and 1,5 MPa was applied. Figure 91 examines the strain comportment and the reactivity of the material to the cyclical changing relative humidity.

The humidity range was chosen according to the linear zone of figure 89, which also corresponds to the realistic range of an underground construction site. The aim was to determine whether deterioration or cracks could be caused due to an increased "fluctuation number" provoked by periodical strain changes. The humidity range between 35% and 75% is not believed to cause any cracks or deterioration after one dehydration rehydration cycle.

The material reacted immediately to each humidity change and took only about 18 hours to stabilize in the first two cycles. After the first two cycles the time interval was shortened for each cycle. The aim was to observe, if the reactivity would remain – it did. At the end of the test the humidity changing interval was 2 hours. The material changed its axial length by 0,1% caused by hydration and about 0,15% due to dehydration.

The result shows the maximum strain range of both specimens correlates to values between 35% and 75% humidity represented in figure 89 (constantly varying humidity). The total strain for both samples is in the same magnitude of 0,5% for #40 and 0,55% for #39. But the first two dehydration/rehydration cycles had different shrinkage and swelling amplitudes and convergent tendencies. The curve of the 1,5 MPa charged material seems to move upwards, as the hydration cycle starting after 90 hours took only 10 hours to reach the strain level of the preceding hydration cycle, which took 20 hours.

Neither micro cracks nor any other deterioration was observed in the 2D X-ray µCR images of specimen #39. The material exhibited identical properties after the test. (cf. figure 92).

As only two full cycles were done in the first cyclical test, a long term test with the same humidity program was conducted with specimens #44 and #45 05664, well 205/482 m (cf figure 93).

axial deformation of shale from Est, well #205/482m, exposed to a cyclical changing rel. humidity, 35% to 75%,
sample # 39/40, axial stress is 1,5 MPa and 4 MPa, Temp. = 41°C

Figure 91: axial strain of #39 and #40 under different stress, exposed to a cyclically varying relative
humidity between 35% and 75%.
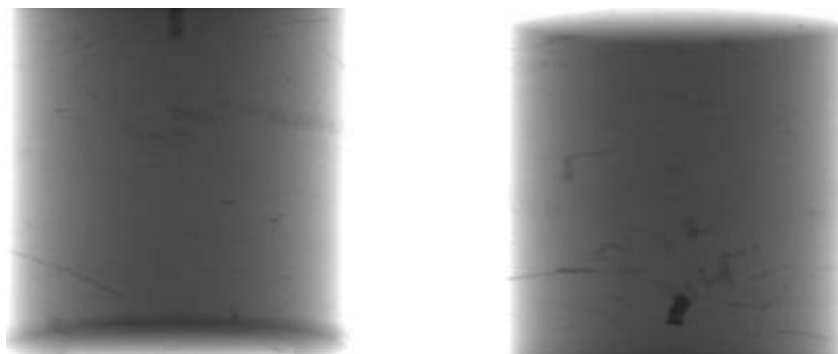
Figure 92a) b): 2D X-ray µCR of specimen #39. a) lower part after the test and b) upper part
of the specimen after the test. The material was exposed to a cyclically changing humidity
from 35% to 75% and a charge of 4 MPa. T =41°C, picture width = 16mm, µCR=22µm

At a first glance, the results of the long term cyclical test, the swelling and shrinking cycles, seem
very uniform and reproducible. But the diagram also clearly shows the previously observed
convergence between the two curves, similar to the result of the first cyclical test. The analysis of
the cycles of specimen #45 (4 MPa load) identified three phases of this convergence (cf figure 93).

The first phase starts at the first rehydration and ends after three rehydration/dehydration cycles.
The value of the swelling strain is lower than the absolute value of the following shrinkage strain.
In addition to that, the values of the swelling and the shrinkage strain are not constant. In this
phase the swelling strain grows from 0,4% to 0,46% and the corresponding shrinkage strain
decreases from -0,46 to -0,5%. The result is a rapid movement of the dehydration coverage curve
of the cycles from -0,30% to -0,44% absolute strain, within the first 9 days.

axial deformation of shale from Est, well #205/482m, exposed to a cyclical changing rel. humidity, 35%/75%, sample # 44/45, axial stress = 1,5 MPa and 4 MPa, Temp. = 41°C
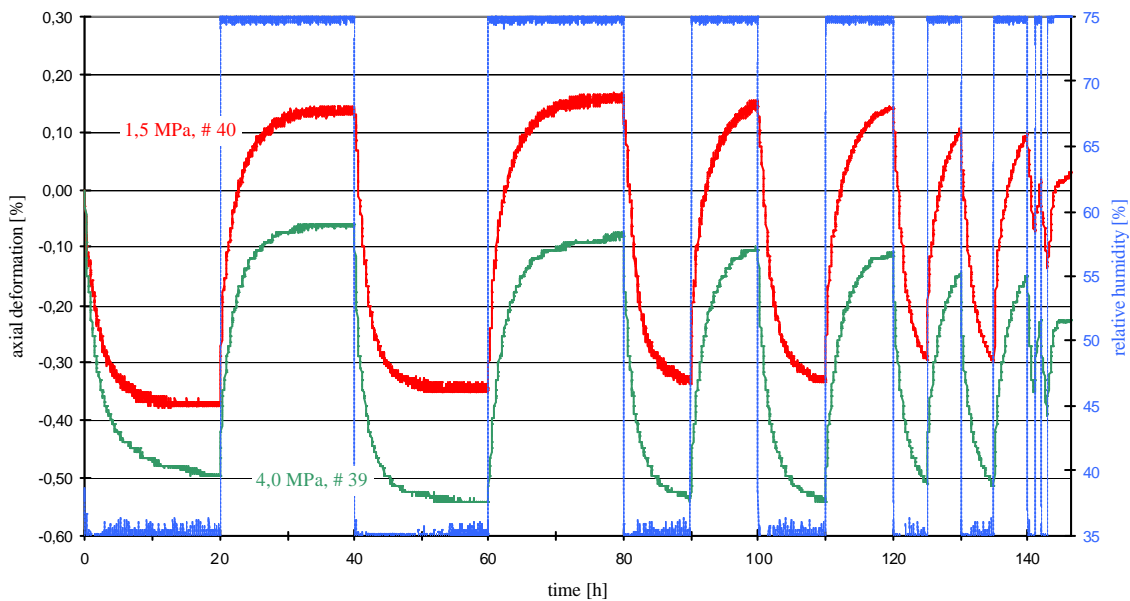

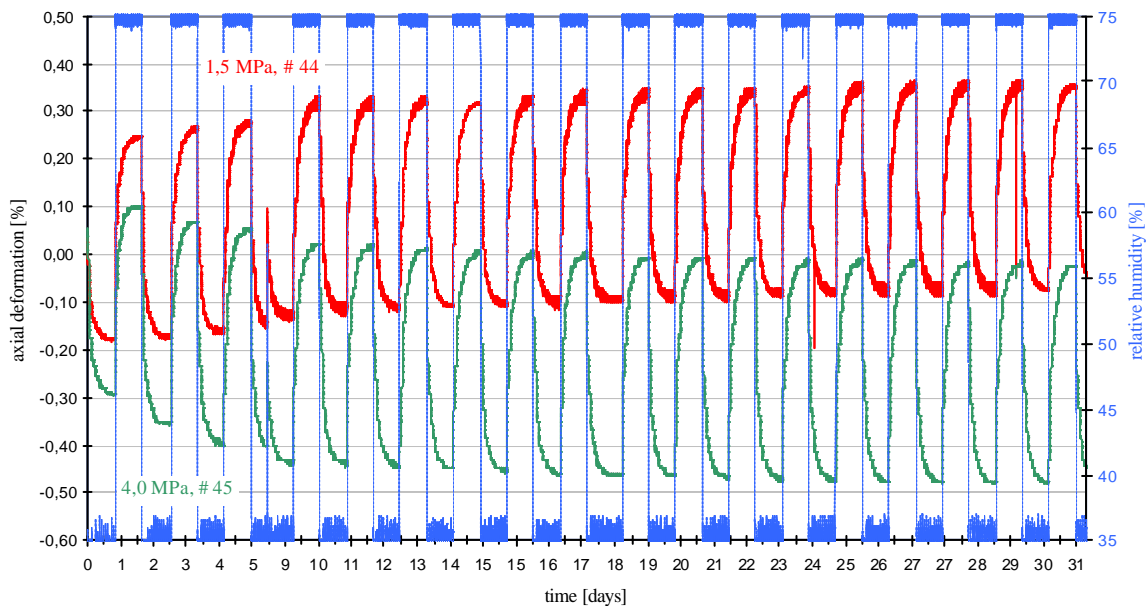Figure 93: axial strain of #44 and #45 under different stress, exposed to a cyclically varying relative humidity between 35% and 75%. The irregularity between the 5th and the 7th day was caused by a power failure.

In the second phase, which is between the end of the third rehydration/dehydration and the end of the eleventh cycle the absolute value of the shrinkage strain is still higher than the preceding swelling strain. But both strains are now constant. In this phase the swelling strain is 0,46% and the corresponding shrinkage strain is 0,47%. The result is a linear and lower movement of the coverage curve of the cycles from -0,44% to -0,48% absolute strain within 12 days.

After 21,5 days and eleven rehydration/dehydration cycles the system stabilized, which can be considered as the third phase. Both, the swelling and the shrinkage strain had the same absolute value of 0,46% and the envelope curve of the cycles shows no inclination – the cycles are constant.

In summary, the material of #45 developed a maximum total shrinkage strain of -0,48% in the constant third phase at 35% relative humidity. This value corresponds to the strain of 0,5% obtained through the constantly varying humidity test between 35% and 75% RH.

The behaviour of specimen #44 is in complete contradiction to the comportment of #45. In this case the value of the swelling strain is higher than the shrinkage strain. The envelope curve of the cycles therefore moves upwards - towards an increasing total swelling strain value. At 75% relative humidity, the swelling strain was 0,25% at the beginning of the test and 0,35 at the end of the test. No stabilization of the system was observed, as the envelope curve exhibits a gradient for the whole testing period.

A possible explanation for this phenomenon can be found in the arrangement of the clay particles of the material. The cylindrical specimen have the bedding plane perpendicular to the z-axis. This means the particles are parallel to the x/y plane. But initially these particles are not perfectly parallel orientated to the x/y plane.

In the case of the 4 MPa loaded specimen, an orientated reorganisation of the clay particles during each dehydration cycle takes place. In the third phase, after the 11th cycle, their orientation is more parallel to the x/y plane than they were at the beginning of the test – a paralellisation took place.

The mechanical load was thus strong enough to reorganize the particles during the dehydration cycles. The result is a descent of the envelope curve of the cycles towards lower values of negative strain – a constant shrinkage of the specimen.

The reason for the increase of the negative strain is comparable to the fatigue behaviour of metallic materials. The de/hydration cycles represent the fluctuation number of the load. In the case where the shale is stabilized, it reached the "fatigue strain" after a certain number of cycles.

A schematic description of the first phases, in which the total negative strain increases , is given in figure 94. The scheme shows a z/x cross section of clay particles, which is represented by an exaggerated inclination.

THS_i is the total hydration strain at the cycle i. THS_i is increasing (absolute value) in this phase, with the number of cycles, due to the remaining negative strain. TDS_i is the total dehydration strain at the cycle i and is also increasing (absolute value). But THS_i and TDS_i have a different increment between the two cycles. ADS_i is the strain amplitude of the dehydration cycle i and AHS_i is the strain amplitude of the hydration cycle i.

Figure 94: schematic description of the behaviour of the clay particles and the negative strain in the first unstable phases of the cyclical test under 4 MPa load. The envelope curves have a different gradient.
$THS_{i-1} < THS_i < THS_{i+n}$ / $ADS_{i-1} < ADS_i < ADS_{i+n}$ / $AHS_{i-1} < AHS_i < AHS_{i+n}$ / $TDS_{i-1} < TDS_i < TDS_{i+n}$

In the second phase we have a constant dehydration (ADS) and hydration (AHS) strain amplitude. ADS_i is bigger than AHS_i and the remaining negative strain for both envelop curves develops with the same gradient. The total remaining strain of hydration (THS_i)and dehydration (TDS_i) have therefore the same linear growth (cf figure 95).

Figure 95: schematic description of the behaviour of the clay particles and the negative strain in the second unstable phases of the cyclical test under 4 MPa load. Both envelope curves have the same gradient.
$THS_{i-1} < THS_i < THS_{i+n}$ / $ADS_{i-1} = ADS_i = ADS_{i+n}$ / $AHS_{i-1} = AHS_i = AHS_{i+n}$ / $TDS_{i-1} < TDS_i < TDS_{i+n}$

The third phase, in which the amplitudes of the hydration and dehydration strain have the same value, is presented in figure 96. The system is stable and the envelope curve has no inclination – the total strain is constant between the hydration and dehydration maxima. TDS_i = constant, ADS_i = constant, AHS_i = constant and $ADS_i = AHS_i$. The total strain thus varies constantly between the

two maxima. This could be interpreted as an indication, that micro cracks could act like a valve – they open and close under certain humidity conditions without changing their characteristics.
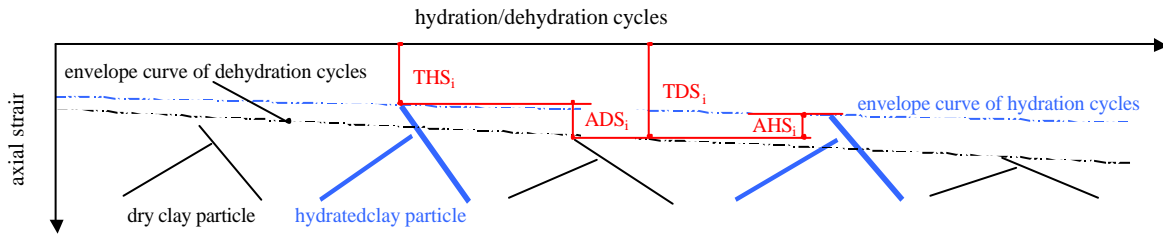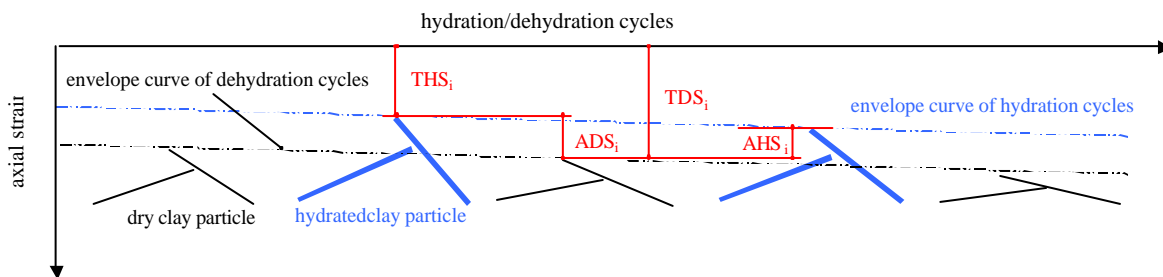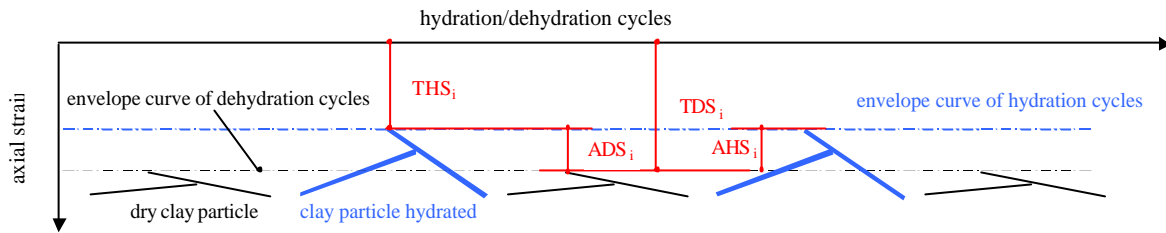

Figure 96: schematic description of the behaviour of the clay particles and the negative strain in the third and stable phases of the cyclical test under 4 MPa load. Both envelope curves have no gradient.
$THS_{i-1} = THS_i = THS_{i+n}$ / $ADS_{i-1} = ADS_i = ADS_{i+n}$ / $AHS_{i-1} = AHS_i = AHS_{i+n}$ / $TDS_{i-1} = TDS_i = TDS_{i+n}$

In the case of the 1,5 MPa loaded material, this reorganization effect does not occur (cf figure 97). The clay particles show less parallel orientation to the x/y plane after each dehydration cycle, compared to their initial orientation – the degree of disorder of the particles increases. The mechanical load is too low to reorganize the particles in the dehydration cycles. The particles stay blocked and disordered. The sample is constantly growing, which is reflected by the ascent of the envelope curve of the cycles. The process exhibits the opposite mechanisms to that of the first phase of the 4 MPa specimen.

THS_i is increasing in this phase, with the number of cycles, due to remaining positive strain. TDS_i is also increasing, but at a different rate to THS_i. ADS_i is smaller than AHS_i and they are both variable.
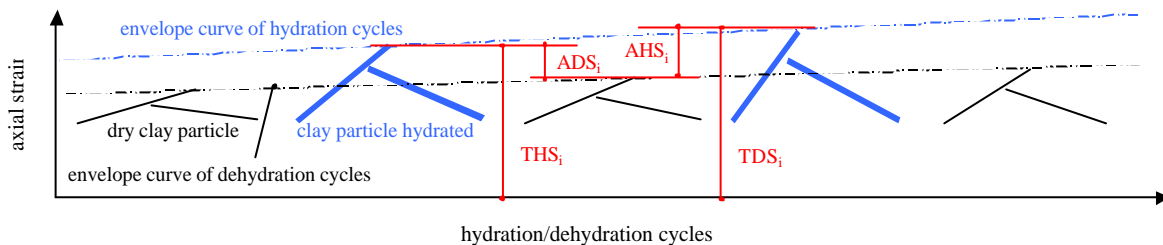
Figure 97: schematic description of the behaviour of the clay particles and the positive strain in during the whole cyclical test under 1,5 MPa load. Both envelope curves have a different gradient.
$THS_{i-1} < THS_i < THS_{i+n}$ / $ADS_{i-1} < ADS_i < ADS_{i+n}$ / $AHS_{i-1} < AHS_i < AHS_{i+n}$ / $TDS_{i-1} < TDS_i < TDS_{i+n}$

Even though no deterioration or micro cracks were detected after the long term test between 35% and 75% relative humidity, it is very likely that deterioration could occur for cycles with a larger humidity interval. The larger the humidity range, the greater the required force will be to reorganize the particles.

In addition to the previously presented tests with 1.5 MPa and 4 MPa, some hydration tests with unloaded material and a charge of 2 MPa were done. The swelling heave of specimens #42 and #46 from sample 05664, well 205/482 m is given in figure 98. The strain of 2,3% for the unloaded material and 1,6% for a load of 2 MPa is in accordance with the 2,0% strain obtained with 1,5 MPa stress and the 0,8% with 4 MPa load.

The observed reduction of the swelling heave due to an increased axial load supports the assumption that: there exists a certain load, under which the material does not swell under 99%RH. Nevertheless it is very likely that the material would fail, as the stress would be to high for the structure (first of all the matrix) of the material.

axial deformation of shale from Est, well 205/482 m, exposed to 99 % relative humidity,
sample # 42/46, axial stress = 0 MPa and 2 MPa, Temp.= 41°C
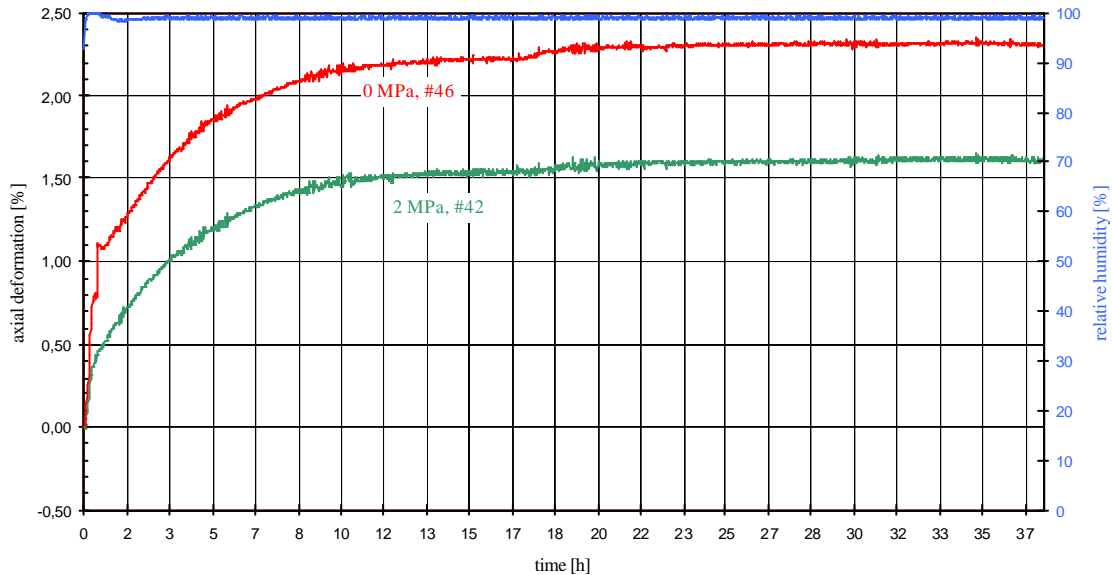
Figure 98: axial strain of #42 and #46 under different stress, exposed to a relative humidity of 99%.

The 2D X-ray analysis of the specimen #46 clearly shows the micro cracks due to hydration. The whole cross section is interstratified with big and smaller crack systems (cf figure 99). The result clearly shows intrinsic cracking of the material, caused by an increased humidity. The term intrinsic is used with reference to the explanations given in chapter 3.1, pp.55.
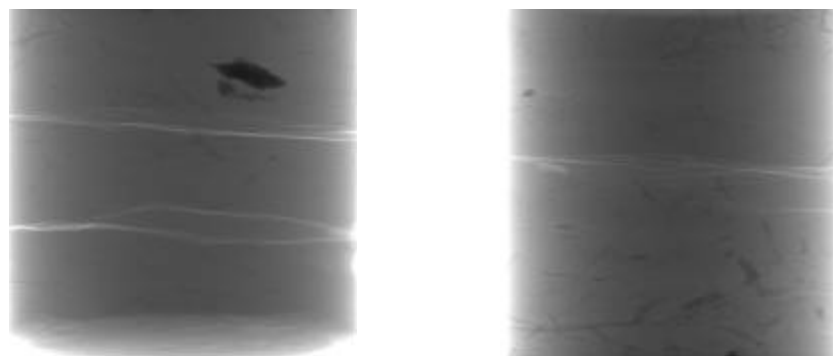
Figure 99a) b): 2D X-ray μCR of specimen #46. a) lower part after the test and b) upper part of the specimen after the test. The material was exposed to a relative humidity of 99% and no charge. 0 MPa, T =41°C, picture width = 16mm, μCR=22μm

Specimen #42 was equally interstratified with cracks, comparable to specimen #37, which was exposed to a charge of 1,5 MPa.

In general, the axial swelling strain results are in accordance with the general reactivity of the material observed in the solution test. The different strain values can be directly related to the mineralogical composition of the material (cf chapter 4.3).

The relation of the Smectite Illite portion to the content of carbonates seems to govern the strain behaviour. A high Smectite Illite portion combined with a low portion of Carbonates allows the high swelling strains observed in material from sample 05664, and vice versa from sample 02517.

Figure 100 presents the swelling heaves of the three different obtained Callovo Oxfordian materials under a load of 1,5 MPa and exposed to a relative humidity of 99%.

axial deformation of shale from Est under 99 % relative humidity and different stress states,
sample # 35/37 (205/481m), # 48/49 (205/445m), # 60/61 (104/511m)
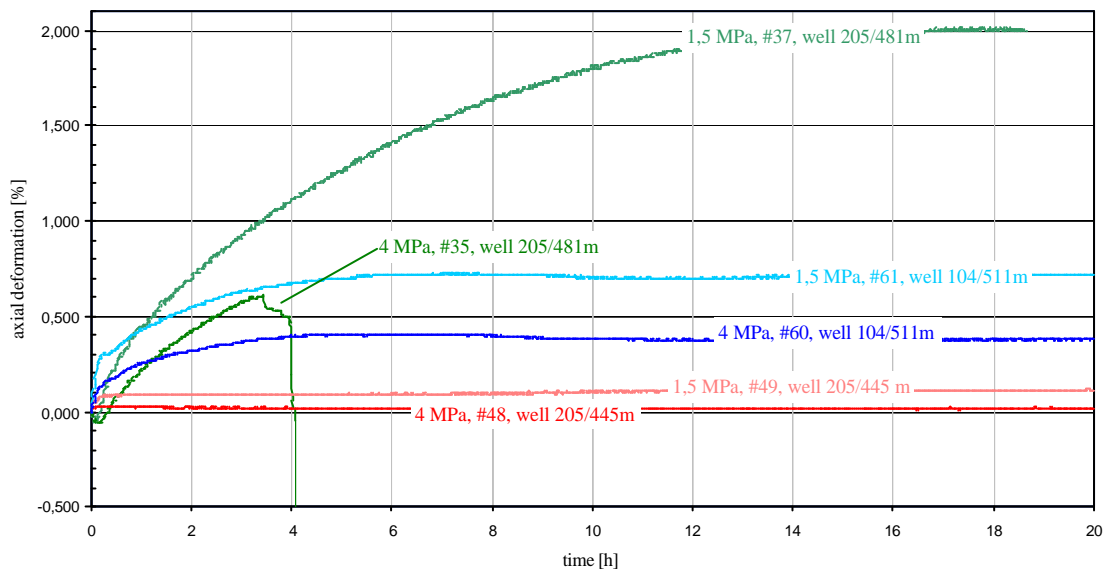
Figure 100: axial strain of the Callovo Oxfordian shale from different zones, under different stress and exposed to a relative humidity of 99%. (#35 and # 37 from sample 05664, well 205/482m, #48 and #49 from sample 05514, well 205/445m, #60 and #61 from sample 02517, well 104/511m)

2D X-ray analyses of specimens #60 and #61 exhibited micro cracks, but the sample was not completely interstratified with small cracks as in the case of #37 (cf figure 101).
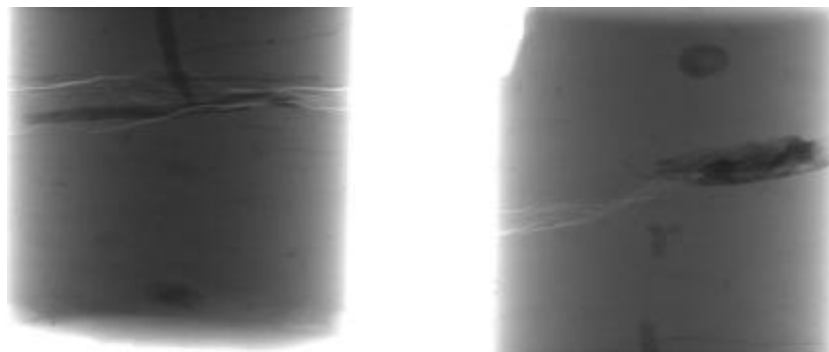
Figure 101a) b): 2D X-ray µCR of specimen #61 a) lower part after the test and c) upper part of the specimen after the test. The material was exposed to a relative humidity of 99% and a charge of 14,5 MPa. T =41°C, picture width = 16mm, µCR=22µm

Several 2D X-ray analyses of the specimens #48, #49, did not detect any micro cracks or other deterioration after the test with 99% relative humidity.

In all previously described kinetic tests the material did not disperse or lose its solid character, as was often the case in the solution test. Even though some of the specimens failed, the characteristics of the failure were different to those in the solution test. The material broke into several bigger pieces, but did not completely deteriorate. The samples which did not fail during the test, hardly had any macroscopic surface cracks or other signs of damage.

Finally, we briefly want to discuss the nature of the swelling and shrinking curve of the material, when exposed to a 99% and 5% relative humidity. Both curves clearly approach asymptotically a threshold, where the suction of the material is in equilibrium - due to its saturation - with the suction caused by the environmental conditions.

The values of specimen #37 were therefore plotted in a logarithmic graph (cf. figure 102). The almost linear relation between the time and the axial deformation shows that the strain behaviour obeys an exponential law.

The gradient of the line was not determined. It would be too great an approximation to conclude from the existing limited amount of strain data of one type of core material, a general exponential constant for this type of shale. Furthermore, there is a large variance in swelling heaves between the different core samples we obtained from ANDRA (cf figure 100).

axial deformation of shale of Est under 99 % relative humidity and different stress states,
sample # 37
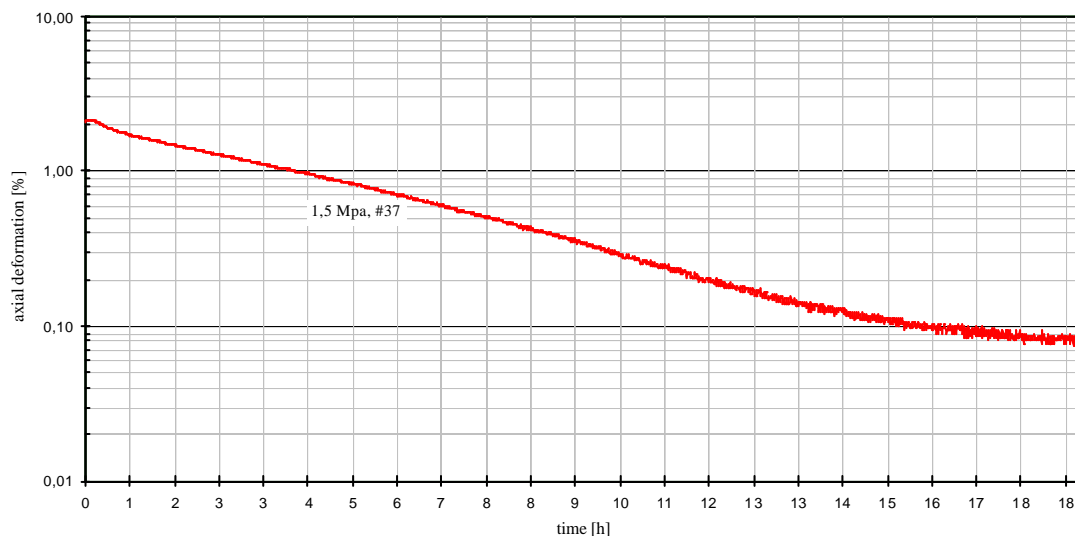
Figure 102: axial strain of #37 under 1.5 MPa stress, exposed to a relative humidity of 99%.

4.7.3 Conclusion

The strain and cracking comportment of different shale from the Callovo Oxfordian layer were analyzed. The material was tested under uniaxial load conditions from 0 MPa to 4 MPa and exposed to distinct relative humidity (RH) conditions in a range from 5% to 99%. For the first time ever, the relation between environmental humidity, axial strain, axial load condition and micro cracks was analyzed.

It was clearly shown that the test arrangement, which comprises the Vötsch air conditioning system, the sample holding device, the electronic strain sensors, cylindrical specimen and the X-ray microfocus radiography, is an effective way to conduct these kinetic tests.

Material from sample 05664, well 205/482 m:

The material reacts to suction variations with axial deformation. The total axial strain is in the range of 1,6% (4 MPa) to 2,5 % (1,5 MPa) between 5% and 99% RH. The swelling heave of the initial material is between 0,8% (4 MPa) to 2,5% (0 MPa) at 99% RH. The shrinkage is between -0,6% (1,5 MPa) and -0,8% (4 MPa) at 5% RH. The total strain at between 35% and 75% RH is in the range of 0,45% to 0,48% (1,5 MPa, 4 MPa) under cyclical conditions.

The swelling comportment seems to obey an exponential law and the highest swelling gradient was observed at between 90% and 99% RH.

It was proven, that micro cracks with an aperture of more than 30μm are generated at 99%RH under all load conditions (0 MPa to 4 MPa). The material therefore exhibits intrinsic cracking at 99% RH (0 MPa). In all cases at 99% RH the whole specimen was interstratified with micro cracks. Micro cracks with a rather small aperture (30μm to 80μm) could also be observed at 5% RH for 1,5 MPa and 4 MPa. The crack density is lower by comparison to the cracks generated at 99% RH.

The cyclical change of humidity between 35% and 75% RH does not create micro cracks with an aperture bigger than 30μm. No cracks or other deterioration could be observed with a X-ray resolution of 22μm. The observed convergence comportment of the envelope curves for the different load conditions is thought to arise from the reorganization of the clay particles.

In general the material can be classified as highly reactive to suction variations, with reference to the strain and micro crack comportment, with a very sensitive range between 90% RH and 99% RH.

Material from sample 05514, well 205/445 m:

The material showed nearly no axial deformation when exposed to 99% RH. The measured strain was between 0,02% (4 MPa) and 0,1% (1,5 MPa). The material did not show any deterioration or micro cracks after the test. The material is nearly unaffected by different humidity levels.

Material from sample 02517, well 104/511 m:

The material reacted to humidity variations with axial strain in the range of 0,7% (1,5 MPa) and 0,4% (4 MPa) at 99% RH. The material generated micro cracks at 99% RH under 1,5 MPa and 4 MPa. The distribution density of the cracks is lower in comparison to material 05664, well 205/482 m. The fossil inclusions in the material seem to support micro cracks due to axial strain.

In terms of its strain and cracking reactivity, the material is sensitive to humidity changes, but not to the same degree as material from sample 05664, well 205/482 m.

The comportment of all three materials can be related to their mineralogical composition (see chapter 4.3). The relation of the Smectite Illite portion to the content of Carbonates, which acts as the matrix, seems to govern the strain behaviour. A high Smectite Illite portion in combination with a low percentage of Carbonates enables the high strains and the creation of micro cracks. The ratio of the swelling clay minerals to the Carbonates is ~ 1,5 for sample 05664 (well 205/482 m) ~ 0,8 for sample 02517 (well 104/511m) and ~ 0,4 for sample 05664 (well 205/445 m).

_____

4.8 The combined test

The aim was to determine whether the material reacts in a different way to pure water after being saturated in the ACS chamber, compared to its reaction in the solution test. The material was initially exposed to 5% and 99% relative humidity and subsequently immersed into pure water.

The first test was the continuation of the previously described test to evaluate the maximum possible strain in a range from 5% to 99% relative humidity. After 67 hours, specimens #38 (1,5 MPa) and #41 (4 MPa), were immersed into pure water under load. The whole sample holding devices, including the electronic strain sensors, were put into big glass cylinders, which were filled with water (the sensors were not in contact with water). The strain behaviour of the material is presented in figure 103.

axial deformation of shale from Est, well #205/482 m, exposed to a relative humidity of 5%, 99% and subsequently immersed into pure water: sample # 38/41, axial stress = 1,5 MPa and 4 MPa, Temp. = 41°C/25°C
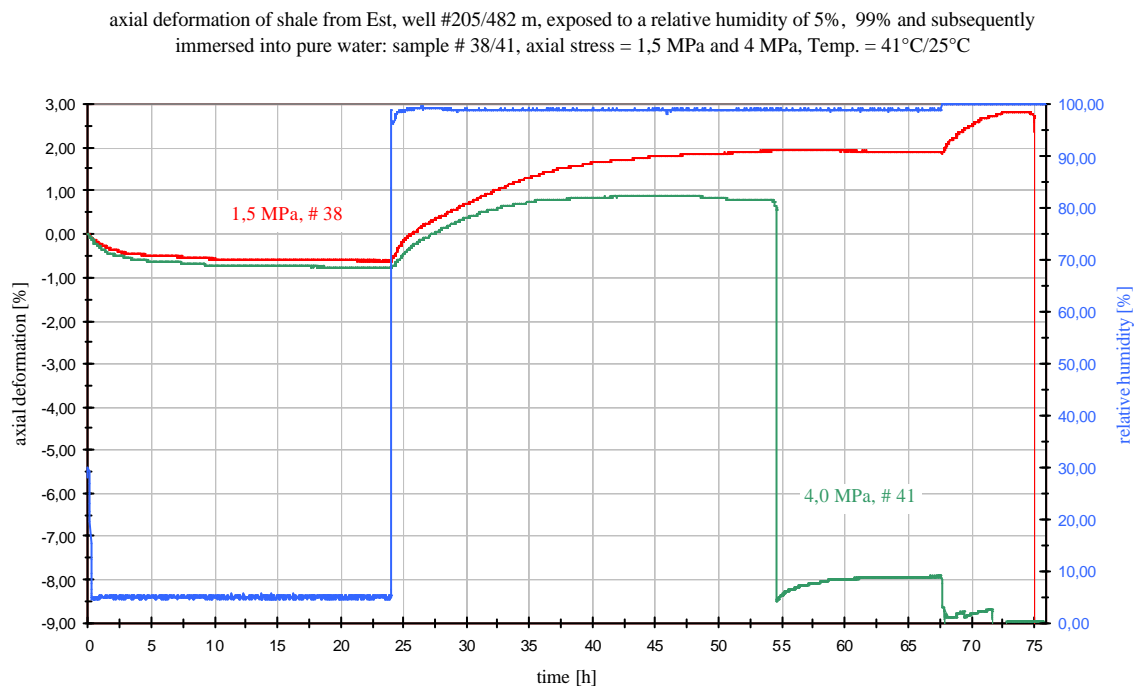
Figure 103: axial strain of #38 and #41 under different stress states, exposed to a relative humidity of 99% followed by immersion into pure water..

Specimen #38 started to swell immediately after the cylinder was filled with water and broke about 7 hours later at a strain of 2,8%. Contrary to that #41, which had already failed at 99% relative humidity, initially shrank and had some swelling shrinking cycles afterwards.

The first thing, which was obviously different to the solution test, was the magnitude of the swelling. It was 0,2% for pure water in the solution test and 2,8% in the combined test.

But the most striking distinction was the characteristic of the failure. No plastification was observed before the rupture. The sample broke into a few solid peaces without any signs of material dispersion. In the solution test the material dispersed completely after 38 minutes.

The biggest fragment of #38 was taken out of the sample holding device, placed in a smaller cylinder, and filled with pure water. To demonstrate the difference of the "standard" reaction of untreated initial material to pure water, specimen #13 was also immersed into pure water. The result after more than 100 hours is given in figure 104.

The material did not react at all to pure water, no dispersion or damage occurred for 150 hours.

_____

_____
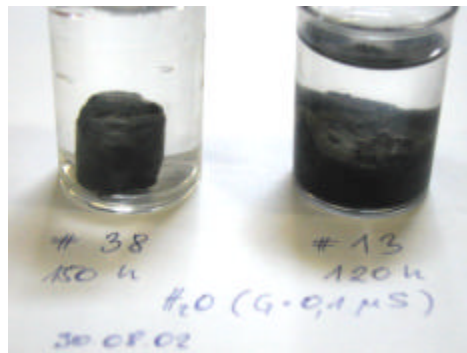
Figure 104: comparison of a fragment of specimen #38 and specimen #13 after more than 100 hours. #38 did not react at all, where as #13 dispersed completely. #38 was immersed into pure water after being exposed to 5% and 99% relative humidity under 1,5 MPa. #13 was immersed with initial properties.

As this very remarkable phenomenon was created under incompatible conditions, #38 was loaded when put into contact with water and #13 was not, another test was realized.

Specimens #14 and #15, both from sample 05664, well 205/482m, were immersed into pure water in the same glass cylinder. #15 was in initial untreated material state. #14 had been exposed to 99% relative humidity in the ACS chamber, under unloaded conditions for 20 hours, before it was immersed into water. Both specimen were put into contact with water at the same time (series 11).
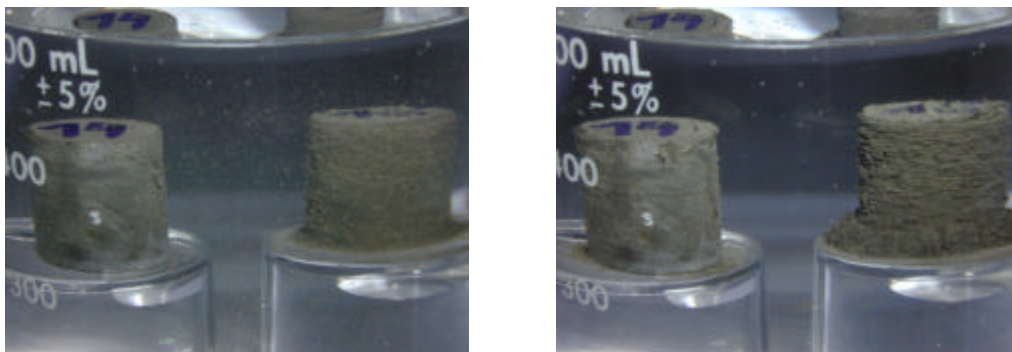
Series 11 a), b), c), d): a) #14 and #15 immediately after the glass cylinder was filled and b) after 10 minutes c) after 20 minutes and b) after 30 minutes. #14 was unloaded hydrated in the ACS chamber at 99% RH before being immersed into pure water (G=0,1 µS). #15 was immersed in initial state conditions.

_____
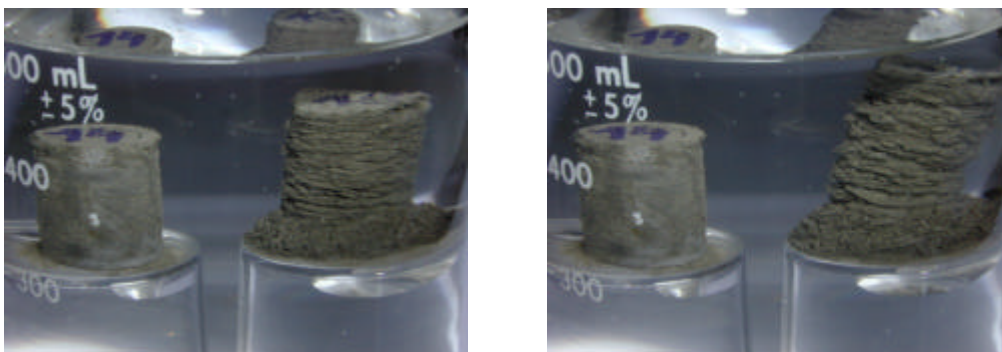
The pictures of series 11 clearly show the difference. The untreated material (#15) shows an intense reaction, where as (#14), the 99% RH saturated specimen, does not. #15 collapsed after 30 minutes and dispersed completely into fine particles. #14 exhibited the first cracks after 10 minutes, but did not disperse or deteriorate as the other specimen did. The specimens were left in the cylinder for two weeks. The result was the same after two weeks as after the first hour. #14 had not reacted, it exhibited the same cracks and had the same shape.

The question was now whether this inert character of the 99% RH saturated material is a remaining permanent material property, or if it could be changed back into a reactive material. If it is not a remaining property, the phenomenon is caused by the different mechanisms between a hydration with humid air and a hydration with liquid water.

The fragment of specimen #38 was therefore taken out of the water after 150 hours - it still had no signs of deterioration – and dehydrated in the ACS chamber at 5% RH. The fragment was subsequently immersed into pure water (series 12).

The process of deterioration was much faster and more powerful for the dry material, than was observed with the initially untreated material. This acceleration is obviously due to the fact, that the material was completely dehydrated when immersed into water. The test clearly shows, that the reactivity can also be changed from inert to very reactive.
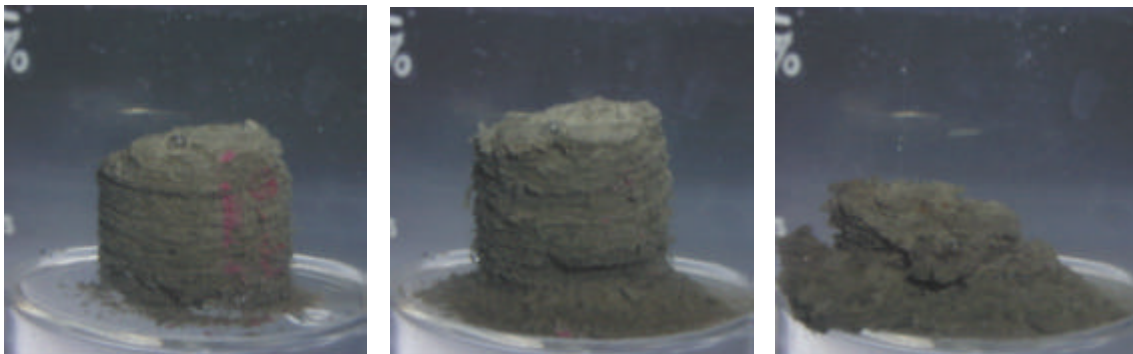
series 12: a), b), c): fragment of specimen #38 immediately after the glass cylinder was filled, b) after 7 minutes and c) after 15 minutes. #38 was hydrated under 1,5 MPa load at 99% RH, immersed into water under 1,5 MPa load, immersed into water without load, dehydrated without load at 5% RH and finally again immersed into water without load.

As the fragment of specimen #38 is not 100% representative due to its long "history" of treatment, the test was again conducted with initial material from sample 05664, well 205/482 m (#47) and sample 02517, well 104/511 m (#67).

Material from sample 02517, well 104/511 did not disperse as much as material from sample 05664, well 205/482 m, when immersed at initial untreated conditions. The material also deteriorated completely, but the pieces at the end of the process were bigger compared to those of the other material.

The reaction of the 99% RH saturated material to water was very weak in both cases. Contrary to this, the reaction of the 5% RH dried material to water was very aggressive. The reaction of the dry material to water was similar to the reaction of the initially untreated material to water. The difference was a higher and more powerful deterioration rate for the 5% RH dried material.

Series 13 represents the reaction of specimen #67 (sample 02517, well 104/511). The test was repeated with several other specimen and always produced the same result. The only exception was material from sample 05664, well 205/445 m. The material did not react at all, neither at 5% RH

dried conditions nor in a 99%RH saturated state, which can be explained by its mineralogical composition (cf chapter 4.3)
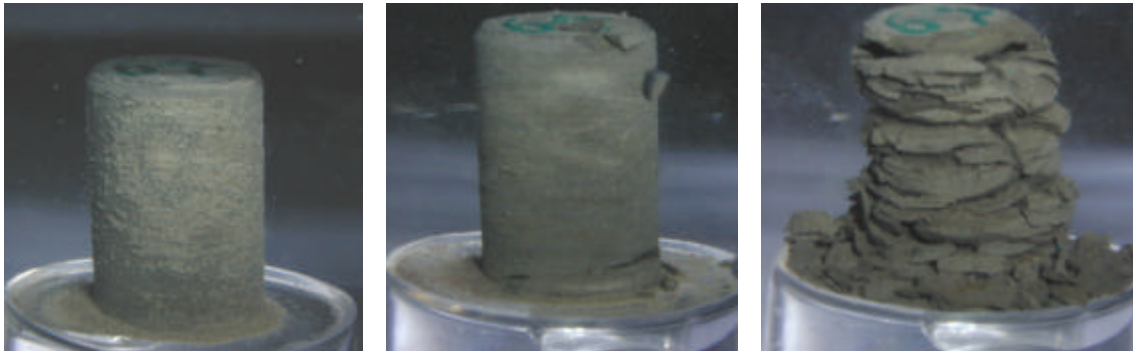
series 13: a), b), c):specimen #67, a) after 20 minutes in pure water at rehydrated state conditions (99% RH, 20 h, unloaded) and b) immediately after the glass cylinder was filled, at dehydrated state (5% RH, 20 h) and c) after 25 minutes

A high saturation gradient inside the material could foster high local swelling stress differences, which leads to deterioration. This is the case when dry material is immersed into water. If the material passed the air entry point before being immersed into water, air penetrates the material. These air bubbles could be entrapped in tiny pores and pressurized by the capillary pressure. This could also cause the deterioration of the material (cf chapter 2.3.6).

In the case of the hydration in the ACS chamber, the material can probably deaerate. The humid air smoothly condenses in the pores of the material and allows the air to escape. The saturation gradient is lower within the different regions of the material and thus causes a more homogenous swelling of the material. Material already hydrated at 99%RH causes a small saturation gradient when immersed into water and in addition to that there is no air inside the material.

The created saturation gradient inside the specimen and whether or not air is inside the specimen therefore seems to govern the reaction of the material.

This theory is supported by the fact that in most cases small ascending air bubbles were observed when 5%RH dried material was immersed into water. Furthermore the reaction was more powerful and faster for the 5% RH dried material than was observed for the material in its initial state. But this could also mean that the initial material we used, was already partially desaturated. This could be caused by the sampling and storage process (cf chapter 4.1).

If this phenomenon also occurs under high stress conditions, the message is clear: Shale must not be resaturated with liquid water, nor under high stress. This could produce incorrect results for the mechanical material parameters. Instead it has to be done in controlled humidity conditions. But today's common standard procedure for triaxial shale testing comprises the resaturation of shale under triaxial load conditions with liquid water.

Unfortunately there was not enough "reactive" material left from sample 05664, well 205/482 m and sample 02517, well 104/511 m, to conduct the required tests under high triaxial load conditions. But the author highly recommends these tests be conducted.

4.8.1 Conclusion

The comportment of shale from sample 05664, well 205/482 m, sample 05514, well 205/445 m and sample 02517, well 104/511 m was analyzed when in contact with pure liquid water.

It was clearly shown that the reaction of the material to pure liquid water is partially governed by the saturation level of the material.

Material which was hydrated in the ACS chamber at 99% relative humidity did not react to pure water as material in its initial untreated state and dry material did. The 99% RH hydrated material seems to be inert against the destruction mechanisms, which lead to complete deterioration and dispersion of the dry and untreated, initial material. The 5%RH exhibited the most powerful reaction to water. The untreated material reacted in a similar way to the dry material, but the deterioration rate was slower, as was the degree of dispersion.

This phenomenon is thought to be governed by two factors. The saturation gradient inside the specimen when immersed into water and whether or not air is inside the specimen. The lower the saturation gradient, the higher the mechanical destruction of the material when hydrated with liquid water.

If dry material is immersed into water, a high saturation gradient is created within the material, which leads to local swelling stress differences and deterioration. The air, which could enter the material when it passes the air entry point, could be entrapped and pressurized by the capillary pressure, which could also lead to deterioration.

It is very likely, that the hydration in the ACS chamber enables the air to evade the material and that the saturation gradient is rather low within the different regions of the material. This causes a much smaller swelling differences within the material.

Except the material from sample 05514, well 205/445 m, which is known was unreactive due to its mineralogical composition, this could be observed during all tests.

From the authors point of view it is very important to evaluate if this phenomenon also occurs under high load conditions, as it is common practice to put shale under triaxial load conditions into contact with liquid water, to resaturate the material.

If this phenomenon is also created under high stress conditions, it would be indispensable to resaturate the material in a controlled humidity environment before running a test.

Another point of interest would be the conduction of the solution test with specimen, which are already 99% RH saturated. These tests would separate the chemical influence of the solutions from the physical influence of the hydration. The chemical influence could therefore be better assessed.

5. General conclusion

A critical introduction into the theory, which describes the different micro mechanisms of the fluid solid interaction of shale, was presented. This theory was used to understand and to analyse the observed macro behaviour of shale under different testing conditions.

The X-ray microfocus technology was used, for the first time ever, to analyse the comportment of shale under different conditions. It was demonstrated that this non-destructive technology is a very useful additional tool for analysing argillaceous material. New insights into the liquid solid interaction of shale were made possible by using this technology.

The material used in the tests originates from the site of Est, where the underground laboratory of ANDRA is located. The variation of the mineralogical composition of the material is very high within a small depth range. The reactions of the received samples were therefore also different. The ratio of swelling clay minerals to the content of Carbonates of the material seems to have a momentous influence on the behaviour. A high Smectite/Illite content in combination with a small portion of Carbonates (reactive shale) provoked very strong reactions and vice versa.

The X-ray microfocus technology was used to visualize and to asses the real time behaviour of shale under uniaxial load when exposed to different aqueous solutions and to water. The analysed material reacted differently to distinct solutions and is chemically sensitive. The development of micro cracks as well as the general deterioration of the material is influenced by the concentration and the ion species of the solution. The geometrical orientation of the micro cracks and their density seems to influence the mechanical behaviour of the material. The observed plastification of the material is believed to arise from micro cracks, which are not orientated in the bedding plane, but under different angles to this plane. Chemical cracking and intrinsic cracking was observed for reactive shale when exposed to aqueous solutions.

The material was exposed to different relative humidity and uniaxial load conditions in the kinetic test arrangement. A computer controlled air conditioning system with online data transfer of the axial strain and the environmental parameters was used. The micro crack comportment of the shale was analysed by using the X-ray microfocus technology.
It was clearly shown, that the axial strain comportment can be directly related to the geochemical composition of the shale. High reactive shale produced the highest strains and vice versa. A relative humidity range from 90% to 99% causes the highest swelling gradients. The exposure of shale to 99% relative humidity under load conditions from 0 MPa to 4MPa resulted in a complete interstratification of micro cracks within the material. Intrinsic cracking of the material, caused by a high suction, therefore exists.
The swelling curves as well as the shrinkage curves always reached a threshold value, which marks equilibrated conditions of the material. It is very likely that the strain comportment of the material obeys an exponential law. The cyclical test showed, that the material is not crack sensitive in a range from 35% RH to 75% RH. But the material exhibits a kind of fatigue behaviour, caused by the reorganisation of the clay particles. This reorganisation depends on the load conditions and can either lead to an increased disorder or reorder of the particles.

The discovered hydration phenomenon is of great importance and has to be further analysed. It clearly shows the difference between hydration in controlled humidity environments and water. This phenomenon is thought to be governed by two factors. The saturation gradient inside the specimen when immersed into water and whether or not air is inside the specimen. The higher the saturation gradient is, the higher the mechanical destruction of the material when hydrated with liquid water. If it turns out that this phenomenon occurs under high stress conditions, some standard testing procedures for shale have to be substantially changed.
But it also opens new possibilities to separate the different mechanisms (physical, chemical), which govern the shale behavior. This is in turn very important for defining reliable models to predict the behavior of shale and would help to better understand the micro-macro relation of shale.

6.   A possible future program at the CGES

The X-ray microfocus technology is a very useful additional tool for further analysing the micro – macro relation of argillaceous materials and rocks in general. The presented results are only of a qualitative nature and the full possibilities of this technology were not used. A very high resolution in combination with the three-dimensional tomography analysis could lead to completely new quantitative insights.

A resolution of about 5 μm should allow us to separately analyse clay particles and to reach conclusions about the influence of the micro behaviour on the overall macro comportment. Creep and plastification of the material could probably be better understood and modelled afterwards.

As the tests conducted in this thesis were of a qualitative nature, a quantitative evaluation of these tests should be done, with reference to growth, orientation and propagation of the cracks and the deteriorations, in order to use them in a numerical simulation.

To better integrate the results of these tests in a numerical model, the tests have to be improved. The mass as well as the volume variations of the specimens should be permanently measured and documented during the tests. Even though these conditions require a very complex test arrangement, it is believed that the results would allow a very advanced numerical modelling of shale under different stress and saturation conditions.

Another point of interest is the relation of the stratification plane to the applied stress. The existing results were all obtained by using a stratification perpendicular to the main stress. But shale exhibits a high anisotropy with reference to the failure stress and the bedding plane.

It is indispensable to further analyse the observed hydration phenomenon. The most important issue is to determine whether this phenomenon occurs under high stress states. If this is the case, the reliability of certain tests, which comprise the resaturation of the shale with liquid water, have to be discussed.

The long term goal is clear: to establish a numerical model, which addresses the geochemical composition of the material, as well as the saturation, the load conditions and the stratification. The results presented in this thesis clearly show the high variety of shale properties as a function of the mineralogical composition. In the case of the material from the site of Est it is believed that the ratio of the portion of Smectite Illite to the portion of Carbonates plays a major role concerning the mechanical comportment. This could be the basis for a first simplified approach for taking the geochemical composition of the material into account in a new numerical model.

IV   Literature reference

1.   Al-Harthy S., Jing X., et al, (1999)"Petrophysical Properties of Sandstone under True Triaxial Stresses: Directional Transport Characteristics and Pore Volume Change"; SPE paper Nr.:57287

2.   Amanullah M., Marsden J., et al, (1994):"Effects of rock fluid interactions on the petrofabric and stress strain behaviour of mudrocks", Eurock 94 Balkema Rotterdam ISBN 905410502X

3.   ANDRA, (1997):"Etude de l'Est du Bassin Parisien"; ISBN: 2-86883-411-6

4.   ANDRA, (2001):"essais recenses dans le cadre de l'étude, synthèse des expérimentations conduites en geomécanique sur des échantillons du site de l'est depuis 1994"; ANDRA Nr.: D RP 0.ENG 01.0073/A

5.   ANDRA, (2002):"Laboratoire de recherche souterrain meuse/haute-marne - lot3 - forages d'investigation geologique complementaire rapport de synthese"; text, figures and appendix - ANDRA Nr.: D RP 0ANT 01-022

6.   Aumann J., (1988):"A Laboratory Evaluation of Core Preservation Materials"; SPE paper Nr.:15381

7.   Ballaed, Tracey J., et al, (1993):"Fundamentals of Shale Stabilization: Water Transport Through Shales"; SPE paper Nr.:24974

8.   Barbour S. L., (1988):"Mechanisms of osmotic flow and volume change in clay soils", Dept. Civil engineering University of Saskatchewan S7N 0W0

9.   Barron J., Weakly R., et al, (1990):"Pore Pressure Analysis Indicates Abnormal Pressure as Reason for Shale Instability in Offshore California Field"; SPE paper Nr.:19993

10. Bauer-Plaindox C., Tessier D., et al, (1997):"Propriétés mécaniques des roches argileuses carbonatées: importance de la relation calcite-argile", Earth & Planetary Sci. 1998. 326 231-237

11. Beihoffer T., Dorrough D., et al, (1988):"The Separation of Electrolyte Effects from Rheological Effects in Studies of Inhibition of Shales with Natural Moisture Contents"; SPE paper Nr.:18032

12. Blanton L., Teufel L., (1983):"A Field Test of the Strain Recovery Method of Stress Determination in Devonian Shale"; SPE paper Nr.:12304

13. Bol G., (1986):"The Effect of Various Polymers and Salts on Borehole and Cutting Stability in Water Base Shale Drilling Fluids"; SPE paper Nr.:14802

14. Bol G., Wong S-W, et al, (1993):"Borehole Stability in Shales"; SPE paper Nr.:24975

15. Broch E. (1979):"Changes in rock strength caused by water", EMF(3012(4))

16.   Cabrera Nunez J. et al, (2001):"Projet Tournemire, synthese des programmes de recherche 1995-1997", IPSN, DPRE/SERGD 01-19

17.   Capuano R., (1993):"Evidence of fluid flow in microfractures in geopressured shales"; American Association of Petroleum Geologists, Vol. 77, No.8, p. 1303-1315

18.   Carminati S., Santarelli F., et al, (1997):"The activity concept applied to shales:consequences for oil, tunneling and civil engineering operations"", Int. J. Rock Mech. & Min. Sci. 34:3-4 paper N°038

19.   Chenevert M. E., Amanullah M., (1997):"Shale Preservation and Testing Techniques for Borehole Stability Studies"; SPE paper Nr.:37672

20.   Chenevert M. E., Osisanya S., (1988):"Shale/Mud Inhibition Defined with Rig-Site Methods"; SPE paper Nr.:16054

21.   Chenevert M. E., Pernot V., (1998):"Control of Shale Swelling Pressures Using Inhibitive Water-Base Muds"; SPE paper Nr.:49263

22.   Chenevert M. E., Sharma A., (1992):"Permeability and Effective Pore Pressure of Shales"; SPE paper Nr.:21918

23.   Chenevert M.E., Amanullah M., (1996):"Assessment of the degree of water saturation in shales", Rock Mech. 96 Balkena Rotterdam ISBN 905410838X

24.   Cheng Y., Yan J., et al, (1996):"A Comprehensive Study of Wellbore Stability in Shale Formation and its Application to Horizontal Drilling Operations"; SPE paper Nr.:37080

25.   Chesser B., (1986):"Design Considerations for an Inhibitive, Stable Water Based Mud System"; SPE paper Nr.:14757

26.   Chiarelli A., Ledesert B. et al, (1999):"Study of the influence of mineralogy and moisture content on plasticity and induced anisotropic damage of shales acting as geological barriers in nuclear waste disposals"

27.   Clauer N., Chauduri S., (1995):"Clay in Crustal Environments, Isotope Dating and Tracing", Springer-Verlag, ISBN: 3-540-58151-0

28.   Comité français de mécanique des roches (2000):"manuel de mécanique des roches", ENSMP les presses: IBSN: 2-911762-23-1

29.   Daupley X., (1997):"Etude du potentiel de l'eau interstitielle d'une roche argileuse et de relations entre ses propriétés hydriques et méchaniques", PhD thèse, ENSMP

30.   Decker K., (1985):"Decker Maschinenelemente, Gestaltung und Berechnung", Carl Hanser Verlag München, ISBN 3-446-14362-9

31.   Ecole Polytechnique, (1998):"Mesure de la perméabilité des argiles sous contrainte et température", Revue Francaise de Geotechnique N°82 98

32. Einfalt H., Fecker E., (1979):"The three phase system clay anhydrit gypsum and its time dependent behaviour on saturation with water based solutions",EMF(3012(4))

33. Einstein H., (1989):"suggested methods for testing of argillaceous swelling rocks", Int. J. Rock Mech. & Min. Sci. 26 N°5 (89) 415-426

34. Fine J., (1997):"Comportement des roches gonflantes compte rendu d'essais sur argilite HTM", école des mines de paris cges

35. Fine J., (1997):"Comportement des roches gonflantes compte rendu d'essais sur argilite HTM", ENSMP CGES

36. Fine J., Gallet S., (1997):"projet d'extension etude geotechnique de dimensionnement", école des mines de paris cges

37. Fooks J., Dusseault M., (1996):"Strength of piere I shale as function of moisture content", Eurock 96 Balkema Rotterdam ISBN 9054108436

38. Forsans T., Schmitt L., (1994):"Capillary forces: the neglected factor in shale instability studies?, Eurock 94 Balkema Rotterdam ISBN 905410502X

39. Fritz S. et al, (1983):"Experimental support for a predictive model of clay membranes", Geochemica et Cosmochemica Acta Vol 47 pp 1515-1522

40. Gasc Barbier M., Ghoreychi M., (1999):"Comportement de roches argileuses profondes: incidence de la texture"

41. Gilmore W., Sanclemente J., (1989):"A Case History Review of the Effects of Drilling Fluids on Shale Stability in the Central Gulf of Mexico"; SPE paper Nr.:18640

42. Hale A., Mody F., et al, (1993):"Mechanism for Wellbore Stabilization with Lime Based Muds"; SPE paper Nr.:25706

43. Hale A., Mody F., et al, (1993):"The Influence of Chemical Potential o Wellbore Stability"; SPE paper Nr.:23885

44. Hand J., Pinczewski W., (1990):"Interpretation of Swelling Extraction Tests"; SPE paper Nr.:19471

45. Heinemann Z., (1995):"Flow in Porous Media", MUL textbook series volume 1, Mining University of Leoben Austria, Dept. for petroleum reservoir physics

46. Holt R., Sonstebo E., et al, (1996):"Fluid effects on acoustic wave propagation in shales", Eurock 96 Balkema Rotterdam ISBN 9054108436

47. Horsrud P., Bostrom B., et al, (1998):"Interaction between Shale and Water-Based Drilling Fluids: Laboratory Exposure Tests Give New Insight Into Mechanism and Field Consequences of KCL Contents"; SPE paper Nr.:48986

48. Huang S., Augenbauch N., et al, (1986):"Swelling Pressure Studies of Shales"; Int. J. Rock Mech. & Min. Sci. 23 N°5 (86) 371-377

49.   Jasmund K., (1955):"Die silicatischen Tonminerale", Monographien zu angewandte Chemie und chemische Ingenieur-Technik, Verlag Chemie GmbH, WeinheimVerlg. Nr.:5482-III-18-127 5000/122/53

50.   Kiehl J., Wittke W., (1991):"Interpretation of the results of large scale in situ swelling tests by means of three dimensional numerical analyses", EMF(3012(7))

51.   Krilov Z., Wojtanowicz A., (1989):"Low pH Ammonium Nitrate Methanol Completion Fluid: A Promising Alternative for Calcareous, Argillaceous Sand Formations"; SPE paper Nr.:18479

52.   Lebon P., Hoteit N., (1996):"Research on the mechanics of clayed rocks in the french program on radioactive waste disposal in deep geological formations", Rock Mech. 96 Balkena Rotterdam ISBN 905410838X

53.   Madsen F., (1979):"Determination of the swelling pressure of claystones and marlstones using mineralogical data", EMF(3012(4))

54.   Madsen F., (1999):"Suggested methods for laboratory testing of swelling rocks", Int. J. Rock Mech. & Min. Sci. 36 (99) 291-306

55.   Manohar L., (1999):"Shale Stability: Drilling Fluid Interaction and Shale Strength"; SPE paper Nr.:54356

56.   Maury V., Sauzay J., (1987):"Borehole Instability: Case Histories, Rock Mechanics Approach, and Results"; SPE paper Nr.:16051

57.   Miehe B., (2002):"Analyse de l'ensemble des essais mechaniquees - court terme et long terme", journee des thesrds Andra 27 juin 2002, pp. 172-191

58.   Milliken K., et al, (1994):"Evidence of fluid flow in microfractures in geopressured shales: discussion"; American Association of Petroleum Geologists, Vol. 78, No.10, p. 1637-1640

59.   Millot G., (1964):"Géologie des Argiles, Altérations Sédimentologie Géochemie", Masson et Cie Paris

60.   Mody F., Hale A., et al, (1993):"A Borehole Stability Model to Couple the Mechanics and Chemistry of Drilling Fluid Shale Interaction"; SPE paper Nr.:25728

61.   Morriss S., Chenevert M. E., et al, (1996):"Time Laps Resistivity and Water Content Changes in Shales"; SPE paper Nr.:36507

62.   Mortimer E., (1987):"Chemie - Das Basiswissen der Chemie"; Georg Thieme Verlag Stuttgart, ISBN: 3-13-484305-6

63.   Nesbitt L., King G., et al, (1985):"Shale Stabilization Principles"; SPE paper Nr.:14248

64.   Nguyen Minh D., Bergues J., (1999):"Determination du comportement mécanique des roches argileuses"

65. Niandou H., Shao J., et al, (1997):"Laboratory investigation of the mechanical behaviour of Tournemire Shale"", Int. J. Rock Mech. & Min. Sci. 34 N°1 (97) 3-16

66. Obara Y., Sugawara K., et al, (1996):"Influence of water vapour pressure on strength of rocks under uniaxial compression", Rock Mech. 96 Balkena Rotterdam ISBN 905410838X

67. Olgaard D., Urai J., et al, (1997):"The influence of swelling clays on the deformation of mudrocks", Int. J Rock Mech. & Min. Sci. 34 3-4, paper N°235

68. Pappas D., Vallejo L., (1997):"The settlement and degradation of nondurable shales associated with coal mine waste embankments", Int. J. Rock Mech. & Min. Sci. 34:3-4 paper N°241

69. Per Horsrud, Rune M., et al, (1994):"Time Dependent Borehole Stability: Laboratory Studies and Numerical Simulation of Different Mechanism in Shale"; SPE paper Nr.:28060

70. Pimentel E., (1999):"Swelling and permeability tests on high compressed bentonite and mixtures of bentonite and sand"; Inst. f. Bodenmechanik, Universität (TH) Karlsruhe

71. Potter P., et al, (1980):"Sedimentology of shale", New York Springer Verlag"

72. Ramambasoa N., (1999):" Revue bibliographique sur les interactions hydromechanique dans les materiaux argileux", IPSN, 47103004 E

73. Ritter A., Geraut R., (1985):"New Optimization Drilling Fluid Programs for Reactive Shale Fromations"; SPE paper Nr.:14247

74. Robert A., Saita A., et al, (1997):"Modelisation numerique des effets du gonflement dans le ouvrages souterrains", tunnels et ouvrages souterrains 301-306 N°143

75. Rowe K. R. et al, (1997):"Clayey barrier systems for waste disposal facilities", E&FN Spon, ISBN: 0 419 19320 0 (HB)

76. Rutang W., Tianyun J., et al, (1988):"A Method for Evaluating Shale Stabilityand its Application in the Field"; SPE paper Nr.:17838

77. Salisbury D., Ramos G., (1991):"Wellbore instbility of shales using a downhole simulation test cell", Rock Mech. Multi Dis. Sci. 91 Balkema Rotterdam ISBN 906191194X

78. Sanjit Roy, Cooper G., (1991):"Effect of electro-osmosis on the indentation of clays", Rock Mech. Multi Dis. Sci. 91 Balkema Rotterdam ISBN 906191194X

79. Santarelli F., Carminati S., (1995):"Do Shales Swell? A Critical Review of Available Evidence"; SPE paper Nr.:29421

80. Santarelli F., Chenevert M. E., et al, (1992):"On the Stability of Shales and its Consequences in Terms of Swelling and Wellbore Stability"; SPE paper Nr.:23886

81. Santarelli F., Forsans T., et al, (1994):"Shale Testing and Capillary Phenomena", Int. J. Rock Mech. & Min. Sci. 31 N°5 (94) pp 411-427

82. Santos H., Rego L., et al, (1997):"Integrated Study of Shale Stability in Deepwater Brazil" ; SPE paper Nr.:38961

83. Santos H., Roegiers J., et al, (1996):"Can clay swelling be easily controlled?", Eurock 96 Balkema Rotterdam ISBN 9054108436

84. Santos H., Roegiers J., et al, (1996):"Investigation of the effects of sample handling procedures on shale properties ",Rock Mech. 96 Balkena Rotterdam ISBN 905410838X

85. Santos H., Rogiers J., et al, (1997):"Shale Reactivity test: a novel approach to evaluate shale-fluid interaction", Int. J. Rock Mech. & Min. Sci. 34:3-4 paper N°268

86. Simpson J., Walker T., et al, (1994):"Environmentally Acceptable Water Base Mud Can Prevent Shale Hydration and Maintain Borehole Stability"; SPE paper Nr.:27496

87. Sonstebo E., Horsrud P., (1996):"Effects of brines on mechanical properties of shales under different test conditions", Eurock 96 Balkema Rotterdam ISBN 9054108436

88. Steiger R., Leung P., (1991):"Consolidated undrained triaxial test procedure for shales", Rock Mech. Multi Dis. Sci. 91 Balkema Rotterdam ISBN 906191194X

89. Steiger R., Leung P., (1991):"Critical state shale mechanics", Rock Mech. Multi Dis. Sci. 91 Balkema Rotterdam ISBN 906191194X

90. Stepkowska E., (1990):"Aspects of the clay electrolyte water system with special reference to geotechnical properties of clays", engineering geology, Nr.28: 249-268

91. Tan P., Richards B., et al, (1997):"Effects of Swelling and Hydrational Stress in Shales on Wellbore Stability" ; SPE paper Nr.:38057

92. Tjong T. Xuan M., (1983):"Swelling rocks and the stability of tunnels", EMF(3012(5))

93. Van Geet M., (2001):"Optimisation of microfocus X-ray computer tomography for geological research with special emphasis on coal components (macerals) and fracture (cleats) characterisation"; PhD thesis, Katholieke Universiteit Leuven Belgium, Fac. Wetenschappen

94. Van Oort E., Hale A ., et al, (1994):"Critical Parameters in Modelling Chemical Aspects of Borehole Stability in Shales and in Designing Improved Water-Based Shale Drilling Fluids"; SPE paper Nr.:28309

95. Velde B., (1992):"Introduction to Clay Minerals", Chapman & Hall, ISBN: 0 412 37030 1

96. Wan R., Achari G., et al, (1996):"Effect of drilling fluids on shear strength properties of fermie shales", Rock Mech. 96 Balkena Rotterdam ISBN 905410838X

97. Wendell I., et al, (1981):"Osmotic model to explain anomalous hydraulic heads": Water Resources Research 17 N°1 (82) 73-82

98. Wong S-W, Kenter C., et al, (1993):"Optimising Shale Drilling in the Northern North Sea: Borehole Stability Considerations"; SPE paper Nr.:26736

99.   Wu B., Tan C., et al, (1997):"Specially designed techniques for conducting consolidated undrained triaxial tests on low permeability shales"", Int. J. Rock Mech. & Min. Sci. 34:3-4 paper N°336

100.   Yamashita S., Sugimoto F., et al, (1999):"The relationship between the failure process of the creep or fatigue test and the conventional compression test on rock"; Fac. of engineering and resource science, Akita university, Japan

101.   Yizehn L., (1988):"Study of Property of Cationic Surfactants for Preventing Clay from Swelling"; SPE paper Nr.:17826

102.   Young A., Low P., (1965):"osmosis in argillaceous rocks", bulletin of the american association of petroleum geologists vol.49, N°7 (65) 1004-1008

103.   Zhou Z., Huang R., et al, (1992):"Constitutive Equations of Shale and Clay Swelling: Theoretical Model and Laboratory Test under Confining Pressure"; SPE paper Nr.:22382

104.   Zhou Z., Kadatz B., et al, (1996):"Clay Swelling Diagrams: Their Applications in Formation Damage Control"; SPE paper Nr.:31123

III   Appendix

Nr	Mass	Hight	diam.	time	vitesse	density	specimen #1 to #47 from core sample #05664, well 205/482 m	test
[ ]	[g]	[mm]	[mm]	[µs]	[m/s]	[kg/m3]		[ ]
1	23,604	50,00	15,93	21,6	2315	2369		KC
2	23,728	50,02	15,96	21,9	2284	2371		
3	23,199	49,60	15,98	16,5	3006	2332		KCl solution (c
4	23,511	49,50	15,94	16,3	3037	2380		NaCl solution (c(
5	18,324	38,60	15,94	14,8	2608	2379		KCl solution (c(
6	18,522	39,22	15,93	15,5	2530	2370		H2
7	28,411	59,99	15,92	25,8	2325	2379		MgCl2 sol
8	27,938	58,99	15,93	22,5	2622	2376		
9	27,924	58,90	15,94	22,7	2595	2376		
10	no data							KCl solution (c(KCl)=1,5mol, T=
11	no data							
12	23,502	50,00	15,93	20,4	2451	2358		atmos
13	14,199	30,01	15,94	12,4	2420	2371		
14	9,470	20,39	15,97	8,9	2291	2319		ACS fast hydration + H2O pure (G=0,
15	9,471	20,38	15,97	8,8	2316	2320		
16	14,209	29,98	16,01	12,5	2398	2354		H2O pure (C
17	14,204	30,11	15,95	12,7	2371	2361		H2O pure (G=5
18	14,190	30,06	15,98	13,2	2277	2354		reconditionned pore
19	14,194	30,02	16,00	12,7	2364	2352		NaCl solution (c(NaCl) = 1,
20	14,318	30,08	15,92	13,0	2323	2391		MgCl2 solution (c(MgCl2) = 1,
21	14,186	30,04	16,01	14,1	2130	2346		NaCl solution (c(NaCl) = 0,
22	14,199	30,07	16,00	12,6	2387	2349		reconditionned pore l
23	15,252	30,10	15,97	12,7	2370	2530		H2O pure (G=5
24	14,260	30,02	15,98	12,4	2421	2368		KCl solution (c(KCl) = 0,
25	14,276	30,02	15,96	13,0	2309	2377		sample broke during P w
26	14,193	29,94	15,96	12,6	2376	2370		KCl solution (c(KCl) = 1,
27	14,299	30,00	15,95	15,0	2000	2385		
28	14,347	30,08	16,02	12,6	2387	2366		CaCl2 solution (c(CaCl2) = 1,
29	14,061	30,10	16,00	13,4	2246	2323		CaCl2 solution (c(CaCl2) = 0,
30	14,209	30,03	16,00	13,8	2176	2353		ACS slow hydration (35% to

specimen #1 to #47

Nr	Mass	Hight	diam.	time	vitesse	density	test
[ ]	[g]	[mm]	[mm]	[µs]	[m/s]	[kg/m3]	[ ]

from core sample #05664, well 205/482 m

Nr	Mass	Hight	diam.	time	vitesse	density	test
[ ]	[g]	[mm]	[mm]	[µs]	[m/s]	[kg/m3]	[ ]
31	14,254	30,07	16,00	13,0	2313	2358	ACS slow hydration (35% to
32	14,209	30,04	15,96	13,4	2242	2364	ACS fast dehydration (5%R
33	14,235	30,04	15,95	14,0	2146	2372	ACS fast dehydration (5%R
34	14,223	30,01	15,98	12,7	2363	2363	H2O pure (G:
35	13,841	29,40	15,94	13,0	2262	2359	ACS fast hydration (99%RH, 20h, T = 4:
36	14,203	30,03	15,99	12,9	2328	2355	ACS
37	14,225	30,04	15,94	12,6	2384	2373	ACS fast hydration (99%F
38	14,136	29,95	16,10	12,4	2415	2318	ACS fast de/rehydration (0%/99%RH, T=
39	14,164	29,87	16,09	12,3	2428	2332	ACS cyclic de/rehydration (min/max=35/75%
40	14,083	29,91	15,98	12,8	2337	2348	ACS cyclic de/rehydration (min/max=35/75%
41	14,066	29,84	16,00	13,1	2278	2344	ACS fast de/rehydration (0%/99%RH, T=
42	14,209	30,04	15,96	13,4	2242	2364	ACS fast hydration (99%RH, 37h, T = 4
43	14,063	30,10	15,97	13,4	2246	2332	ACS fast hydr.+H2O+fast dehydr.+H2O(5%/
44	14,187	29,94	15,96	12,9	2321	2369	ACS cyclic de/rehydration (min/max=35/75
45	14,293	30,00	15,95	13,2	2273	2384	ACS cyclic de/rehydration (min/max=35/75%
46	14,061	30,10	16,00	13,4	2246	2323	ACS fast hydration (99%RH, 37h, T = 4
47	14,187	30,03	16,01	14,1	2130	2347	ACS fast hydr.+H2O+fast dehydr.+H2O(5%/

specimen #48 to #55 from core sample #05514, well 205/445 m

Nr	Mass	Hight	diam.	time	vitesse	density	test
[ ]	[g]	[mm]	[mm]	[µs]	[m/s]	[kg/m3]	[ ]
48	16,373	29,90	15,90	8,3	3602	2758	ACS fast hydration (99%RH, 45h, T = 4
49	16,624	30,01	16,00	8,5	3531	2755	ACS fast hydration (99%RH, 45h, T = 45
50	16,625	29,56	15,90	8,2	3605	2833	
51	16,626	29,90	15,90	8,3	3602	2800	ACS fast hydr.+H2O+fast dehydr.+H2O(5%/
52	16,410	29,78	15,99	8,8	3384	2744	ACS fast hydr.+H2O+fast dehydr.+H2O(5%/
53	16,398	29,80	16,00	8,7	3425	2737	ACS fast hydration (99%RH, 45h, T = 4

Nr	Mass	Hight	diam.	time	vitesse	density	test
54	16,476	29,90	15,99	8,9	3360	2744	
55	16,250	30,05	15,89	8,5	3535	2727	ACS fast dehydr.+H2O+fast dehydr.+H2O(5%/

specimen #60 to #70 from core sample #02517, well 104/511 m

Nr	Mass	Hight	diam.	time	vitesse	density	test
[ ]	[g]	[mm]	[mm]	[µs]	[m/s]	[kg/m3]	[ ]
60	14,189	29,07	15,96	11,5	2528	2440	ACS fast hydration (99%
61	14,522	30,08	15,95	11,7	2571	2416	ACS fast hydration (99%F
62	13,579	29,96	15,98	11,3	2651	2260	
63	14,592	30,17	15,94	11,3	2670	2424	ACS fast hydration, power failure, no data
64	14,507	30,16	15,99	12,0	2513	2395	ACS fast hydration, power failure, no data
65	14,340	30,00	15,94	11,6	2586	2395	ACS fast hydr.+H2O+fast dehydr.+H2O(5%/
66	14,550	29,96	15,99	11,7	2561	2418	
67	14,489	30,24	15,94	12,1	2499	2401	ACS fast hydr.+H2O+fast dehydr.+H2O(5%/
68	13,296	27,36	16,10	11,0	2487	2387	KCl solution (c
69	9,058	18,80	16,09	7,5	2507	2370	ACS fast dehydr.+F
70	9,096	18,56	15,98	7,9	2349	2444	